Lipid – protein interactions:
from signal transduction to drug delivery

By

Aparna Krishnamoorthy

A dissertation submitted in partial satisfaction of the

requirements for the degree of

Doctor of Philosophy

in

Molecular and Biochemical Nutrition

in the

Graduate Division

of the

University of California, Berkeley

Committee in charge:

Professor Robert O. Ryan (Co-Chair)
Professor Danica Chen (Co-Chair)
Professor Jen Chywan (Wally) Wang
Professor Henk Roelink

Spring 2017

Abstract

Lipid – protein interactions: from signal transduction to drug delivery

by

Aparna Krishnamoorthy

Doctor of Philosophy in Molecular and Biochemical Nutrition

University of California, Berkeley

Professor Robert O. Ryan, (Co-Chair)
Professor Danica Chen (Co-Chair)

Based on the hydrophobic tendencies exhibited by certain groups of molecules, the primary focus of this dissertation has been to create environments enriched in lipids and amphipathic molecules to explore the effect on their biological behavior. To this effect, ternary complexes of phospholipid, an apolipoprotein scaffold and a hydrophobic bioactive MDM2 inhibitor, nutlin-3a were used to form nanoassemblies of nutlin-3a nanodisks (ND). Nutlin-3a, as a part of ND was conferred with aqueous solubility, formed a homogeneous population of ND particles and associated reversibly with the ND. Biological activity of nutlin-3a ND was examined in three distinct glioblastoma cell lines, U87MG, SF763 and SF767. An overall robust decrease in cell viability, increase in apoptosis, increase in protein levels of p53 and MDM2 was observed in U87MG cells in response to nutlin-3a ND incubation while the other two cell lines remained mostly unresponsive. The nanoscale size of the formulation particles, their facile assembly and nutlin-3a solubilization capability suggest ND represent a potentially useful vehicle for *in vivo* administration of this anti-tumor agent.

"Wnt" family of signaling molecules regulates cell fate and proliferation in tissues of many multicellular organisms. Structure function studies of Wnts have been impeded due to the high propensity of isolated Wnts to self-associate. Stably transfected *Drosophila* S2 cells were used to improve recovery of recombinant murine Wnt3a. As a part of Wnt3a characterization, modulators of Wnt3a signaling were evaluated. Based on the central role played by low density lipoprotein receptor related protein 5 or 6 (LRP5/6) in Wnt3a signaling and apolipoprotein (apo)E3 lipoprotein metabolism, the ability of apoE3 to modulate Wnt signaling was evaluated. Wnt3a canonical signaling was down regulated in the presence of lipid-free apoE3 N-terminus however, this interaction appeared to be mediated through apoE3 binding with Wnt3a rather than LRP5/6. Additionally, while dissecting the supporting scaffolds of Wnt3a using thrombin mediated limited proteolysis, a site-specific cleavage within the N-terminal domain of Wnt3a was identified. Within the N-terminal (NT) domain there exists a motif that is superimposable upon saposin-like protein (SAPLIP) family

members. SAPLIPs possess lipid surface seeking activity. Further inspection into the Wnt3a saposin-like sub-domain (SLD) revealed that neighboring structural elements within full-length Wnt3a affect SLD conformational stability. Overall, SLD function(s) in Wnt proteins appear to have evolved away from those commonly attributed to SAPLIP family members.

ACKNOWLEDGEMENTS

"The goal of a Ph.D. is that you enjoy the journey", were the first words Robert Ryan (Bob) told me when I joined his lab as a graduate student. I thank Bob for standing by his words as I developed my scientific acumen under his guidance. With a penchant for details and always wearing a smile, Andrzej Witkowski has been my technical-hiccups-resolving-guru and I thank him for providing me with incredible insight throughout my research.

I acknowledge Trudy Forte, Jennifer Beckstead and Nahal Lalefar for their presence by my side during all the successful and not-so-successful experiments in the lab and infusing me with renewed energy. I thank Jens Simonsen for his moral support. I thank my committee members for thought provoking ideas and useful feedback on my research.

I thank Maureen Mitra for always accommodating my requests to edit numerous fellowship applications and her valuable insight in helping me convey scientific material to a non-scientific audience.

I thank the Children's Hospital Oakland Research Institute (CHORI) for maintaining a positive and collaborative research environment for me. I thank the department of nutritional sciences and toxicology at UC Berkeley for supporting me with a generous stipend and giving me the opportunity to be a part of the UC Berkeley legacy.

Wild and urban expeditions outside the lab helped me maintain a healthy perspective for which I owe a big thank you to the ever optimistic, Jayaram Natarajan. I thank Anusha Krishnamoorthy, Murali Bharathan and Mrdah Murali for creating a home away from home for me in Simi Valley. My parents have been a huge influence in laying the foundation for a good education and reminding me to always do my best. I thank them for being supportive through the years.

TABLE OF CONTENTS

LIST OF FIGURES

INTRODUCTION

The body of work compiled as part of my dissertation originated as a result of two independent events that took place in 2012. The first was a Gordon conference on lipoproteins that I attended in June 2012 in New Hampshire. Lipoproteins are complex mixtures of protein and lipid that facilitate cholesterol transport through the vascular system. Plasma lipoproteins usually undergo a maturation process starting with their synthesis followed by their eventual catabolism. High density lipoproteins (HDL) facilitates extraction of cholesterol from tissues and transport to the liver. Among the numerous proteins that make up these lipoprotein particles, apolipoprotein E3 (apoE3) and apolipoprotein A-I (apoA-I) play key roles (1–3). The aqueous nature of plasma forces hydrophobic molecules in circulation to associate with lipoprotein particles as a protective shield. In the Ryan lab, this principle is used to combine synthetic phospholipids and a suitable apolipoprotein scaffold to form reconstituted HDL (rHDL) particles. One of the many applications of rHDL particles is their use as nanodisks, to confer improved solubility to certain hydrophobic compounds. Nanodisks are thus delivery vehicles with the potential to solubilize and shield hydrophobic compounds of therapeutic value for *in vivo* administration (4). These are nanoscale assemblies comprising a disk-shaped lipid bilayer stabilized by an apolipoprotein scaffold in complex with hydrophobic agents. Combining my interest that was sparked from attending the lipoprotein conference and available expertise within the Ryan lab, survey for a suitable agent to incorporate into nanodisks began. Nutlin-3a, is a small molecule inhibitor that was originally developed in 2004 by Roche (5). Nutlin-3a is a cis-imidazoline drug that is used to bind and prevent mouse double minute 2 (MDM2) molecule from ubiquitinating p53, the tumor suppressor protein, for degradation (6). Nutlin-3a is thus an effective compound that can be used in tumor cells that express wild type MDM2 and p53 pathways. However, one of the major limitations that have stalled the use of nutlin-3a in clinical trials relates to their intrinsic hydrophobicity. Poor water solubility poses practical problems with respect to mode of administration, bioavailability, toxicity and transit across the blood brain barrier. I decided to address the solubilization and characterization of nutlin-3a as part of rHDL (nutlin-3a nanodisks) and the efficacy of nutlin-3a nanodisks on glioblastoma multiforme (GBM) cell lines, an aggressive type of brain tumor. Details of this work are covered in **Chapter 1**.

The other event in 2012 that played a key role in shaping the course of my dissertation was a breakthrough in the field of ‘Wnt’ biology. Almost three decades earlier, in 1982, a proto-oncogene called int1 was identified in mouse mammary tumors which was found to be activated by a retroviral insertion (7). Later, a discovery was made that the gene involved in segment polarity and larval development called Wingless in *Drosophila melanogaster* was an int1 homologue (8) and subsequently, the term Wnt (Wingless-related integration site) was coined (9). Wnt signaling plays a critical role during embryogenesis and adult tissue homeostasis through regulation of cell fate decisions and is largely conserved among metazoans (10). In 2012, the X-ray crystal structure of a member of the Wnt family was reported for the first time that revealed details about the organization of Wnt and how it interacts with its receptors.

The structure revealed that Wnt exists as a two-domain protein comprised of an

N-terminal domain that contains a single covalently bound, monounsaturated fatty acyl chain and a C-terminal domain that adopts a cytokine like fold. Coexpressing Wnt in the presence of a subdomain of one its receptors facilitated burial of its fatty acyl group that prevented its aggregation and enabling X-ray crystallography (11). With the Wnt structure in hand it was possible to address many speculations that exist in the 'Wnt' field around how this lipidated protein is transported to neighboring cells in the aqueous plasma and what are its binding interactions at the cell surface with receptors and other ligands. Complexes of Wnt with its receptor are not optimal for biochemical analysis as they may compete with natural receptors that mediate Wnt signaling activity. It was necessary to have sufficient amounts of Wnt protein to work with. In **Chapter 2,** I describe an improved procedure built upon an existing protocol to isolate recombinant Wnt3a (one of the most commonly studied Wnt family members), validation of Wnt3a biological activity and its use in molecular studies.

In mammals, the complexity of Wnt signaling arises from the spatiotemporal expression of 19 different Wnts that engage with 10 unique frizzled receptors and 2 co-receptors, low density lipoprotein receptor related protein 5 or 6 (LRP5/6). Wnt binding to frizzled and LRP5/6 induces stabilization of the transcriptional coactivator, β-catenin, thereby leading to enhanced expression of Wnt responsive genes. In the absence of Wnt, a proteasomal degradation complex rapidly degrades β-catenin (12). Many modulators in the form of enhancers or inhibitors exist in vivo that regulate Wnt signaling activity (13). It has been previously reported that LRP5/6 regulates serum cholesterol levels by binding to apoE3. Considering LRP5/6 function(s) at the intersection of cell proliferation (Wnt) and cholesterol metabolism (apoE3), I was curious to determine if apoE3 could function as a modulator of Wnt signaling by competition or by directly binding to LRP5/6. In **Chapter 3**, I describe details of the interplay between LRP5/6 protein, Wnt3a and N terminus receptor binding domain of apoE3 and the differences observed in the canonical Wnt3a signaling in cultured mouse embryonic fibroblasts in the presence of apoE3 in lipid free and lipid associated forms.

The X-ray crystal structure of Wnt opened the door to deeper inspection into the supporting scaffolds of Wnts that contact the frizzled receptor via both the N and C terminal domains (14). Interestingly, covalent attachment of the palmitoleic acid is required for Wnt trafficking within the cell as well as binding to the cysteine rich domain of frizzled (15). A portion of the N-terminal domain that contains the palmitoleic acid post-translational modification adopts a structure similar to the saposin family of proteins (16). Within the human genome, there are 11 physiologically diverse saposin-like proteins with functions clustered in three main groups: membrane binding, pore formation and cell lysis – all of which share an ability to interact with lipid (17). The significance of a saposin-like motif within the Wnt N-terminal domain in relation to the function of the protein was an evolutionary question that remained unaddressed. In **Chapter 4**, I describe the design of different constructs of the saposin like domain of Wnt3a, their expression, isolation, solubilization and characterization to understand its function in the broader context of full length Wnt3a.

References

1. Gogonea, V. (2016) Structural Insights into High Density Lipoprotein: Old Models and New Facts. *Front. Pharmacol.* **6**, 318
2. Hegele, R. A. (2009) Plasma lipoproteins: genetic influences and clinical implications. *Nat. Rev. Genet.* **10**, 109–121
3. Hauser, P. S., Narayanaswami, V., and Ryan, R. O. (2011) Apolipoprotein E: From lipid transport to neurobiology. *Prog. Lipid Res.* **50**, 62–74
4. Ryan, R. O. (2010) Nanobiotechnology applications of reconstituted high density lipoprotein. *J. Nanobiotechnology*. **8**, 28
5. Vassilev, L. T., Vu, B. T., Graves, B., Carvajal, D., Podlaski, F., Filipovic, Z., Kong, N., Kammlott, U., Lukacs, C., Klein, C., Fotouhi, N., and Liu, E. A. (2004) In vivo activation of the p53 pathway by small-molecule antagonists of MDM2. *Science*. **303**, 844–8
6. Vassilev, L. T. (2004) Small-molecule antagonists of p53-MDM2 binding: research tools and potential therapeutics. *Cell Cycle*. **3**, 419–21
7. Nusse, R., and Varmus, H. E. (1982) Many tumors induced by the mouse mammary tumor virus contain a provirus integrated in the same region of the host genome. *Cell*. **31**, 99–109
8. Rijsewijk, F., Schuermann, M., Wagenaar, E., Parren, P., Weigel, D., and Nusse, R. (1987) The Drosophila homolog of the mouse mammary oncogene int-1 is identical to the segment polarity gene wingless. *Cell*. **50**, 649–57
9. Nusse, R., Brown, A., Papkoff, J., Scambler, P., Shackleford, G., McMahon, A., Moon, R., and Varmus, H. (1991) A new nomenclature for int-1 and related genes: the Wnt gene family. *Cell*. **64**, 231
10. Nusse, R. (2008) Wnt signaling and stem cell control. *Cell Res.* **18**, 523–527
11. Janda, C. Y., Waghray, D., Levin, A. M., Thomas, C., and Garcia, K. C. (2012) Structural basis of Wnt recognition by Frizzled. *Science*. **337**, 59–64
12. Schulte, G. (2015) Frizzleds and WNT/β-catenin signaling – The black box of ligand–receptor selectivity, complex stoichiometry and activation kinetics. *Eur. J. Pharmacol.* **763**, 191–195
13. Lu, B., Green, B., Farr, J., Lopes, F., and Van Raay, T. (2016) Wnt Drug Discovery: Weaving Through the Screens, Patents and Clinical Trials. *Cancers (Basel).* **8**, 82
14. Kumar, S., Žigman, M., Patel, T. R., Trageser, B., Gross, J. C., Rahm, K., Boutros, M., Gradl, D., Steinbeisser, H., Holstein, T., Stetefeld, J., and Özbek, S. (2014) Molecular dissection of Wnt3a-Frizzled8 interaction reveals essential and modulatory determinants of Wnt signaling activity. *BMC Biol.* **12**, 44
15. Takada, R., Satomi, Y., Kurata, T., Ueno, N., Norioka, S., Kondoh, H., Takao, T., and Takada, S. (2006) Monounsaturated fatty acid modification of Wnt protein: its role in Wnt secretion. *Dev. Cell*. **11**, 791–801
16. Bazan, J. F., Janda, C. Y., and Garcia, K. C. (2012) Structural architecture and functional evolution of Wnts. *Dev. Cell*. **23**, 227–32
17. Bruhn, H. (2005) A short guided tour through functional and structural features of saposin-like proteins. *Biochem. J.* **389**, 249–57

CHAPTER 1

Nutlin-3a nanodisks induce p53 stabilization and apoptosis in a subset of cultured glioblastoma cells

1.1. Abstract

Nanodisks (ND) are ternary complexes of phospholipid, one or more hydrophobic bioactive agents and an apolipoprotein scaffold. These nanoscale assemblies are organized as a disk-shaped lipid bilayer whose perimeter is stabilized by an apolipoprotein scaffold. Solubilization of hydrophobic bioactive agents is achieved by their integration into the ND lipid milieu. When the *cis*-imidazoline, nutlin-3a, was incubated with phosphatidylcholine and apolipoprotein A-I, it was conferred with aqueous solubility as judged by spectroscopic analysis. Nondenaturing polyacrylamide gel electrophoresis yielded evidence of a homogeneous population of ND particles ~9 nm in diameter. Gel filtration chromatography experiments revealed the association of nutlin-3a with ND is reversible. Biological activity of nutlin-3a ND was examined in three distinct glioblastoma cell lines, U87MG, SF763 and SF767. Incubation of U87MG cells with nutlin-3a ND induced concentration-dependent cell growth arrest and apoptosis. SF763 cells demonstrated modest cell growth arrest only at high concentrations of nutlin-3a ND and no apoptosis. SF767 cells were unaffected by nutlin-3a ND. Immunoblot analysis revealed nutlin-3a ND induced time-dependent stabilization of the master tumor suppressor, p53, and up regulation of the E3 ubiquitin ligase, murine double minute 2 in U87MG cells, but not the other glioma cell lines. The nanoscale size of the formulation particles, their facile assembly and nutlin-3a solubilization capability suggest ND represent a potentially useful vehicle for *in vivo* administration of this anti-tumor agent.

Keywords: nutlin-3a, nanodisk, apoptosis, glioblastoma, p53, MDM2.

1.2. Introduction

Healthy cells maintain low levels of the tumor suppressor protein, p53 through the action of the E3 ubiquitin ligase, murine double minute 2 (MDM2). Continuous ubiquitinylation of newly expressed p53 by MDM2 targets it for degradation by the 26S proteasome (1). At the same time, other regulatory proteins, including $p14^{ARF}$ and nucleophosmin (NPM) are sequestered in the nucleolus as part of larger protein complexes. In response to cellular stress (e.g. oncogene activation, genotoxic drugs or disruption of rRNA synthesis by chemotherapeutic drugs), $p14^{ARF}$ and/or NPM redistribute to the nucleoplasm where they function as inhibitors of MDM2 ubiquitin ligase activity (2–5). As a result, p53 levels rise, promoting transactivation of genes involved in cell cycle arrest and DNA damage repair (6). An important gene target of p53 is MDM2 itself, creating an auto-regulatory feedback loop that limits the duration of the stress response (7–9). If the damage is irreparable, p53 stabilization leads to activation of an apoptotic response (10). Given its central role in the regulation of cell fate, many cancers are caused by mutations in the p53 pathway (8, 11).

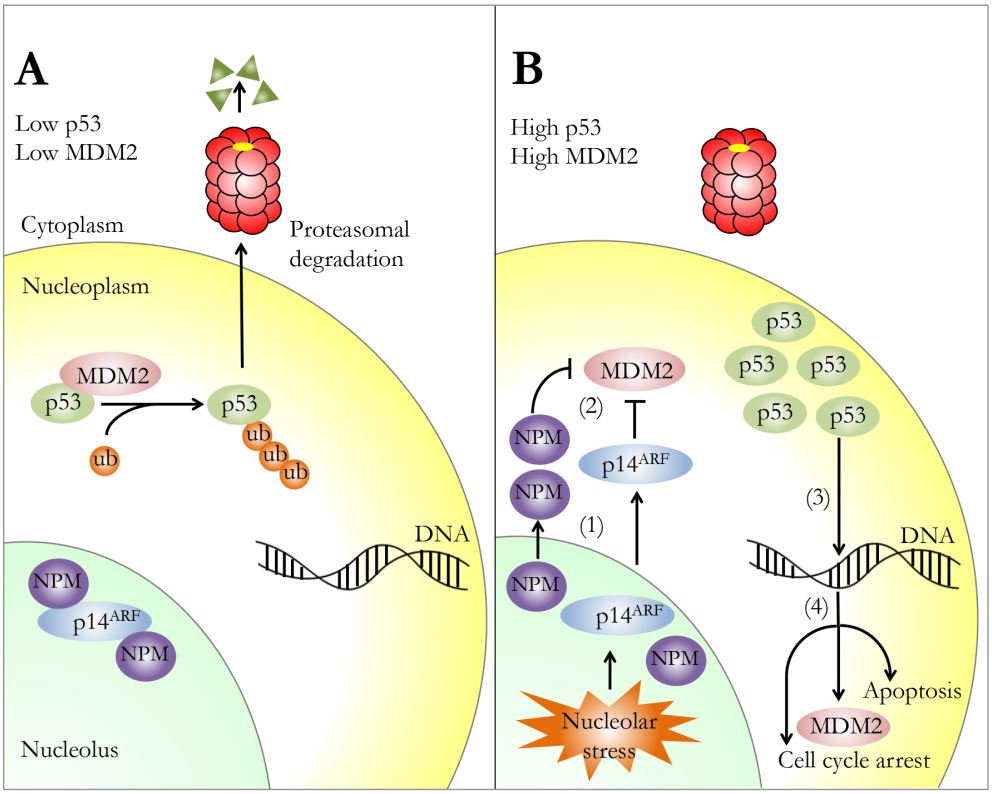

Figure 1-1. The response of p53, MDM2, $p14^{ARF}$ and NPM to nucleolar stress. In healthy cells (panel A), p53 is targeted for proteasomal degradation by MDM2, and $p14^{ARF}$ binds NPM in the nucleolus. In response to nucleolar stress (panel B), $p14^{ARF}$ and/or NPM migrate from the nucleolus to the nucleoplasm (1) and binds MDM2, inhibiting its E3 ubiquitin ligase activity (2). As a result, levels of p53 rise, promoting its function as a transcriptional activator (3) of genes of cell cycle arrest, MDM2 expression and apoptosis (4).

Astrocytic gliomas are one of the most common intracranial malignant tumors, with four classification grades (I - IV). The most severe form (Grade IV), referred to as glioblastoma multiforme (GBM), is one of the most aggressive and least effectively treated solid tumors in humans (12). Close to 78% of GBMs have a disrupted p53 pathway, including deletion of $p14^{ARF}$, overexpression of MDM2 or mislocalization of p53 to the cytoplasm (13). The current standard of care for newly diagnosed patients with GBM involves surgical resection, with concurrent radiotherapy and administration of the cytotoxic alkylating agent, temozolomide (14, 15). Despite this aggressive and invasive treatment strategy, nearly all GBMs recur within 15 months, resulting in high rates of morbidity and mortality (16).

In 2004, a family of chemically related *cis*-imidazoline based compounds, termed nutlins, were shown to inhibit MDM2 activity (17). X-ray crystallography of a nutlin-2-MDM2 complex revealed it binds to a tryptophan-rich pocket in MDM2 previously identified as a p53 binding site (18). Thus, it is postulated that nutlins compete with, or displace, p53 from MDM2 (19). It may be anticipated that pharmacological inhibition of MDM2's ubiquitin ligase activity by nutlin represents a plausible therapeutic approach in tumors that possess a wild type (WT) p53 pathway (20–22). However, a general problem with nutlins relates to their intrinsic hydrophobicity. Poor water solubility poses practical problems with respect to mode of administration, bioavailability, toxicity and transit across the blood brain barrier (23).

One approach to overcoming these obstacles is to solubilize nutlin in a delivery vehicle. Toward this end, nanoscale disk-like miniature membranes, termed nanodisks (ND), have been documented to solubilize various hydrophobic bioactive agents including amphotericin B (24), all *trans* retinoic acid (25) and curcumin (26). ND self assembly occurs upon incubation of specific phospholipids with members of the class of exchangeable apolipoproteins (27, 28). Based on its structural properties, solubility profile and potent biological activity, nutlin-3a has been identified as a candidate for integration into ND. In the current study, nutlin-3a ND were formulated and shown to elicit variable effects on cultured GBM cells, depending on their p53 pathway status.

1.3. Material and Methods

Reagents

Nutlin-3a (the most active member of this inhibitor class) was obtained from Cayman Chemical (Ann Arbor, MI) and dissolved in dimethylformamide (DMF). Dimyristoylphosphatidylcholine (DMPC) was obtained from Avanti Polar Lipids Inc. (Alabaster, AL). Bicinchoninic acid (BCA), bovine serum albumin (BSA) and GelCode Blue stain reagent were purchased from Thermo Fisher Scientific. Mouse anti-p53 (clone DO-1) and mouse anti-MDM2 were from Sigma Aldrich. Anti-GAPDH was from EMD Millipore (San Diego, CA). Horseradish Peroxidase (HRP) conjugated goat anti-mouse IgG secondary antibody was from Vector laboratories (Burlingame, CA). WesternBright ECL HRP substrate was from Advansta (Menlo Park, CA). Halt Protease Inhibitor cocktail was from Thermo Scientific (Rockford, IL). Rabbit anti-$p14^{ARF}$ was purchased from Novus Biologicals (Littleton, CO). Mouse anti-NPM was purchased from Abcam (Cambridge, United Kingdom). FITC conjugated goat polyclonal anti-rabbit IgG secondary antibody (probe for $p14^{ARF}$) was purchased from Abcam (Cambridge, United Kingdom) and Texas Red conjugated goat monoclonal anti-mouse IgG secondary antibody (probe for NPM) was purchased from Santa Cruz Biotechnology (Dallas, TX). Recombinant WT human apolipoprotein (apo) A-I and tryptophan (W)-null variant apoA-I (the four W residues in apoA-I were replaced by phenylalanine) were expressed in *E. coli* and isolated as described previously (29). The GBM cell lines, SF763 and SF767, were kindly provided by Dr. Eleanor Blakely (Lawrence Berkeley National Laboratory). U87MG cells were purchased from the UC Berkeley Cell Culture Facility. Cells were maintained in high glucose DMEM (Thermo Scientific Hyclone, South Logan, UT) supplemented with 10% fetal bovine serum, 100 U/ml penicillin and 100 µg/ml streptomycin. Cells were cultured at 37°C in a humidified atmosphere of 5% CO_2 and 95% air. CellTiter 96 Non-Radioactive Cell Proliferation (MTT) assay kit was purchased from Promega (Madison, WI). FITC - Annexin V Apoptosis kit was purchased from Invitrogen (Carlsbad, CA).

Nutlin-3a ND formulation

Five mg DMPC was dissolved in chloroform / methanol (3:1 v/v) and dried under a stream of N_2 gas, forming a thin film on the vessel wall. Residual organic solvent was removed under vacuum. The prepared lipid was dispersed in 0.5 ml phosphate buffered saline (PBS; 20 mM sodium phosphate, 150 mM sodium chloride, pH 7.4) and 400 µg nutlin-3a (from a 20 mg/ml stock solution) added. Following this, 2 mg apoA-I (from a 4 mg/ml stock solution in PBS) was added and the sample (1 ml final volume) was bath sonicated between 22°C and 25°C for approximately 45 min. The sonication step induced the turbid sample to clarify, indicating that the complexes of apolipoprotein and phospholipid (i.e. ND) had formed. The sample was centrifuged at 10,000 rpm for 10 min to remove unincorporated material and filter sterilized (0.22 µm). Control ND (termed empty ND) was prepared in a similar manner except nutlin-3a was omitted from the reaction mix.

UV/Vis absorbance spectroscopy

Absorbance spectroscopy was performed on a Perkin-Elmer Lambda 20 spectrophotometer. Samples were scanned from 260 - 350 nm.

Non-denaturing polyacrylamide gel electrophoresis (PAGE)

Samples (~6 µg protein) were electrophoresed on 4-20% acrylamide slab gels at a constant 150V for 2 h at 22°C and stained with GelCode Blue.

Gel filtration

A sterile filtered sample (200 µl) of nutlin-3a ND was applied to a Zorbax GF-250 column equilibrated in PBS containing additionally 0.15M NaCl. Chromatography was performed on a Perkin-Elmer Series 200 System at a flow rate of 1 ml/min. Fractions (0.5 ml) were collected over a period of 30 min. For comparison, a sample containing empty ND was applied to the column.

Cell viability assay

Cells were plated in 96-well culture plates at 10,000 cells per well and allowed to attach overnight. Subsequently, the cells were replenished with fresh medium supplemented with specified concentrations of nutlin-3a ND or a corresponding amount of empty ND. The range of nutlin-3a concentrations tested (20 µM to 100 µM nutlin-3a) was limited by the amount of nutlin-3a that could be solubilized in ND. Furthermore, in preliminary experiments on nutlin-3a ND stability, it was determined that storage of nutlin-3a ND for two weeks at 4°C resulted in decreased biological activity toward U87MG cells. To avoid this, all experiments reported were performed using freshly prepared nutlin-3a ND. After 24 h incubation with ND, cell proliferation assays were performed. Briefly, cells were incubated with MTT (3-[4,5-dimethylthiazol-2-yl]-2,5-diphenyltetrazolium bromide) for 4 h at 37 °C. Viable cells converted the tetrazolium into purple colored formazan crystals that were solubilized upon incubation for 1 h at 37 °C, prior to absorbance measurement at 570 and 650 nm.

Apoptosis assay

Cells were plated in 12-well culture plates at 0.5 x 10^6 cells per well and allowed to attach overnight. Subsequently, the cells were replenished with fresh medium supplemented with specified concentrations of nutlin-3a ND or a corresponding amount of empty ND. Twenty-four h after treatment, apoptosis was measured by flow cytometry. Briefly, cells were scraped from the plate, washed with ice cold PBS and re-suspended in 106 µl binding buffer containing 0.5% BSA, 5 µl FITC-annexin V and 1 µl propidium iodide and incubated, shielded from light for 30 min at room temperature. Cells were pelleted to remove unbound dye and re-suspended in binding buffer containing 0.5% BSA. Flow cytometry measurements were obtained on BD LSR Fortessa and data analyzed using FlowJo v10 software.

Immunoblot analysis

Cells were plated in 12-well culture plates at $0.5x10^6$ cells per well and allowed to attach overnight. Cells were then incubated with fresh medium supplemented with 50 μM nutlin-3a ND, a corresponding amount of empty ND or PBS. At indicated time points, cells were lysed with RIPA buffer (50 mM Tris, 150 mM NaCl, 0.1% SDS, 0.5% sodium deoxycholate, 1% Triton X-100 and 1 x Halt Protease Inhibitor cocktail). Protein concentrations were determined and 10 μg protein from each lysate were separated on a 4% to 20% acrylamide SDS gel, transferred to a PVDF membrane and blocked with 5% (w/v) non-fat milk. Target proteins were visualized using the ECL detection system after incubation with anti-p53 (1:1000), anti-MDM2 (1:200) or anti-GAPDH (1:2000) antibodies. Goat anti-mouse HRP-conjugated secondary antibody was used at (1:5000) dilution.

Confocal fluorescence microscopy

U87MG and SF767 cells were plated in 12-well culture plates with coverslips at $0.5x10^6$ cells per well and allowed to attach overnight. Cells were incubated with 50 μM nutlin-3a (as ND) for 4 h at 37°C. Coverslips were washed, the cells were fixed with 4% paraformaldehyde for 15 min on ice and washed with PBS containing 1% BSA. Cells were permeabilized with 0.1% Triton X-100 in PBS for 10 min at room temperature followed by 3 washes with PBS containing 1% BSA. Fixed cells were incubated with anti-NPM (1:100) and anti-$p14^{ARF}$ (1:100) for 2 h at room temperature, then washed and incubated again with Texas Red conjugated goat anti-mouse IgG (1:200) for NPM detection and FITC conjugated goat anti-rabbit IgG (1:200) for $p14^{ARF}$ detection. Finally, cells were stained with Hoeschst 33342 (1:2000) in PBS for 10 min at room temperature and washed before mounting with Vectashield. Coverslips on slides were allowed to dry overnight before image acquisition on a Zeiss LSM710 confocal microscope.

Statistical analysis

Statistical significance between groups was calculated using the two-tailed Student's t-test. Data are presented as mean ± standard error (SE) of three independent experiments performed in triplicate, with p-values < 0.05 considered significant.

1.4. Results

Nutlin-3a ND formulation

Nutlin-3a is poorly soluble in aqueous media yet fully miscible in organic solvents. In preliminary experiments, nutlin-3a in DMSO was observed to absorb light in the range of 260 – 320 nm, a property that was used to monitor solubilization of nutlin-3a in ND. When nutlin-3a was incubated with DMPC and recombinant WT apoA-I, although the solution appearance indicated nutlin-3a ND had formed, spectral overlap from the four tryptophan (W) residues in apoA-I (absorbance max = 280 nm) interfered with spectroscopic quantitation of nutlin-3a solubilization efficiency. To circumvent this, a W-null-apoA-I variant was generated and employed in lieu of WT apoA-I as ND scaffold. As with experiments using WT apoA-I, the sample transitioned from an opaque, turbid suspension into a clear solution, indicating ND formation. Following centrifugation and sterile filtration (0.22 μm), a UV-visible absorbance spectrum was recorded. In contrast to empty ND (no nutlin-3a) prepared with W-null-A-I, nutlin-3a ND gave rise to an absorbance spectrum consistent with nutlin-3a solubilization (**Figure 1-2A**). The minor absorbance observed in the empty ND sample can be attributed to the 7 tyrosine residues in W-null-apoA-I. After subtracting the absorbance contribution from W-null-apo-A-I, the UV-vis absorbance pattern of nutlin-3a ND was found to superimpose with a spectrum of the same amount of nutlin-3a in organic solvent (**Figure 1-2B**) indicating that, at this concentration, nutlin-3a efficiently incorporates into ND. Nondenaturing gradient PAGE of nutlin-3a ND revealed a population of particles with a diameter ~9 nm, similar to the size of control empty ND (**Figure 1-3**)**.** Upon gel filtration chromatography both nutlin-3a ND and empty ND eluted between 8 and 12 min post-injection. However, nutlin-3a was not detected in the elution fractions containing ND, indicating nutlin-3a association with ND is reversible without destruction of the ND vehicle.

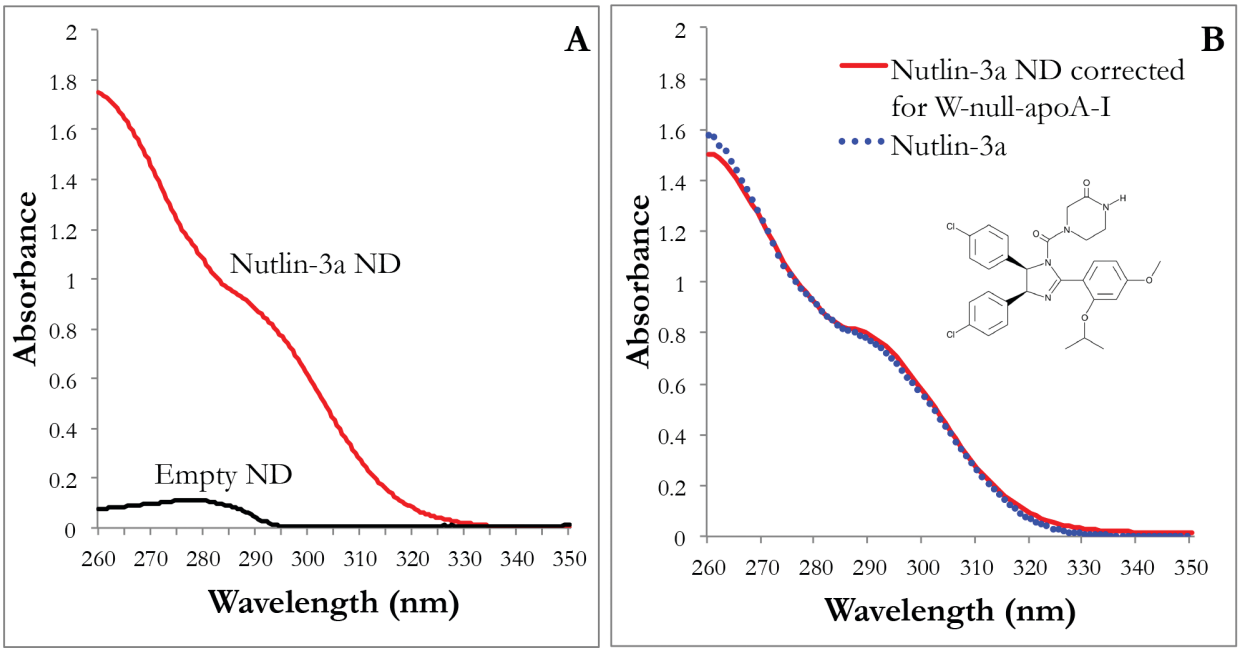

Figure 1-2. UV-Visible absorbance of nutlin-3a ND, empty ND and nutlin-3a. (A) 400 µg nutlin-3a in nutlin-3a ND or equivalent volume of DMF in empty ND (both prepared using W-null apoA-I as ND scaffold protein) in 1 ml final volume of PBS, were scanned. **(B)** Absorbance of 400 µg nutlin-3a (in DMSO) and nutlin-3a ND (in DMSO) (spectrum of empty ND (in DMSO) was subtracted from nutlin-3a ND (in DMSO) to account for absorbance from W-null apoA-I. Spectrum of DMSO was subtracted from spectrum of nutlin-3a).

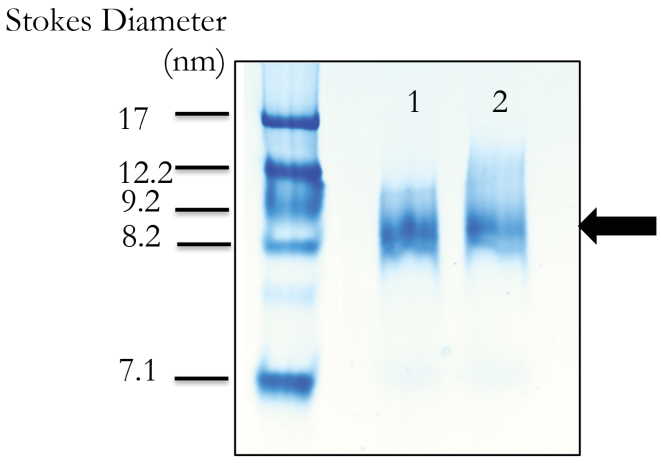

Figure 1-3. Nondenaturing PAGE of ND preparations. A 4-20% nondenaturing PAGE gel was electrophoresed at 150V for 2 h. Lane 1) empty ND; Lane 2) nutlin-3a ND. Stokes diameter was estimated from the migration of known molecular markers run on same gel. Black arrow depicts the band corresponding to ND.

Effect of nutlin-3a ND on cell viability

To assess the biological activity of nutlin-3a ND, three distinct GBM cell lines were examined. U87MG cells possess a WT p53 pathway (30, 31) while SF763 cells harbor a mutant p53 (30, 32) and SF767 cells have a different mutation that results in constitutively elevated MDM2 protein levels (33, 34). Each of these GBM cell lines were incubated with nutlin-3a ND or empty ND for 24 h, followed by MTT assay of cell viability as described in Methods. Of the three cell lines examined, U87MG cells displayed the greatest response to nutlin-3a ND (**Figure 1-4**). SF763 cell viability was modestly affected at the highest concentration of nutlin-3a ND while SF767 cell viability was largely unaffected by incubation with nutlin-3a ND.

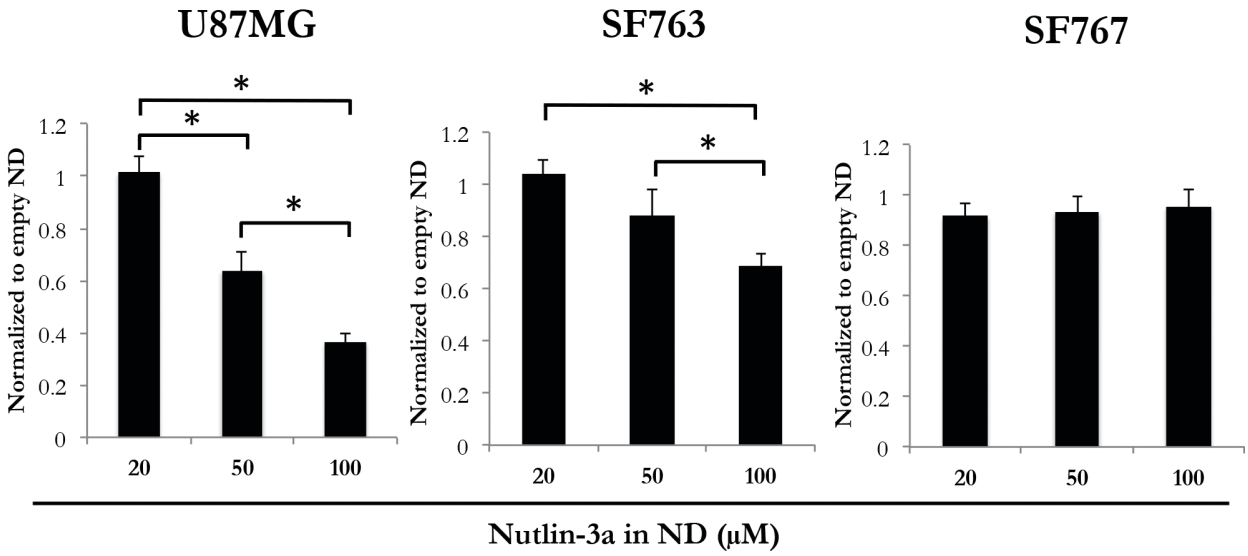

Figure 1-4. The effect of nutlin-3a on the viability of cultured glioma cells. Three GBM cell lines (U87MG, SF763 and SF767) were incubated with nutlin-3a ND or empty ND at indicated concentrations. The cells were processed as described in Materials and Methods and cell viability measured by the MTT assay. Samples treated with nutlin-3a ND were compared to samples treated with a corresponding amount of empty ND. Values reported are the mean ± SE of 3 independent experiments performed in triplicate. * $p<0.05$ as determined by student t-test between different concentrations used.

Nutlin-3a ND induced apoptosis

To evaluate the ability of nutlin-3a ND to induce cell death via apoptosis, U87MG, SF763 and SF767 cells were incubated with increasing concentrations of nutlin-3a (as ND) or a corresponding amount of empty ND for 24 h followed by flow cytometry analysis of apoptosis based on FITC-annexin V binding and propidium iodide fluorescence intensity. Complementing the cell viability results, U87MG cells displayed a pronounced apoptotic response when treated with nutlin-3a ND (**Figure 1-5**) while SF763 and SF767 were unresponsive over this nutlin-3a concentration range.

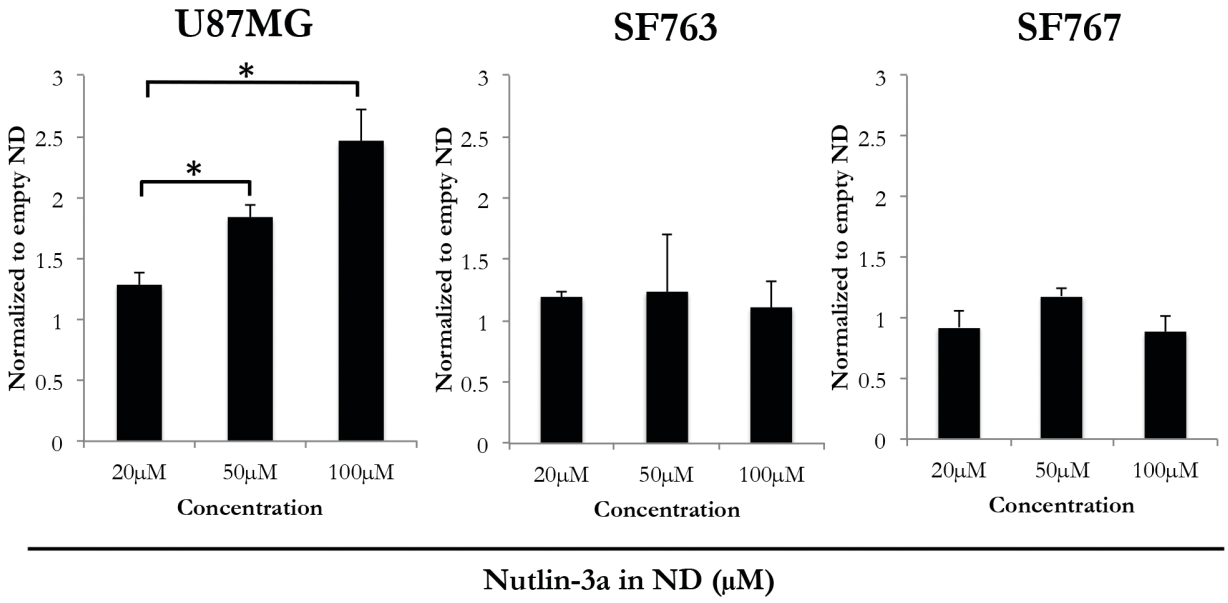

Figure 1-5. Effect of nutlin-3a ND on GBM cell apoptosis. Three GBM cell lines (U87MG, SF763 and SF767) were incubated with nutlin-3a ND or empty ND at the indicated concentrations. After 24 h, the cells were processed as described in Materials and Methods. The cells were incubated with FITC labeled annexin-V and propidium iodide and after washing, subjected to flow cytometry. Cells treated with nutlin-3a ND were compared to cells treated with empty ND. Values reported are the mean ± SE of 3 independent experiments. * $p<0.05$ as determined by student t-test between different concentrations.

Effect of nutlin-3a on p53 and MDM2 levels

To further investigate the effects of nutlin-3a on cell viability and apoptosis, immunoblot analysis of p53 and MDM2 was performed. Each of the three GBM cell lines were incubated with 50 μM nutlin-3a (as ND), empty ND or buffer and harvested after 2, 4 and 8 h. Following cell lysis, 10 μg cell protein was separated by SDS-PAGE, immunoblotted and probed with antibodies against p53, MDM2 and GAPDH. As shown in **Figure 1-6**, compared to incubations with buffer (labeled C) or empty ND (E), U87MG cells treated with nutlin-3a ND (N) showed a time dependent increase in p53 and MDM2 content. In the case of SF763 cells, MDM2 was barely detectable and p53 levels were elevated under all incubation conditions. Conversely, in SF767 cells, MDM2 levels were elevated regardless of the incubation condition and p53 was undetectable.

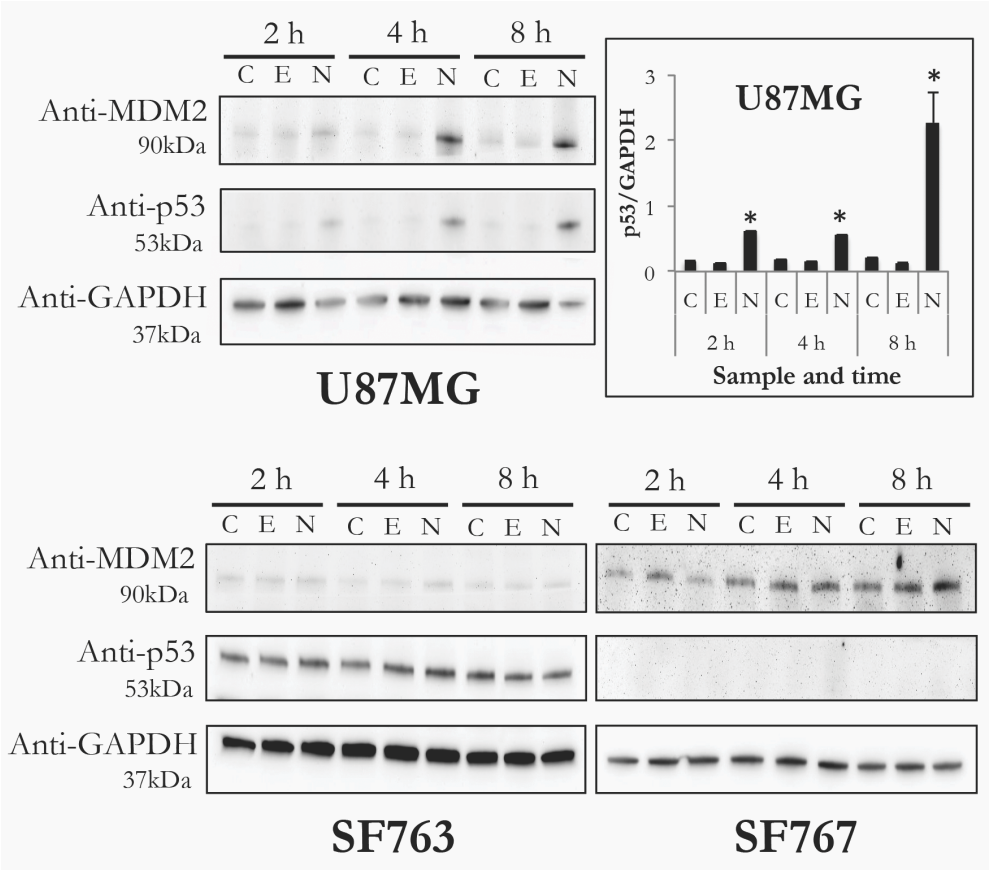

Figure 1-6. Effect of nutlin-3a ND on cellular levels of p53 and MDM2. U87MG, SF763 and SF767 cells were incubated with PBS, empty ND or 50 μM nutlin-3a (as ND) for 2, 4 and 8 h. At indicated time points, cells were harvested, lysed and 10 μg cell protein separated by SDS PAGE, immunoblotted and probed with antibodies directed against MDM2, p53 and GAPDH. Lane assignments: C, PBS treated control; E, empty ND; N, nutlin-3a ND. Bar graph represents densitometric analysis of p53 band intensity in U87MG cells, normalized to internal loading control (i.e. GAPDH). Values reported are the mean ± SE of 3 independent experiments. * $p<0.05$ versus empty ND and PBS treated cells.

Effect of nutlin-3a ND on $p14^{ARF}$ and NPM distribution

To investigate the effect of nutlin-3a ND on the cellular localization of p53 pathway regulatory proteins $p14^{ARF}$ and NPM, U87MG and SF767 cells were incubated with 50 μM nutlin-3a (as ND) for 4 h and analyzed by confocal fluorescence microscopy. In U87MG cells, no $p14^{ARF}$ was detected in control or nutlin-3a ND treated cells (**Figure 1-7A**). Whereas NPM localized to the nucleolus in U87MG cells incubated with PBS, it displayed a more diffuse nuclear distribution pattern in cells treated with nutlin-3a ND (**Figure 1-7B**). In SF767 cells, $p14^{ARF}$ and NPM remained localized in the nucleolus in the absence and presence of nutlin-3a ND.

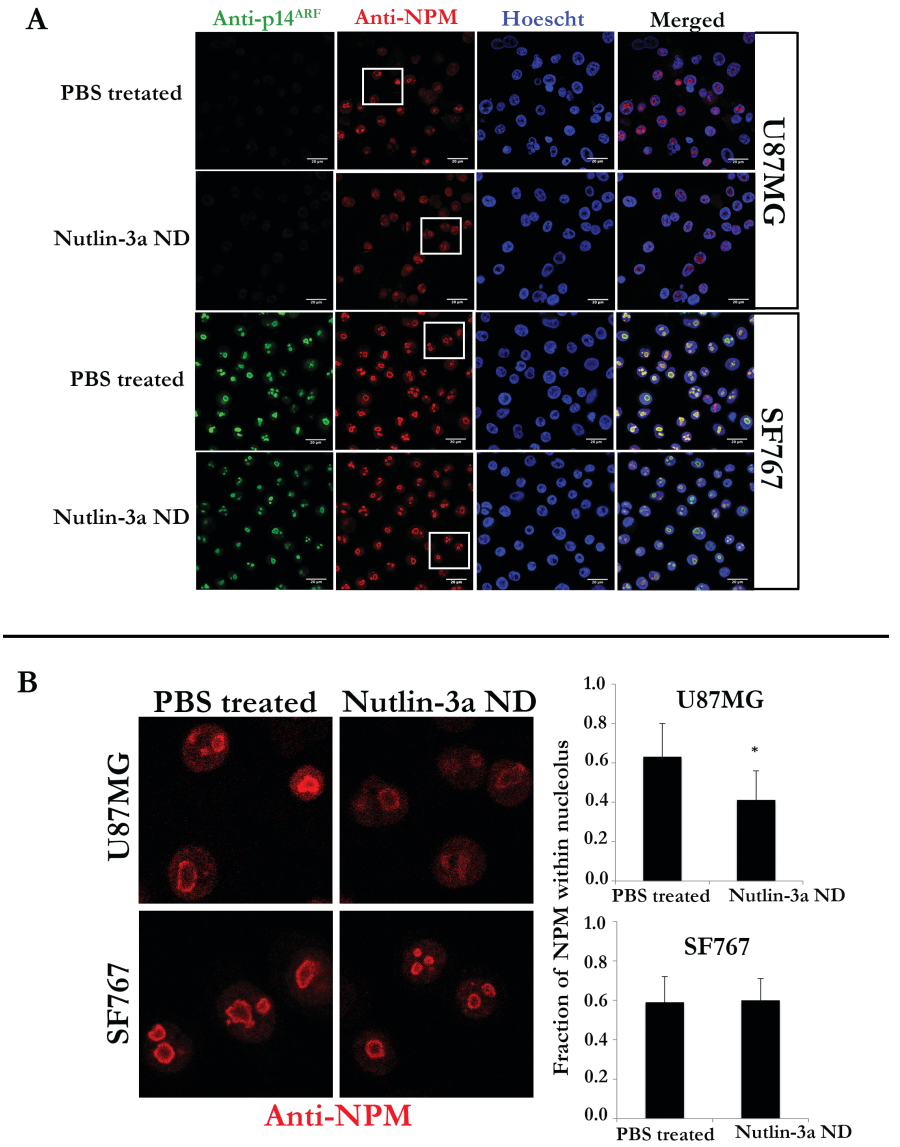

Figure 1-7. Effect of nutlin-3a ND on the sub nuclear localization of p14^{ARF} and NPM. Panel A) U87MG and SF767 cells grown on cover slips were incubated with PBS or 50 μM nutlin-3a (as ND) for 4 h at 37^{o}C. Anti-p14^{ARF} and anti-NPM was added to the fixed cells and secondary antibodies tagged with FITC (p14^{ARF}) or Texas Red (NPM) was used for detection. Cell nuclei were stained with Hoescht. Scale bar 20 μm. **Panel B)** Higher magnification images of cells bordered by white boxes in the anti-NPM region of panel A. Bar graph represents densitometric analysis of immunofluorescence intensity processed in grayscale mode using ImageJ software. Values reported are mean ± SE of 15 or more cells in each group examined for NPM localization. * $p < 0.05$ versus PBS treated. Background readings were corrected using the formula: Corrected Total Cell Fluorescence (CTCF) = Total Fluorescence – (Area of selected cell x Mean fluorescence of background readings). Fraction of NPM within nucleolus = (CTCF nucleolus)/(CTCF nucleus). Integrated density values were used for calculations.

1.5. Discussion

Nutlins have been used to treat different types of cancer, usually in combination with chemotherapeutic drugs, anti-mitotic agents and radiation (35–39). However, little progress has been made in terms of their use to treat glioblastomas. One reason for this is poor solubility of nutlin-3a in aqueous media, a property that poses a challenge for administration and likely affects bioavailability. In an effort to confer water solubility, nutlin-3a was incorporated into ND, particles previously shown to function as a transport vehicle for hydrophobic bioactive compounds (27). Nutlin-3a was originally identified based on its ability to induce apoptosis and cell cycle arrest by activating upstream regulators of the tumor suppressor protein, p53 (17). Thus, in cells possessing a WT p53 pathway, nutlin-3a administration induces cell cycle arrest and/or apoptosis. To examine the effect of nutlin-3a ND, three GBM cell lines were studied. Among these grade IV gliomas, U87MG cells possess a functional p53 / MDM2 pathway while the other two cell lines harbor mutations that result in constitutively elevated p53 (SF763 cells) or MDM2 (SF767 cells) protein levels (30, 31, 33). Upon incubation with nutlin-3a ND, U87MG cells were most responsive in terms of compromised cell viability and increased number of apoptotic cells. At the same time, SF763 cells showed reduced cell viability only at high doses of nutlin-3a ND and SF767 cells were unaffected. In cells with a mutant p53 protein (i.e. SF763), p53 levels were elevated to begin with and nutlin-3a ND did not induce any change in p53 content. SF767 cells failed to show a biological effect despite reports that it possesses a functional p53 (34). It is conceivable, however, that the constitutively high MDM2 protein levels in this cell line could not be overcome by the nutlin-3a concentrations examined such that residual E3 ubiquitin ligase activity of MDM2 promoted continued degradation of p53.

Although U87MG cells are deficient in $p14^{ARF}$ (40), they responded to nutlin-3a ND by increasing p53 protein levels. The observation that nutlin-3a ND induced NPM redistribution from nucleolus to nucleoplasm suggests that either nutlin-3a is capable of directly activating a cellular stress response or NPM redistribution is a consequence, rather than a cause, of the cellular stress response induced by nutlin-3a ND. Considering the response of the 3 GBM cell lines to nutlin-3a ND, the data indicate that detailed knowledge of a patients' p53 pathway status is key to determining whether nutlin-3a treatment may be of therapeutic benefit.

At present, surgical resection followed by radiation and chemotherapy is the standard of care for GBM. Many drug delivery systems have been investigated including targeted delivery via overexpressed receptors not present (or present at low levels) in normal tissue, convection enhanced delivery and intra-arterial delivery with blood brain barrier disruption (41). Despite advances in treatment options, median patient survival remains an abysmal 8 – 22 months, most likely due to the highly infiltrative nature of these tumors (42). In order to eliminate remnant tumor cells, it is conceivable that, following surgical resection, insertion of a biologically inert implant containing nutlin-3a ND into the surgical cavity may be effective (43). Release / diffusion of nutlin-3a ND from the implant over time is anticipated to promote apoptosis of remnant tumor cells, thereby improving patient survival. Taken together, the findings reported herein support further evaluation of nutlin-3a ND as a therapy option for GBMs that possess an intact p53 pathway.

1.6. References

1. Michael, D., and Oren, M. (2003) The p53–Mdm2 module and the ubiquitin system. *Semin. Cancer Biol.* **13**, 49–58
2. Brodská, B., Holoubek, A., Otevřelová, P., and Kuželová, K. (2016) Low-Dose Actinomycin-D Induces Redistribution of Wild-Type and Mutated Nucleophosmin Followed by Cell Death in Leukemic Cells. *J. Cell. Biochem.* **117**, 1319–1329
3. Di Matteo, A., Franceschini, M., Chiarella, S., Rocchio, S., Travaglini-Allocatelli, C., and Federici, L. (2016) Molecules that target nucleophosmin for cancer treatment: an update. *Oncotarget*. **7**, 44821–44840
4. Sherr, C. J. (2006) Divorcing ARF and p53: an unsettled case. *Nat. Rev. Cancer*. **6**, 663–73
5. Suzuki, A., Kogo, R., Kawahara, K., Sasaki, M., Nishio, M., Maehama, T., Sasaki, T., Mimori, K., and Mori, M. (2012) A new PICTure of nucleolar stress. *Cancer Sci.* **103**, 632–637
6. Lane, D. P. (1992) Cancer. p53, guardian of the genome. *Nature*. **358**, 15–6
7. Barone, G., Tweddle, D. A., Shohet, J. M., Chesler, L., Moreno, L., Pearson, A. D. J., and Van Maerken, T. (2014) MDM2-p53 interaction in paediatric solid tumours: preclinical rationale, biomarkers and resistance. *Curr. Drug Targets*. **15**, 114–23
8. Wasylishen, A. R., and Lozano, G. (2016) Attenuating the p53 Pathway in Human Cancers: Many Means to the Same End. *Cold Spring Harb. Perspect. Med.* 10.1101/cshperspect.a026211
9. Zhao, Y., Yu, H., and Hu, W. (2014) The regulation of MDM2 oncogene and its impact on human cancers. *Acta Biochim. Biophys. Sin. (Shanghai).* **46**, 180–9
10. Roos, W. P., and Kaina, B. (2006) DNA damage-induced cell death by apoptosis. *Trends Mol. Med.* **12**, 440–450
11. Vijayakumaran, R., Tan, K. H., Miranda, P. J., Haupt, S., and Haupt, Y. (2015) Regulation of Mutant p53 Protein Expression. *Front. Oncol.* **5**, 284
12. Rao, J. S. (2003) Molecular mechanisms of glioma invasiveness: the role of proteases. *Nat. Rev. Cancer*. **3**, 489–501
13. Cancer Genome Atlas Research Network, T. C. G. A. (TCGA) R. (2008) Comprehensive genomic characterization defines human glioblastoma genes and core pathways. *Nature*. **455**, 1061–8
14. Hau, E., Shen, H., Clark, C., Graham, P. H., Koh, E.-S., and L McDonald, K. (2016) The evolving roles and controversies of radiotherapy in the treatment of glioblastoma. *J. Med. Radiat. Sci.* **63**, 114–23
15. Fritz, L., Dirven, L., Reijneveld, J., Koekkoek, J., Stiggelbout, A., Pasman, H., and Taphoorn, M. (2016) Advance Care Planning in Glioblastoma Patients. *Cancers (Basel).* **8**, 102
16. Ramakrishna, R., and Pisapia, D. (2015) Recent Molecular Advances in Our Understanding of Glioma. *Cureus*. 10.7759/cureus.287
17. Vassilev, L. T., Vu, B. T., Graves, B., Carvajal, D., Podlaski, F., Filipovic, Z., Kong, N., Kammlott, U., Lukacs, C., Klein, C., Fotouhi, N., and Liu, E. A. (2004) In vivo activation of the p53 pathway by small-molecule antagonists of MDM2. *Science*. **303**, 844–8
18. Kussie, P. H., Gorina, S., Marechal, V., Elenbaas, B., Moreau, J., Levine, A. J.,

and Pavletich, N. P. (1996) Structure of the MDM2 oncoprotein bound to the p53 tumor suppressor transactivation domain. *Science*. **274**, 948–53
19. Laurie, N. A., Donovan, S. L., Shih, C.-S., Zhang, J., Mills, N., Fuller, C., Teunisse, A., Lam, S., Ramos, Y., Mohan, A., Johnson, D., Wilson, M., Rodriguez-Galindo, C., Quarto, M., Francoz, S., Mendrysa, S. M., Guy, R. K., Marine, J.-C., Jochemsen, A. G., and Dyer, M. A. (2006) Inactivation of the p53 pathway in retinoblastoma. *Nature*. **444**, 61–6
20. Khoo, K. H., Hoe, K. K., Verma, C. S., and Lane, D. P. (2014) Drugging the p53 pathway: understanding the route to clinical efficacy. *Nat. Rev. Drug Discov.* **13**, 217–36
21. Villalonga-Planells, R., Coll-Mulet, L., Martínez-Soler, F., Castaño, E., Acebes, J.-J., Giménez-Bonafé, P., Gil, J., and Tortosa, A. (2011) Activation of p53 by nutlin-3a induces apoptosis and cellular senescence in human glioblastoma multiforme. *PLoS One*. **6**, e18588
22. England, B., Huang, T., and Karsy, M. (2013) Current understanding of the role and targeting of tumor suppressor p53 in glioblastoma multiforme. *Tumour Biol.* **34**, 2063–74
23. Burgess, A., Chia, K. M., Haupt, S., Thomas, D., Haupt, Y., and Lim, E. (2016) Clinical Overview of MDM2/X-Targeted Therapies. *Front. Oncol.* **6**, 7
24. Oda, M. N., Hargreaves, P. L., Beckstead, J. A., Redmond, K. A., van Antwerpen, R., and Ryan, R. O. (2006) Reconstituted high density lipoprotein enriched with the polyene antibiotic amphotericin B. *J. Lipid Res.* **47**, 260–7
25. Redmond, K. A., Nguyen, T.-S., and Ryan, R. O. (2007) All-trans-retinoic acid nanodisks. *Int. J. Pharm.* **339**, 246–50
26. Ghosh, M., Singh, A. T. K., Xu, W., Sulchek, T., Gordon, L. I., and Ryan, R. O. (2011) Curcumin nanodisks: formulation and characterization. *Nanomedicine*. **7**, 162–7
27. Ryan, R. O. (2010) Nanobiotechnology applications of reconstituted high density lipoprotein. *J. Nanobiotechnology*. **8**, 28
28. Simonsen, J. B. (2016) Evaluation of reconstituted high-density lipoprotein (rHDL) as a drug delivery platform – a detailed survey of rHDL particles ranging from biophysical properties to clinical implications. *Nanomedicine Nanotechnology, Biol. Med.* **12**, 2161–2179
29. Ryan, R. O., Forte, T. M., and Oda, M. N. (2003) Optimized bacterial expression of human apolipoprotein A-I. *Protein Expr. Purif.* **27**, 98–103
30. Geoerger, B., Vassal, G., Opolon, P., Dirven, C. M. F., Morizet, J., Laudani, L., Grill, J., Giaccone, G., Vandertop, W. P., Gerritsen, W. R., and van Beusechem, V. W. (2004) Oncolytic activity of p53-expressing conditionally replicative adenovirus AdDelta24-p53 against human malignant glioma. *Cancer Res.* **64**, 5753–9
31. Cerrato, J. A., Yung, W. K., and Liu, T. J. (2001) Introduction of mutant p53 into a wild-type p53-expressing glioma cell line confers sensitivity to Ad-p53-induced apoptosis. *Neuro. Oncol.* **3**, 113–22
32. van Beusechem, V. W., van den Doel, P. B., Grill, J., Pinedo, H. M., and Gerritsen, W. R. (2002) Conditionally replicative adenovirus expressing p53 exhibits enhanced oncolytic potency. *Cancer Res.* **62**, 6165–71

33. Blough, M. D., Zlatescu, M. C., and Cairncross, J. G. (2007) O6-methylguanine-DNA methyltransferase regulation by p53 in astrocytic cells. *Cancer Res.* **67**, 580–4
34. Trentin, G. A., He, Y., Wu, D. C., Tang, D., and Rozakis-Adcock, M. (2004) Identification of a hTid-1 mutation which sensitizes gliomas to apoptosis. 10.1016/j.febslet.2004.11.034
35. Cao, C., Shinohara, E. T., Subhawong, T. K., Geng, L., Kim, K. W., Albert, J. M., Hallahan, D. E., and Lu, B. (2006) Radiosensitization of lung cancer by nutlin, an inhibitor of murine double minute 2. *Mol. Cancer Ther.* **5**, 411–7
36. Coll-Mulet, L., Iglesias-Serret, D., Santidrián, A. F., Cosialls, A. M., de Frias, M., Castaño, E., Campàs, C., Barragán, M., de Sevilla, A. F., Domingo, A., Vassilev, L. T., Pons, G., and Gil, J. (2006) MDM2 antagonists activate p53 and synergize with genotoxic drugs in B-cell chronic lymphocytic leukemia cells. *Blood*. **107**, 4109–14
37. Kojima, K., Konopleva, M., McQueen, T., O'Brien, S., Plunkett, W., and Andreeff, M. (2006) Mdm2 inhibitor Nutlin-3a induces p53-mediated apoptosis by transcription-dependent and transcription-independent mechanisms and may overcome Atm-mediated resistance to fludarabine in chronic lymphocytic leukemia. *Blood*. **108**, 993–1000
38. Secchiero, P., Barbarotto, E., Tiribelli, M., Zerbinati, C., di Iasio, M. G., Gonelli, A., Cavazzini, F., Campioni, D., Fanin, R., Cuneo, A., and Zauli, G. (2006) Functional integrity of the p53-mediated apoptotic pathway induced by the nongenotoxic agent nutlin-3 in B-cell chronic lymphocytic leukemia (B-CLL). *Blood*. **107**, 4122–9
39. Carvajal, D., Tovar, C., Yang, H., Vu, B. T., Heimbrook, D. C., and Vassilev, L. T. (2005) Activation of p53 by MDM2 antagonists can protect proliferating cells from mitotic inhibitors. *Cancer Res.* **65**, 1918–24
40. Ishii, N., Maier, D., Merlo, A., Tada, M., Sawamura, Y., Diserens, A.-C., and Van Meir, E. G. (1999) Frequent Co-Alterations of TP53, p16/CDKN2A, p14ARF , PTEN Tumor Suppressor Genes in Human Glioma Cell Lines. *Brain Pathol.* **9**, 469–479
41. Laquintana, V., Trapani, A., Denora, N., Wang, F., Gallo, J. M., and Trapani, G. (2009) New strategies to deliver anticancer drugs to brain tumors. *Expert Opin. Drug Deliv.* **6**, 1017–32
42. Young, R. M., Jamshidi, A., Davis, G., and Sherman, J. H. (2015) Current trends in the surgical management and treatment of adult glioblastoma. *Ann. Transl. Med.* **3**, 121
43. Bastiancich, C., Danhier, P., Préat, V., and Danhier, F. (2016) Anticancer drug-loaded hydrogels as drug delivery systems for the local treatment of glioblastoma. *J. Control. Release*. **243**, 29–42

CHAPTER 2

Isolation and characterization of recombinant murine Wnt3a

2.1. Abstract

Wnts are a family of morphogens with diverse biological activity. Challenges in obtaining high yields of biologically active recombinant Wnt and the high propensity of isolated Wnts to self-associate in the absence of detergent have impeded structure function studies. In the current study, stably transfected *Drosophila* S2 cells were used to improve recovery of recombinant murine Wnt3a. S2 cell culture conditioned media was processed by 3-step protocol of dye ligand chromatography, immobilized metal affinity chromatography and gel filtration chromatography. Based on purity, eluted fractions from columns were pooled and purified Wnt3a preparation was obtained. Isolated recombinant murine Wnt3a showed increase in canonical signaling in a concentration dependent manner. Thrombin mediated limited proteolysis of Wnt3a resulted in site-specific cleavage within the N-terminal domain of Wnt3a. To generate a detergent free protein, Wnt3a in CHAPS was eluted in buffer containing methyl-β-cyclodextrin (MβCD). Soluble and biologically active Wnt3a was recovered enabling structure activity studies in the absence of detergent effects.

Keywords: Wnt3a, CHAPS detergent, thrombin proteolysis, chromatography, methyl-β-cyclodextrin, β-catenin

2.2. Introduction

Wnt proteins derive their name from *Drosophila* Wingless gene and the mouse INT-1 gene and are conserved across all metazoans (1). In mammals, the complexity of Wnt signaling arises from the spatiotemporal expression of 19 different Wnts that engage with 10 unique Frizzled receptors and 2 co-receptors, low density lipoprotein receptor related protein 5 or 6 (LRP5/6). In the canonical pathway, Wnt binding to the seven transmembrane spanning Frizzled (Fzd) and single pass transmembrane LRP5/6 receptors induces stabilization of the transcriptional coactivator, β-catenin, by inhibiting a multi protein degradation complex made of adenomatous polyposis coli tumor suppressor protein, axin (the scaffold protein) and glycogen synthase kinase 3. The stabilized β-catenin translocates to the nucleus, interacts with transcriptional regulators of T cell factor/lymphoid enhancer factor family thereby leading to enhanced expression of Wnt responsive genes. In the absence of Wnt, a proteasomal degradation complex rapidly degrades β-catenin (2) **(Figure 2-1)**.

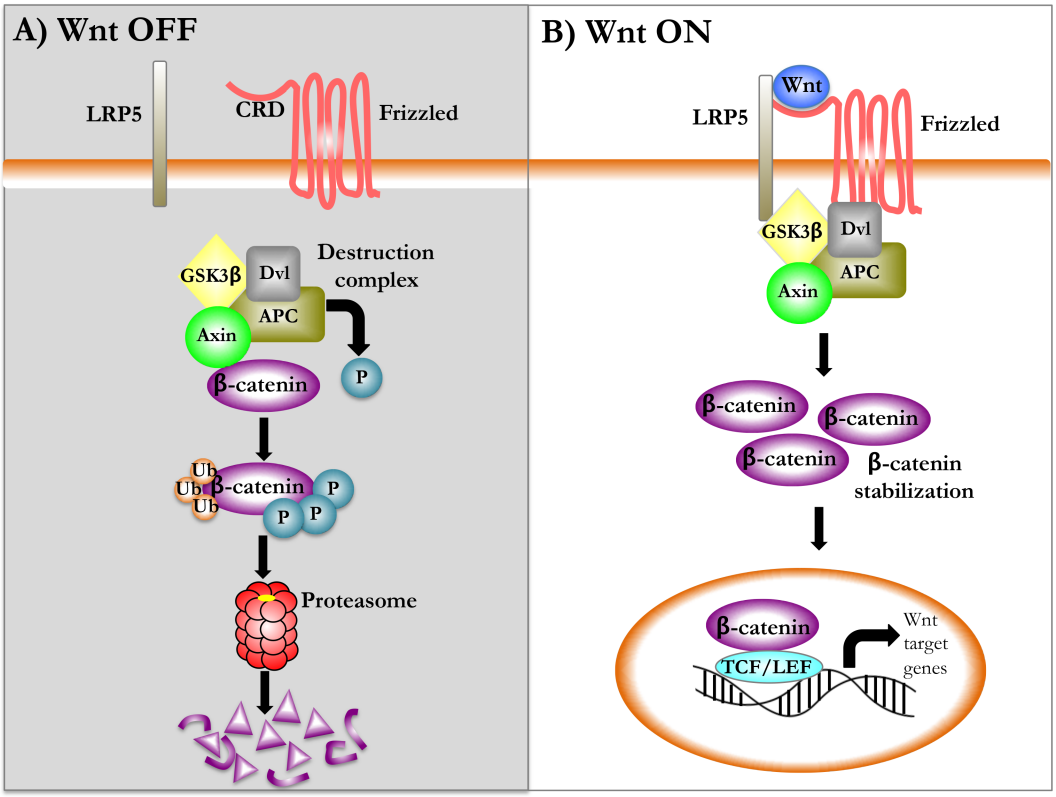

Figure 2-1. Wnt3a canonical signaling. (A) In the absence of Wnt, β-catenin is recruited into the APC/Axin/GSK3/Dishevelled (Dvl) (destruction complex), phosphorylated, ubiquitinated and targeted for proteasome degradation. (B) In the presence of Wnt, LRP5/6 and Frizzled form a ternary complex with Wnt, recruiting the destruction complex to cytoplasmic domain of receptors. As a result, β-catenin is stabilized, increased protein levels of β-catenin translocates to the nucleus, binds to transcription factors TCF/LEF and induces Wnt gene expression.

Secreted Wnt3a is a 334 amino acids long, glycosylated, lipid modified and cysteine enriched protein with a molecular weight of ~40kDa (3). Like other members of the Wnt family, Wnt3a has a unique serine that serves as the site for covalent attachment of a long chain monounsaturated palmitoleic fatty acid chain conferring considerable hydrophobicity to the protein. Mutations in the lipid attachment site of Wnt proteins have revealed that lipid modification is required for proper intracellular processing and biological activity (4). The X-ray crystal structure of *Xenopus* Wnt8 obtained by co-expression with cysteine rich domain (CRD) of Fzd revealed the protection of the fatty acyl moiety from the surrounding aqueous environment by its burial within Fzd-CRD (5). Interestingly almost all recombinant routinely used Wnt preparations include detergent due to its propensity to aggregate in the absence of detergent. Building on a protocol originally developed by (3), an improved procedure is presented here for isolation of recombinant Wnt3a for its use in molecular studies.

2.3. Materials and methods

Cell culture

Drosophila S2 cells stably transfected with murine Wnt3a were obtained from Dr. Roel Nusse and cultured in complete Schneider's media (supplemented with 10% heat inactivated FBS, 100 U/ml penicillin, 50 U/ml streptomycin and 500 mg/L L-glutamine) at 22 °C. After 12-14 days, the cells were used to expand the culture to 3 or 5 liters. Five hundred ml Bellco spinner flasks containing 300 ml complete Schneider's media were seeded with 0.5 – 1.0 x 10^6 cells/ml. The expanded culture was maintained, with stirring, for 14 days. Subsequently, the S2 cell culture was centrifuged in 500 ml bottles at 7,000 rpm for 10 min at 4 °C. The cell pellet was discarded and the conditioned media (CM) collected and stored at 4 °C in 0.02 % sodium azide until further processing. Prior to chromatographic separation of CM components, Tris-HCl was added to 20 mM, the pH was adjusted to 7.45 and the CM stored at 4 °C for an additional 2 to 3 days, during which a mineral precipitate comprised of media components, appeared. Triton X-100 was added to the decanted CM (1%; v/v) and the solution filtered through 0.45 µm membrane.

Dye-ligand Chromatography

Processed CM was applied to a 5 ml bed volume HiTrap Blue HP column (GE Healthcare). The column was protected from residual precipitate by an inline 0.45 µm syringe filter. The sample was applied to the column at ~2 ml/min with a peristaltic pump. The column eluate was collected during loading and SDS-PAGE α-Wnt3a immunoblot analysis performed to monitor Wnt3a binding to the column matrix. After loading up to 5 L processed CM and washing with 40 ml 20 mM Tris HCl, pH 7.45 containing 0.14 M NaCl and 1 % (w/v) CHAPS detergent (buffer A) the column was placed in an AKTA Prime FPLC system (GE Healthcare). All operations up to this point were carried out at 4 °C. The column was washed with 150 ml buffer A at 2.5 ml/min and protein eluted with 1.5 M sodium chloride, 20 mM Tris-HCl, 1% CHAPS, pH 7.45 (buffer B) using the following gradient: 20 ml to 25% B; 5 ml to 35% B; 2.5 ml to 100% B followed by a further 75 ml at 100% B (flow rate = 2.5 ml/min). The collected fractions were pooled based on A_{280} and SDS-PAGE analysis.

Immobilized metal affinity chromatography (IMAC)

Select Wnt3a containing fractions from the dye-ligand chromatography step (see Results) were pooled and applied to a 1 ml Cu^{2+} saturated HiTrap Chelating column at ~1 ml/min with a peristaltic pump. After loading the sample and washing with 5 ml buffer C (20 mM Tris HCl, pH 7.45, 0.5 M NaCl, 1% CHAPS), the column was placed in the AKTA Prime system and proteins eluted with an imidazole gradient using Buffer C and Buffer D (buffer C containing 1 M NaCl and 200 mM imidazole). The gradient was applied as follows: 0 % D to 2 % D (5 ml); 15 ml at 2% D; 2 % D to 16% D (5 ml); 16 %

D to 40% D (5 ml) and 40 % D to 100% D (2 ml) followed by 20 ml at 100% D (flow rate = 1 ml/min). Fractions were pooled based on A_{280} and SDS-PAGE analysis and concentrated to ~2 ml by centrifugal ultrafiltration (Amicon Ultracel 30 K; EMD Milipore, Billerica, MA).

Gel filtration chromatography

Pooled and concentrated Wnt3a-containing fractions obtained following IMAC were applied to an AKTA Prime system equipped with HP Sephacryl S-100 HR, 16 x 60 (GE Healthcare) equilibrated with 20 mM Tris-HCl, 0.3 M sodium chloride, 1% CHAPS, pH 7.45. Proteins were eluted with 70 ml buffer at flow rate 0.5 ml/min (fraction size = 1 ml). Wnt3a containing fractions were combined and concentrated by centrifugal ultrafiltration.

Recombinant Wnt3a analysis

The recovery and purity of Wnt3a following each step of the purification process was assessed on the basis of total protein, protein stain following SDS-PAGE, quantitative immunoblot and cell-based activity assays (see below). α-Wnt3a immunoblot analysis was performed in triplicate and a four point calibration curve constructed using high purity Wnt3a whose concentration was determined by absorbance at 280 nm using a theoretical extinction coefficient = 67,390 M^{-1} cm^{-1}. When necessary, absorbance values at 280 nm were corrected for light scattering using standard methods based on absorbance values at 320 nm and 350 nm (6). SDS-PAGE was performed on 1 mm thick 10% acrylamide slab gels and stained with the Imperial Protein Stain (Pierce, Rockford, IL) or transferred to a PVDF membrane using the Trans-Blot Turbo Transfer System (Bio-Rad Laboratories, Hercules, CA). After blocking the membrane with 5% fat-free milk, α-Wnt3a (ab28472, Abcam, Cambridge, MA; 1:6,000 dilution) was added followed by HRP-conjugated goat anti-rabbit IgG (PI-1000, Vector Labs, Burlingame, CA; 1:10,000 dilution). Horseradish peroxidase-generated light was scanned on a FluorChem Q instrument (Alpha Innotech, San Leandro, CA). Images were quantified using ImageJ software, version 1.47v. Only gray images, containing a limited number of black pixels, were used for quantification. Isolated Wnt3a obtained from the gel filtration column was stable in CHAPS-containing buffer and could be stored without loss of activity at 4° C for a few weeks or, after flash-freezing in liquid nitrogen, at -80 °C for an extended period of time.

β-catenin induction assay

L cells were cultured in high glucose DMEM, 10% FBS, 100 U each penicillin and streptomycin overnight at 37 °C. Cells (0.5 x 10^6 per well, 12-well plate) were incubated with varying concentrations of purified Wnt3a for 3 h at 37 °C and cells harvested using RIPA cell lysis buffer (Santa Cruz Biotechnology, Dallas, TX) with protease inhibitor cocktail mix (Roche). Protein concentration of L cell lysates were measured and 10 µg lysate protein separated on precast 10% polyacrylamide gels (Bio-Rad, Hercules, CA) at 120 V. Separated proteins were transferred to a PVDF membrane and the membrane

blocked as described above. Blots were probed with anti mouse β-catenin (BD Transduction Laboratories, San Jose, CA, 1:2,000 dilution) and anti-GAPDH (Millipore, Billerica, MA, 1:2,500 dilution) and positive bands detected with horseradish peroxidase conjugated anti mouse secondary antibody (Vector Labs, Burlingame, CA, 1:5,000 dilution). Bands detected and analyzed as described above.

Limited proteolysis

Isolated Wnt3a was incubated in the presence and absence of thrombin (Sigma) at a 1:1 ratio for 4 h at 37 °C in 50 mM Tris, pH 7.5, 300 mM NaCl, 2.5 mM $CaCl_2$ and 1% CHAPS. Following incubation, SDS-PAGE was performed on 15% gels that were either stained with Imperial Protein Stain (Pierce, Rockford, IL, USA) or transferred to PVDF membrane for immune-detection or Edman degradation sequence analysis. a-Wnt3a immunoblot analysis was performed as described above and N-terminal sequencing by Edman degradation was performed at the UC Davis Genome Center Molecular Structural Facility.

Detergent removal studies

Removal of CHAPS detergent and replacement with methyl-β-cyclodextrin (MβCD) was performed by binding 10 µg purified Wnt3a (in CHAPS containing buffer) to 0.1 ml Cu^{2+}-charged iminodiacetic acid (IDA) Sepharose beads (Sigma) in a 0.6 ml spin column (Pierce) for 1 h with gentle rotation. The beads were washed three times with 0.6 ml buffer E (40 mM Tris HCl, pH 7.45, 0.5 M NaCl and 30 mM MßCD). Subsequently, the Wnt3a-containing beads were incubated for 0.5 h in 0.25 ml buffer E containing 200 mM imidazole. A brief centrifugation at 100 x g was performed at each step. Two additional experiments were carried out in parallel, one with buffer E containing 1% CHAPS but no MβCD (positive control) and the other with buffer E with no CHAPS and no MβCD (negative control).

2.4. Results

Drosophila S2 cells that were stably transfected with murine Wnt3a were used to enhance the yield of recombinant Wnt3a applying modifications to the original method reported by Willert and group (3).The yields were optimized using 3 chromatographic steps.

Dye ligand chromatography

While a 120ml bed volume Blue Sepharose column was used in the original method, it was determined that a 5ml bed volume Hi Trap Blue Sepharose column bed volume could be used without affecting Wnt3a binding to column. Conditioned media from 5 L processed S2 cells were applied to the column and the flow through was monitored for Wnt3a by immunoblot analysis (**Figure 2-2,** left inset). In comparison to the starting material (CM), eluates from the first and second 2L and final 1L had much less Wnt3a than the starting material. The increased amount of Wnt3a detected in the final liter of CM indicated that the column had reached maximum binding capacity. The column was washed; using 20mM Tris buffered saline containing 1% CHAPS as a non-UV absorbing, low molecular weight micelle detergent alternative to Triton-X-100. A 2-step gradient wash of NaCl from 150mM to 1M (70ml total volume), followed by high salt wash was applied to the column with 2.5ml collection fractions (**Figure 2-2**). The elution profile was monitored for conductivity and the absorbance had a leading edge, main peak and trailing edge. General protein stain of column fractions revealed that Wnt3a was present in fractions across the entire profile. Due to relatively heavier contaminations with other proteins, the main peak (fractions 23-26) was discarded and the fractions on either side of the main peak were combined.

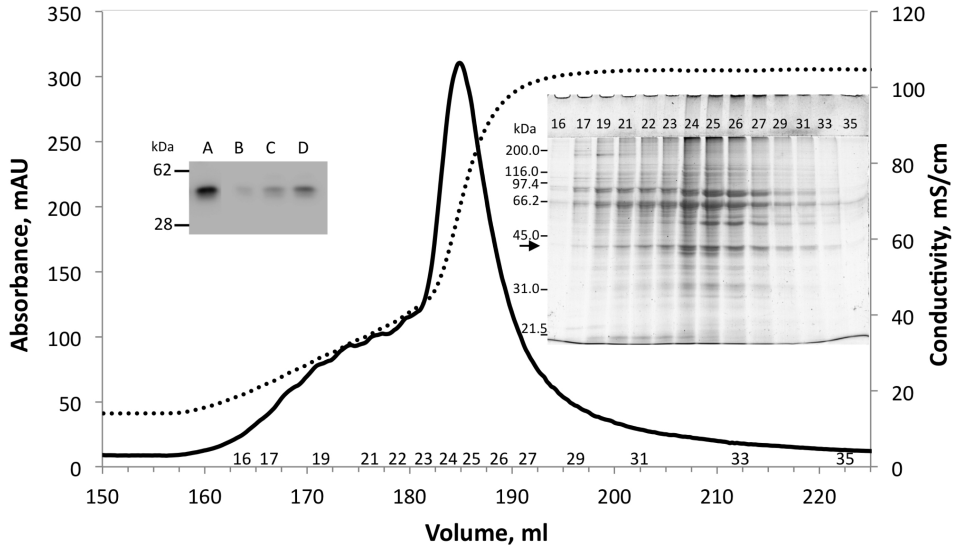

Figure 2-2. Dye-ligand chromatography of S2 cell conditioned media. Five L of processed CM was applied to a 5 ml bed volume HiTrap HP column, unbound proteins were collected and 10 µl aliquots analyzed by α-Wnt3a immunoblot (left inset). Lane A) processed CM; Lane B) first 2 L of column eluate; Lane C) second 2 L of column eluate and D) fifth liter of unbound eluate. Bound proteins were subsequently eluted by application of a NaCl gradient and collection of 2.5 ml fractions. Absorbance at 280 nm (continuous line) and conductivity (dotted line) are shown on the graph. Right inset depicts SDS-PAGE analysis of individual column fractions (indicated by numbers). The arrow depicts the migration position of Wnt3a. Molecular weight markers are shown at left.

Immobilized metal affinity chromatography (IMAC)

The Wnt3a pool from dye ligand chromatography was applied to a 1ml, Cu^{2+} charged, IMAC column. The column was washed and Wnt3a was eluted using a 3-step 5mM to 200mM gradient of imidazole (**Figure 2-3**). The elution profile had a main peak and a trailing edge. Immunoblot analysis indicated Wnt3a was present in all fractions except in the fractions eluted in the region of the sharp peak at 10ml. General protein stain revealed that fractions at the start of trailing edge (Pool 1) had more Wnt3a and contaminating proteins than later eluting fractions (Pool 2). Each pool was concentrated to 2ml by centrifugal ultrafiltration.

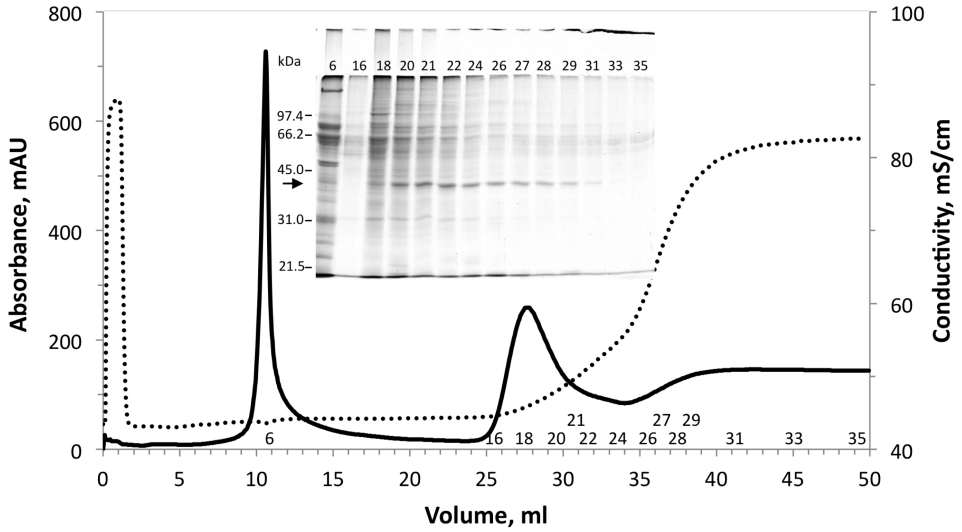

Figure 2-3. IMAC of dye-ligand chromatography pool 1. Select fractions from the dye-ligand column elution profile were pooled and applied directly to a 1 ml IMAC column. After loading, bound proteins were eluted with a three step gradient of NaCl (0.5 M to 1.0 M) and imidazole (5 mM to 200 mM) with collection of 1 ml fractions. Absorbance at 280 nm (continuous line) and conductivity (dotted line) in fractions are shown on the graph. Inset) SDS-PAGE analysis of IMAC column fractions. The band corresponding to Wnt3a is depicted by the arrow at left. Molecular weight markers are shown at left.

Gel filtration chromatography

Concentrated IMAC Pool 2 was subjected to Sephacryl S100 gel filtration chromatography yielding protein profile with a major and a minor peak. The eluates corresponding to minor peak (fractions 10-16) had a more homogeneous content of Wnt3a. Gel electrophoresis was conducted in the presence of β-mercaptoethanol, which contributed to the doublet pattern.

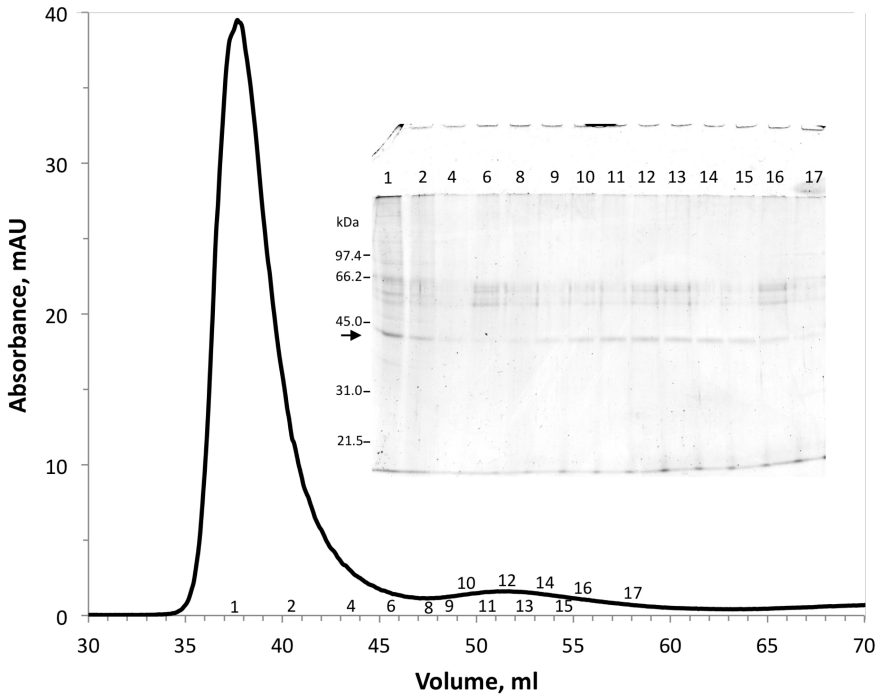

Figure 2-4. Gel filtration profile of IMAC Pool 2. Fractions pooled from the IMAC chromatography step were concentrated to 2 ml and applied to a Sephacryl S100 column. Proteins were eluted in 1 and 3 ml fractions with monitoring of absorbance at 280 nm. Inset) SDS-PAGE analysis of column fractions. The arrow at left depicts the band corresponding to Wnt3a. Molecular weight markers are shown at left.

Purification summary

Figure 2-5 (top panel) shows a summary of the 3-step purification scheme for Wnt3a from S2 cell CM. **Figure 2-5 (bottom panel)** shows the relative purity of the Wnt3a from each stage of the isolation procedure. Pool 2 from dye ligand chromatography was heavily contaminated and relative purities of IMAC pools 1 and 2 can be seen. Finally Wnt3a obtained from Sephacryl S100 gel filtration chromatography of IMAC pools 1 and 2 is depicted.

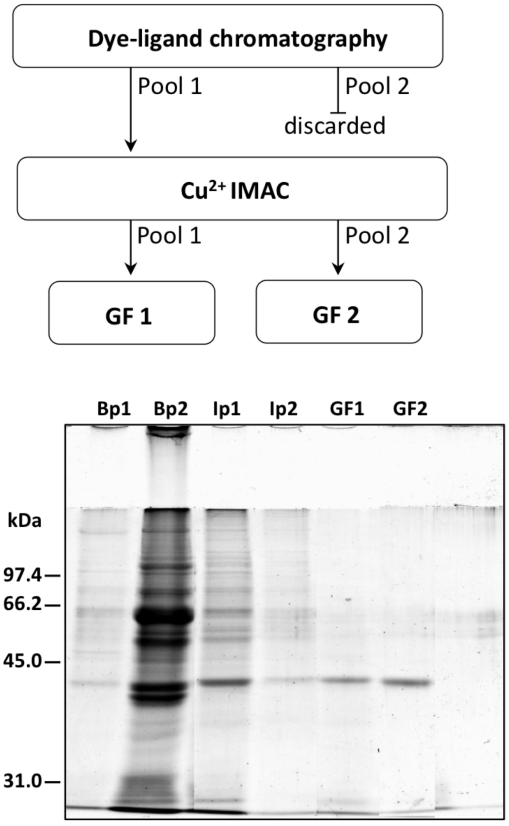

Figure 2-5. Summary of Wnt3a purification scheme. Top Panel) Flow chart of Wnt3a purification scheme. Bottom Panel) SDS-PAGE analysis of samples obtained after each step of the purification procedure including dye-ligand chromatography pool 1 and pool 2 (Blp1 and Blp2), IMAC chromatography pool 1 and pool 2 (Imp1 and Imp2) and gel filtration chromatography of the IMAC pool 1 and pool 2 (GF1 and GF2). The gel was electrophoresed in the presence of β-mercaptoethanol and stained with Imperial protein stain. The last lane shows 2-mercaptoethanol-containing sample buffer alone. Molecular weight markers are shown at left.

Effect of Wnt3a on β-catenin levels in L cells

Wnt interaction with its receptors results in stabilization and production of β-catenin through the canonical signaling pathway (7). Normally, β-catenin functions as a cytoskeletal protein in cells. However, any increases in β-catenin levels upon exposure to Wnt3a will be incremental to basal levels of cytoskeletal β-catenin. Mouse fibroblast L cells do not contain detectable levels of β-catenin in the absence of Wnt stimulation (8). Taking advantage of this fact, L cells were incubated with increasing amounts of isolated Wnt3a that resulted in a concentration dependent increase in the amount of β-catenin in as short as 3 h (**Figure 2-6**). Longer cell incubation times (24 h) with Wnt3a proportionally increased the β-catenin signal intensity (data not shown).

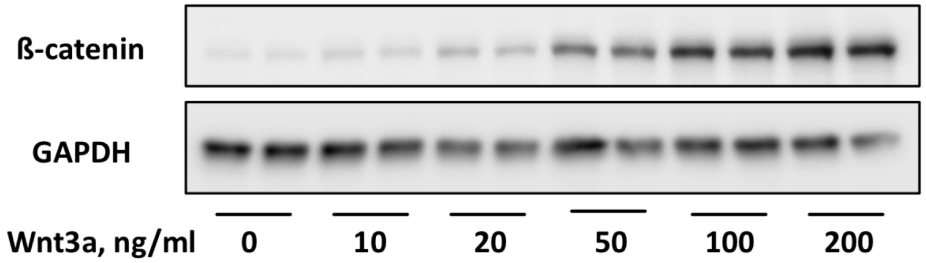

Figure 2-6. Effect of Wnt3a on cellular levels of β-catenin. Mouse L cells were incubated with the indicated concentrations of Wnt3a for 3 h. Following incubation the cells were lysed and 10 µg lysate protein applied to a 10% SDS-PAGE gel. Separated proteins were transferred to PVDF membrane and, after blocking, probed with antibodies directed against β-catenin and GAPDH.

Limited proteolysis

Biochemical tools to study structural limitations have been routinely used as part of protein characterization studies. The X-ray structure of *Xenopus* Wnt8 revealed that the evolutionarily conserved Wnt family of proteins is made of 2 domains. The larger N terminal domain that contains the palmitoleoyl moiety covalently attached to a conserved serine residue within a saposin like motif and the smaller C terminal domain that adopts a cytokine like fold (5). Computer assisted analysis of murine Wnt3a sequence for potential protease cleavage sites predicted a single thrombin cleavage near the C-terminus that under non-reducing conditions should remain attached via an inter chain disulfide bond. Incubation of isolated Wnt3a with thrombin at low thrombin: Wnt3a ratios resulted in no cleavage after 24 h. Upon altering thrombin:Wnt3a ratio to 1:1, quantitative cleavage was detected within 4 h giving rise to two distinct lower molecular weight products. SDS-PAGE under reducing and non-reducing conditions revealed that the size of the two fragments were not as predicted and the fragments were not held together by a disulfide bond as hypothesized. Based on the electrophoretic mobility of the fragments (~26kDa and ~21kDa) it was evident that cleavage had occurred at an alternate site. Immunoblot analysis using α-Wnt3a

antibody specific to C terminal residues (250-350) detected the 26kDa while the lower 21kDa protein remained undetected. In order to identify the alternate site of cleavage, Edman degradation analysis was performed on both fragments. The results revealed the N–terminal sequence of the 26kDa cleavage product corresponded to Wnt3a residues 163-167 (Ser-Ala-Met-Asn) and the 21kDa thrombin cleavage corresponded to N terminus of mature murine Wnt3a (Ser-Tyr-Pro-Ile). Residue 162 of mature murine Wnt3a (the P′ _site) corresponds to Arg, in accordance with the known cleavage specificity of thrombin (9).

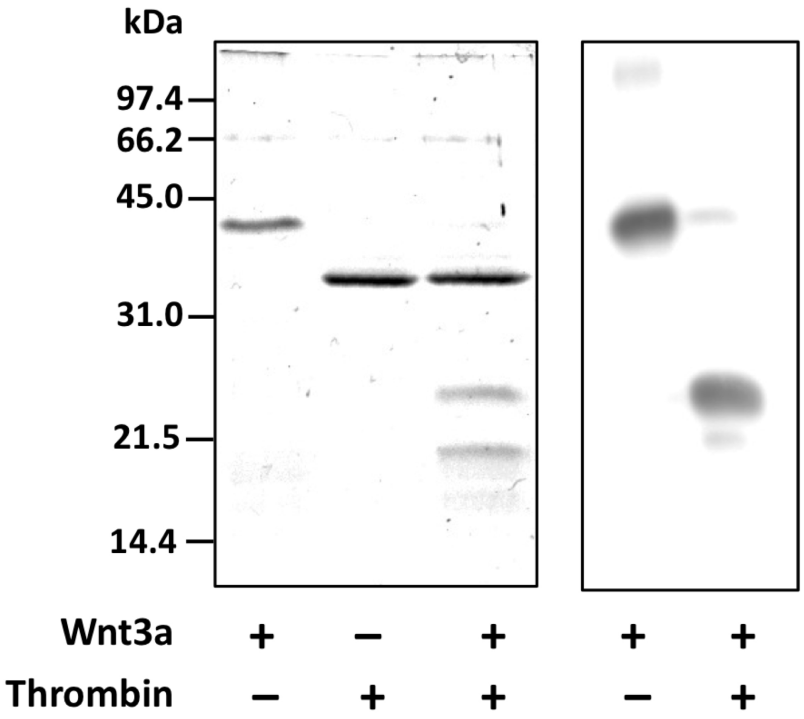

Figure 2-7. Effect of thrombin on isolated Wnt3a. Wnt3a (0.2 µg) was incubated in the absence or presence of 0.2 µg thrombin (10 µl total volume) for 4 h at 37 °C. Following incubation the samples were subject to SDS-PAGE and stained with Imperial protein stain (left panel) or transferred to PVDF and probed with α-Wnt3a (right panel).

CHAPS replacement studies

Cyclodextrins are comprised of 6-8 glucopyranoside units organized as a toroid. The exterior is hydrophilic thus imparting water solubility to cyclodextrins while the interior is used to host hydrophobic molecules. In order to determine a suitable replacement for CHAPS detergent, studies were conducted using MβCD based on its properties and evidence of its interaction with prenylated proteins (10). Purified Wnt3a in CHAPS was bound to 3 separate 0.1ml samples of Cu^{2+} charged IDA Sepharose beads in centrifugal columns. The columns were washed with 0.6ml TBS containing a) 1% CHAPS; b) 30mM MβCD or c) TBS alone, respectively following which, each column was equilibrated with corresponding buffer and bound Wnt3a was eluted with each buffer containing 200mM imidazole. It was found that CHAPS was most efficient at retaining Wnt3a activity and solubility, MβCD showed positive effect in terms of activity compared to TBS alone. In terms of protein recovery, 27±2% of MβCD containing sample was recovered versus 13±2% of TBS alone sample. In order to eliminate aggregated Wnt3a, samples were centrifuged for 4 min at 10,000xg. Relative to Wnt3a in CHAPS TBS, 73±2% of Wnt3a in MβCD containing TBS was recovered in the supernatant while 11±19% of the Wnt3a in TBS alone was present in supernatant. This finding indicates that MβCD is protective against Wnt3a aggregation.

2.5. Discussion

Molecular studies of Wnt structure function relations require the use of purified Wnt protein preparations. An optimized and streamlined expression and purification scheme has been developed to generate sufficient Wnt for characterization studies. Biologically active Wnt3a was produced from stably transfected S2 cells using dye ligand, metal affinity and gel filtration chromatography in the presence of CHAPS detergent to prevent aggregation and maintain solubility. To begin with S2 cell CM had levels of up to 350ug/L of Wnt3a and the final concentration of purified Wnt3a was 6-13ug/L.

In order to study natively lipidated Wnts, it is important to use expression systems that generate lipidated protein that retains its biological activity. Janda et al. were successful in establishing a detergent free expression system of *Xenopus* Wnt8 in complex with Fzd8-CRD (5). This was made possible due to the presence of the CRD of Fzd8 that served as a binding pocket for the interaction of the palmitoleic acid moiety covalently bound to Ser187 of Wnt8. The acyl chain was thus protected from solvent exposure eliminating the need for the presence of detergent during protein expression. Lipid modification is essential for Wnt secretion and biological function (4). One exception is *Drosophila* WntD, which is neither lipidated nor glycosylated and can thus be expressed at relatively high levels in the absence of detergent (11, 12).

Coexpression of Wnt8 with Frizzled CRD is not optimal for biochemical analysis of receptor ligand activity studies since the CRD may compete with natural receptors that mediate Wnt signaling activity. Till date, in vitro studies have been conducted using Wnt3a conditioned media or commercially available Wnt solubilized in CHAPS detergent micelles, which is expensive. CHAPS have attractive properties such as small micelle size 6,600MW, low aggregation number ~10 and critical micelle concentration of 8 to 10mM. However long term studies with CHAPS poses toxicity problems during cell culture (13). For protein characterization studies, based on the zwitterionic nature of CHAPS, it is unclear if Wnt-CHAPS mixed micelles primarily interact with the acyl chain or if the detergent interacts with other regions of the protein.

An alternate approach to replace detergent is the use of liposome associated Wnt3a that have displayed enhanced and sustained signaling activity in vitro potentially mimicking native Wnts in vivo. Wnt3a containing liposomes, following subcutaneous administration was shown to induce hair follicle neogenesis and used in bone regeneration studies establishing their regenerative capacity (14–16). However, liposomal Wnts are bulky complexes and Wnts are in CHAPS, an agent that disrupts liposome structure.

In a separate study, “secreted wingless interacting molecule” or “swim”, a lipocalin like protein was found to bind to Wingless, the *Drosophila* homolog of Wnt (17). Lipocalins are known to have affinity to hydrophobic ligands and in this case may be inferred to bind and sequester the fatty acyl chain of Wingless, conferring water solubility to diffuse as a morphogen. Wingless is also transported between cells in association with the hemolymph lipoprotein, lipophorin that is a noncovalent assembly of lipid and protein (18). Most likely Wingless is stably associated with the particle by insertion of its fatty acid moiety into the lipid rich core of the lipoprotein facilitating its transport to distant cells.

In studies of Wnt mediated effects on myogenic cells, Portilho et al. attempted to deplete cholesterol from membrane raft domains using MβCD. The authors found that exposure of cells to MβCD increased the amount of soluble Wnt3a in CM and concluded that cholesterol depletion alters the cell membrane association properties of Wnt3a (19). Based on the toroid structure and its interaction with prenylated proteins an alternative hypothesis was developed that MβCD interacts directly with Wnt promoting its solubility. In the present study, significant improvement was observed in terms of Wnt3a solubility when compared to buffer alone with overall low yields. It will be interesting to test whether alternate forms of cyclodextrins have a better fit with the fatty acyl chain of Wnt3a that may improve the interaction and thus give better recovery.

A key event in canonical Wnt signaling is the stabilization of a pool of β-catenin to serve as transcriptional activator in the nucleus. Interestingly, β-catenin participates in cell-cell adhesion as part of adherens junctions required to maintain epithelial cell layers and barriers. Taking advantage of the fact that mouse embryonic fibroblast L cells do not use β-catenin as part of cytoskeletal complexes, biological activity of the isolated and purified Wnt3a was tested on these cells by immunoblot analysis of β-catenin levels in whole cell lysates. As part of characterizing the isolated Wnt3a, the effect of limited proteolysis was examined on Wnt3a biological activity. Sequence analysis predicted a single thrombin cleavage site (between residues 295 and 296) in Wnt3a in the C terminus of Wnt3a at Arg-Gly site. However a specific cleavage occurred at an Arg-Ser site in the N terminus between residues 162 and 163. It is possible that C terminal Arg-Gly site may not be accessible to the enzyme due to interference of CHAPS micelles. The N terminal region of Wnt3a where thrombin cleavage occurred is the saposin like domain that adopts a unique fold identical to the family of saposin like protein or SAPLIPs. It will be interesting to explore the Wnt3a saposin like domain for further thrombin sensitivity as a function of lipid interaction as many saposins function via membrane interaction (20). The fatty acylation site on Wnt is part of a hairpin extension from saposin like domain, which suggests an important role played by the domain in modulating Wnt membrane interaction and fatty acyl chain binding to Frizzled.

2.6. References

1. Nusse, R., Brown, A., Papkoff, J., Scambler, P., Shackleford, G., McMahon, A., Moon, R., and Varmus, H. (1991) A new nomenclature for int-1 and related genes: the Wnt gene family. *Cell*. **64**, 231
2. Nusse, R., and Varmus, H. (2012) Three decades of Wnts: a personal perspective on how a scientific field developed. *EMBO J.* **31**, 2670–84
3. Willert, K., Brown, J. D., Danenberg, E., Duncan, A. W., Weissman, I. L., Reya, T., Yates, J. R., and Nusse, R. (2003) Wnt proteins are lipid-modified and can act as stem cell growth factors. *Nature*. **423**, 448–52
4. Takada, R., Satomi, Y., Kurata, T., Ueno, N., Norioka, S., Kondoh, H., Takao, T., and Takada, S. (2006) Monounsaturated fatty acid modification of Wnt protein: its role in Wnt secretion. *Dev. Cell*. **11**, 791–801
5. Janda, C. Y., Waghray, D., Levin, A. M., Thomas, C., and Garcia, K. C. (2012) Structural basis of Wnt recognition by Frizzled. *Science*. **337**, 59–64
6. Mach, H., Middaugh, C. R., and Denslow, N. (2001) Determining the identity and purity of recombinant proteins by UV absorption spectroscopy. *Curr. Protoc. protein Sci.* **Chapter 7**, Unit 7.2
7. MacDonald, B. T., Tamai, K., and He, X. (2009) Wnt/beta-catenin signaling: components, mechanisms, and diseases. *Dev. Cell*. **17**, 9–26
8. Shibamoto, S., Higano, K., Takada, R., Ito, F., Takeichi, M., and Takada, S. (1998) Cytoskeletal reorganization by soluble Wnt-3a protein signalling. *Genes Cells*. **3**, 659–70
9. Le Bonniec, B. F., Myles, T., Johnson, T., Knight, C. G., Tapparelli, C., and Stone, S. R. (1996) Characterization of the P2' and P3' specificities of thrombin using fluorescence-quenched substrates and mapping of the subsites by mutagenesis. *Biochemistry*. **35**, 7114–22
10. Saito, N., Ishida, Y., Seno, K., and Hayashi, F. (2012) Methyl-β-cyclodextrin is a useful compound for extraction and purification of prenylated enzymes from the retinal disc membrane. *Protein Expr. Purif.* **82**, 168–73
11. Chu, M. L.-H., Ahn, V. E., Choi, H.-J., Daniels, D. L., Nusse, R., and Weis, W. I. (2013) Structural Studies of Wnts and identification of an LRP6 binding site. *Structure*. **21**, 1235–42
12. Ching, W., Hang, H. C., and Nusse, R. (2008) Lipid-independent secretion of a Drosophila Wnt protein. *J. Biol. Chem.* **283**, 17092–8
13. Dhamdhere, G. R., Fang, M. Y., Jiang, J., Lee, K., Cheng, D., Olveda, R. C., Liu, B., Mulligan, K. A., Carlson, J. C., Ransom, R. C., Weis, W. I., and Helms, J. A. (2014) Drugging a stem cell compartment using Wnt3a protein as a therapeutic. *PLoS One*. **9**, e83650
14. Morrell, N. T., Leucht, P., Zhao, L., Kim, J.-B., ten Berge, D., Ponnusamy, K., Carre, A. L., Dudek, H., Zachlederova, M., McElhaney, M., Brunton, S., Gunzner, J., Callow, M., Polakis, P., Costa, M., Zhang, X. M., Helms, J. A., and Nusse, R. (2008) Liposomal packaging generates Wnt protein with in vivo biological activity. *PLoS One*. **3**, e2930
15. Minear, S., Leucht, P., Jiang, J., Liu, B., Zeng, A., Fuerer, C., Nusse, R., and Helms, J. A. (2010) Wnt proteins promote bone regeneration. *Sci. Transl. Med.* **2**,

29ra30
16. Popelut, A., Rooker, S. M., Leucht, P., Medio, M., Brunski, J. B., and Helms, J. A. (2010) The acceleration of implant osseointegration by liposomal Wnt3a. *Biomaterials*. **31**, 9173–81
17. Mulligan, K. A., Fuerer, C., Ching, W., Fish, M., Willert, K., and Nusse, R. (2012) Secreted Wingless-interacting molecule (Swim) promotes long-range signaling by maintaining Wingless solubility. *Proc. Natl. Acad. Sci. U. S. A.* **109**, 370–7
18. Panáková, D., Sprong, H., Marois, E., Thiele, C., and Eaton, S. (2005) Lipoprotein particles are required for Hedgehog and Wingless signalling. *Nature*. **435**, 58–65
19. Portilho, D. M., Martins, E. R., Costa, M. L., and Mermelstein, C. S. (2007) A soluble and active form of Wnt-3a protein is involved in myogenic differentiation after cholesterol depletion. *FEBS Lett.* **581**, 5787–95
20. Bruhn, H. (2005) A short guided tour through functional and structural features of saposin-like proteins. *Biochem. J.* **389**, 249–57

CHAPTER 3

Apolipoprotein E modulation of canonical Wnt3a signaling

3.1. Abstract

Low density lipoprotein receptor related protein 5 or 6 (LRP5/6) interaction with “Wnt” family signaling molecules regulates cell fate and proliferation in many tissues. In addition, it has been previously reported that LRP5/6 regulates serum cholesterol levels by binding to apolipoprotein (apo) E. Considering LRP5/6 function(s) at the intersection of cell proliferation (Wnt) and cholesterol metabolism (apoE), it was hypothesized that apoE is capable of modulating Wnt signaling by competition or by directly binding to LRP5/6. *In vitro* experiments conducted in cultured mouse embryonic fibroblasts indicate that in the absence of fetal bovine serum, Wnt3a canonical signaling is down regulated by reconstituted high density lipoproteins (HDL) containing either apoE3 N-terminal domain or apoA-I. On the other hand, Wnt3a mediated signaling activity was attenuated upon incubation of these cells with lipid-free apoE3 N-terminus, but not by lipid-free apoA-I. This effect of apoE3 N-terminus does not appear to be mediated through an apoE3 binding interaction with LRP5/6 but, rather, an interaction between apoE3 and Wnt3a.

Keywords: LRP5/6, apoE3, apoA-I, Wnt3a, liposomes, LDL A repeats

3.2. Introduction

Since LRP5 and LRP6 share 71% nucleotide sequence homology they are commonly referred to as LRP5/6 (1). Based on their characteristic structural features, LRP5/6 (~180kDa) are classified as members of the low density lipoprotein receptor (LDLR) family of endocytic cell surface receptors (2). LRP5/6 harbors 3 "LDL type A" (~40 amino acids long) repeats, 4 epidermal growth factor (EGF) precursor-like repeats, 4 β-propeller motifs, a single transmembrane spanning sequence and a highly conserved cytoplasmic domain with 5 PPPSP motifs (**Figure 3-1A)**. A unique and distinguishing feature of LRP5/6 is the location of its LDL type A repeats directly adjacent to the transmembrane spanning sequence. In all other LDLR family members, including LDLR and LRP1, these repeats are localized towards the N terminus of the receptors where they function as ligand binding sites (3).

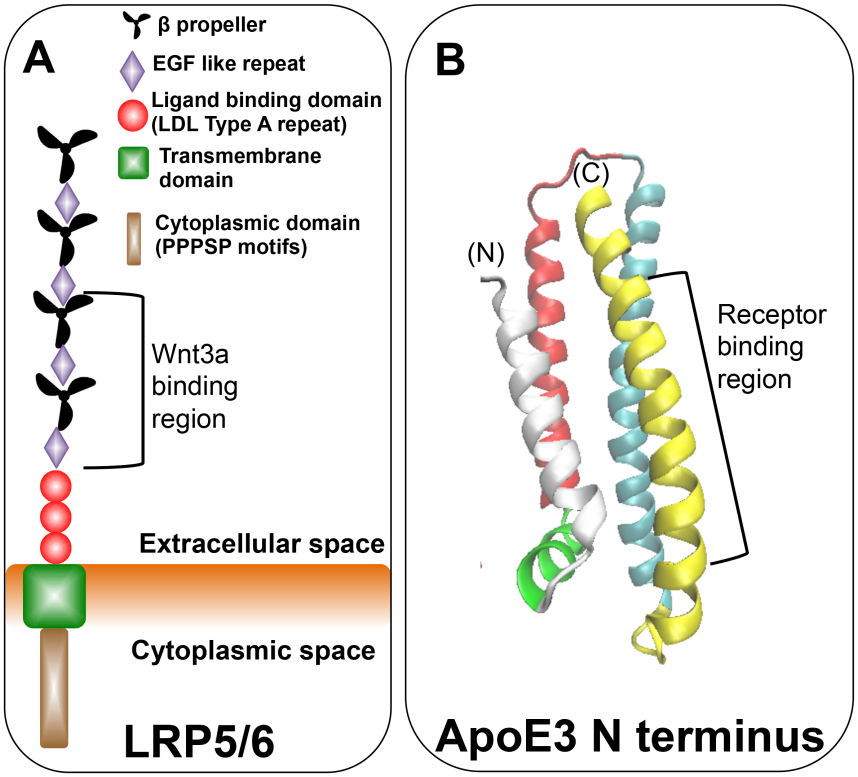

Figure 3-1. Schematic diagram of LRP5/6 and apoE3-NT. Panel A) Cartoon depiction of LRP5/6 modular structure. The receptor has four β propeller motifs (β1-β4) that alternate with 4 EGF-like repeats (E1-E4) in the N-terminus of the receptor. Three adjacent LDL Type A repeats are connected to the transmembrane sequence on the cell exterior. The cytoplasmic domain consists of five PPPSP repeats. Panel B) Secondary structure of apoE3-NT downloaded from Research Collaboratory for Structural Bioinformatics using Protein Data Bank entry (1H7I) and reconstructed using Visual Molecular Dynamics (4). ApoE3-NT exists as a four helical bundle in the lipid-free state. The receptor-binding region of apoE3-NT consists of a series of positively charged amino acids between residues 140 and 150.

LRP5/6 serves as a co-receptor for a large family of cysteine-rich, fatty acylated glycoproteins, termed Wnts (~40kDa). Wnt binding to co-receptors frizzled (Fzd) via its cysteine rich domain (CRD) and LRP5/6 via its β propeller / EGF repeat regions activates a signaling pathway that leads to intracellular accumulation of β-catenin, which translocates to the nucleus and activates transcription factors that transactivate Wnt target genes (5–7). It is important during this process for the Wnt fatty acyl group to be protected due to its propensity to aggregate. The Wnt/β-catenin pathway plays a major regulatory role in proliferation, renewal and subsequent differentiation of progenitor cells in the microenvironment of many tissues, including cardiac mesenchymal stem cells and cardiomyocytes (8–12).

LRP5/6 not only serves as a binding site for Wnts but also for apoE associated lipoprotein particles (13–15). In the non-lipid bound state, the 22kDa N-terminal (NT) domain of apoE3 forms a four-helix bundle (16) (**Figure 3-1B**) linked to a less structured, hydrophobic 10kDa C-terminal (CT) domain. A cluster of positively charged amino acids (in the vicinity of residues 140-150) in the NT domain serves as recognition site for binding to LDLR family members as well as heparan sulfate proteoglycans (17). Several independent studies have revealed that polymorphisms in LRP5/6 and apoE3 lead to dyslipidemia and elevated levels of LDL cholesterol (13–15, 18, 19).

Modulation of Wnt7a canonical signaling by full length apoE has been previously reported in undifferentiated rat adrenal medulla cells transfected with plasmids for constitutive expression of LRP5/6 and Wnt7a (20). Despite LRP5/6's role as a receptor for both apoE3 and Wnt, no studies have fully characterized the interplay between these ligands and LRP5/6. In the present study it was determined that Wnt3a-mediated signaling in cultured mouse embryonic fibroblasts is attenuated by lipid free apoE3 NT domain but not by the structurally related apolipoprotein, apoA-I. It is conceivable that the apoE3 NT elicits this effect by binding to a region outside the predicted LDL-A module in LRP5/6 or by direct interaction with the Wnt ligand.

3.3. Materials and methods

Wnt3a production

Murine Wnt3a was produced as previously described in CHAPTER 2 (21).

ApoE3 production and purification

The NT domain of human apoE3 (residues 1-183), which is necessary and sufficient for binding to LDL receptor family members, was cloned into a pet22b vector (New England Biolabs) and expressed in *E. coli* BL21 cells. Expression and purification procedures for apoE3-NT followed standardized protocol previously established (22). Briefly, overnight cultures grown in 2xYT were inoculated into M9 minimal media containing 50 µg/ml ampicillin, grown to an OD_{600} = 0.6 and induced with 1 mM isopropyl thiogalactopyranoside (IPTG). After 16 h culture at 30 °C, cells were pelleted by centrifugation. The supernatant was concentrated by ultrafiltration (with 10K molecular weight cutoff), dialyzed against 20mM NaPO4, 150mM NaCl, pH 7 and subjected to heparin Sepharose (GE Healthcare) chromatography as per the manufacturer's instructions. Bound protein was eluted in buffer containing 10mM NaPO4, pH 7, 1M NaCl, dialyzed against H_2O and lyophilized. As a final purification step, the protein was dissolved in 20mM sodium phosphate, pH 7.0, 50 mM NaCl, 2 M guanidine HCl and subjected to reversed phase high pressure liquid chromatography (HPLC) on a Perkin Elmer series 200 fitted with a Zorbax R-C8 (Dupont) column. Fractions were analyzed by SDS-PAGE and analytical HPLC and fractions displaying > 90 % protein purity were pooled, lyophilized and stored at -20^{o}C until use.

ApoA-I production and purification

ApoA-I, found on HDL and chylomicrons is a close structural relative to apoE3 and hence, was employed as a control in the present study. Recombinant wild type (WT) human apoA-I was expressed in *E. coli* and isolated as described previously (23). Briefly, human apoA-I was transformed into *E. coli* BL21 (DE-3) pLysS cells using the pET21 vector and cultured in NZCYM medium containing 50 µg/ml ampicillin at 37 °C. Overnight cultures were inoculated at a 1:30 ratio into NZCYM media containing 50 µg/ml ampicillin, grown to OD_{600} = 0.6 and induced with 1 mM IPTG. After 3 h at 37 °C, the cells were pelleted by centrifugation. Expressed proteins were purified via Hi-Trap nickel-chelating columns (GE Biosciences, Inc., Piscataway, NJ) according to manufacturer's instructions. Bound protein was eluted in buffer containing 500 mM imidazole and dialyzed against phosphate buffered saline (PBS) (20 mM sodium phosphate, 150 mM sodium chloride) pH 7.4, filtered and stored at 4 °C for further use.

Reconstituted HDL (rHDL) production

Five mg 1,2-dimyristoyl-sn-glycero-3-phosphocholine (DMPC) was dissolved in chloroform / methanol (3:1 v/v) and dried under a stream of N_2 gas, forming a thin film on the vessel wall. Residual organic solvent was removed under vacuum. The prepared lipid was dispersed in 0.5 ml PBS (20 mM sodium phosphate, 150 mM sodium chloride, pH 7.4) and 2 mg apoE3-NT or apoA-I (from 4 mg/ml stock solutions in PBS) were added and the sample (1 ml final volume) bath sonicated between 22 °C and 25 °C. The sonication step induced the turbid sample to clarify, indicating that the complexes of apolipoprotein and phospholipid (i.e. rHDL) had formed. The sample was centrifuged to remove unincorporated material and filter sterilized (0.22 μm).

Cell culture

L cells (0.5 x 10^6 cells/ml) were cultured in high glucose DMEM containing 10% fetal bovine serum (FBS), 100 U/ml penicillin and 100 μg/ml streptomycin overnight at 37 °C.

Immunoblot analysis

L cells (0.5 × 10^6 cells/well, 12 well plate) that were incubated with specified amounts of each protein for 3 h to 4 h at 37 °C in the presence of high glucose DMEM were harvested using RIPA cell lysis buffer (50 mM Tris HCl, pH 7.4, 150 mM NaCl, 0.1% SDS, 0.5% sodium deoxycholate, 1% Triton X-100) containing 1X Halt protease inhibitor cocktail mix. The protein concentration of cell lysates was measured and 10 μg aliquots heated to 95°C for 10 min in the presence of reducing SDS sample treatment buffer, applied to precast 10% polyacrylamide gels and electrophoresed at 120 V. Separated proteins were transferred to a PVDF membrane, blocked in 5% bovine serum albumin (BSA) and probed with anti-mouse β-catenin (1:2,000 dilution, BD Transduction Laboratories) and anti-mouse GAPDH (1:2,500 dilution, Millipore). Positive bands were detected with Horseradish Peroxidase (HRP)-conjugated anti-mouse secondary antibody (1:5,000 dilution, Vector Labs). Assays were performed in triplicate.

3.4. Results

Effect of FBS on canonical Wnt3a signaling activity in cultured L cells

Serum is a largely undefined, complex mixture of many growth factors, lipoproteins and other constituents that have proven invaluable for cell culture (24). Since the goal of the current study was to address the effect of apoE3 and its associated lipoprotein particles on Wnt3a canonical signaling activity, it was important to eliminate possible extraneous effects contributed by components of FBS in the media. To evaluate the effect of FBS on Wnt3a signaling, L cells were incubated with Wnt3a in media alone or media containing 10 % FBS for 3 h, followed by immunoblot analysis of the cellular content of β-catenin (**Figure 3-2**). Whereas β-catenin was nearly undetectable in control cells not exposed to Wnt3a, a strong signal was detected in cells incubated with Wnt3a. No differences in Wnt3a-induced β-catenin stabilization were observed in cells incubated in media containing or lacking FBS. Based on this result, it was concluded that Wnt3a is fully active in serum-free media, thereby permitting analysis of potential competitors to be investigated under this condition.

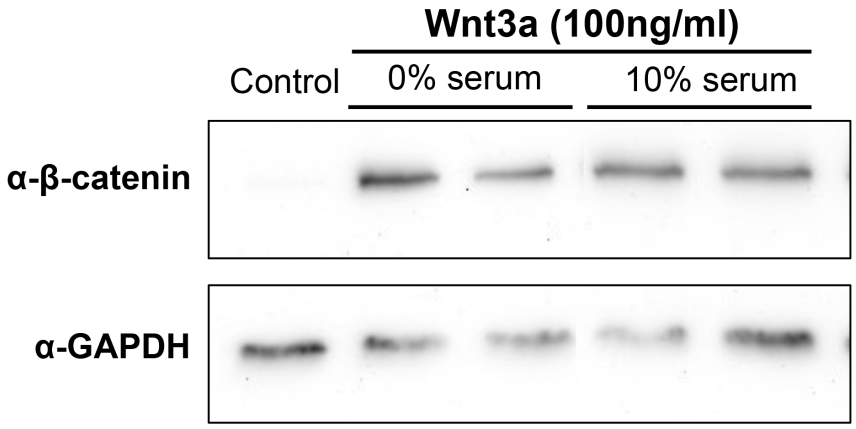

Figure 3-2. Effect of FBS on Wnt3a-stimulated β-catenin stabilization in L cells. L cells were incubated with Wnt3a (100 ng/ml) for 3 h in media lacking (0%) or containing (10%) serum. Following incubation, the cells were lysed and 10 μg lysate protein was applied to a 10% SDS-PAGE gel and electrophoresed. Separated proteins were transferred to a PVDF membrane and, after blocking, probed with antibodies directed against β-catenin and GAPDH.

Effect of rHDL on Wnt3a signaling activity

To test the hypothesis that apoE3-NT modulates Wnt3a signaling, rHDL containing apoE3-NT or apoA-I were formulated and introduced into Wnt3a signaling assays. Given that FBS deficient media had no effect on Wnt3a stimulated β-catenin stabilization, assays were performed in the absence of FBS. L cells were incubated with 100 ng/ml Wnt3a in the absence or presence of rHDL formulated with apoE3-NT or apoA-I as the scaffold protein. Following incubation, cellular β-catenin levels were determined as a measure of Wnt3a signaling activity (**Figure 3-3**). At the rHDL concentrations examined, incubations containing apoE3-NT rHDL or apoA-I rHDL resulted in a significant decline in Wnt3a-induced β-catenin stabilization.

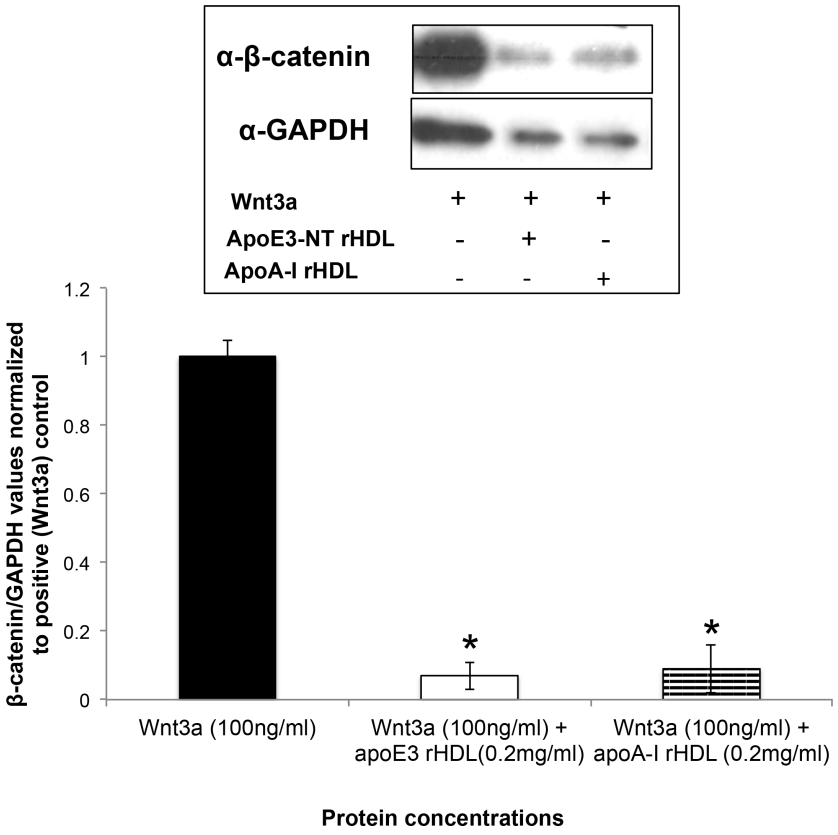

Figure 3-3. Effect of rHDL particles on Wnt3a-stimulated β-catenin stabilization. L cells were incubated with Wnt3a (100 ng/ml) alone or with 0.2 mg/ml rHDL (apoE3-NT rHDL or apoA-I rHDL for 3h. Following incubation, the cells were lysed and 10 μg lysate protein applied to a 10% SDS-PAGE gel. Separated proteins were transferred to a PVDF membrane and, after blocking, probed with antibodies directed against β-catenin and GAPDH. Bar graph depicts results of densitometric analysis of β-catenin/GAPDH signal intensity normalized to Wnt3a (100 ng/ml) only incubations. The results are representative of 3 independent experiments.

Effect of lipid free apolipoproteins on Wnt3a signaling activity

To determine whether the effects of apoE3-NT rHDL and apoA-I rHDL on Wnt3a-induced β-catenin stabilization in L cells may be related to the lipid content of the particles rather than the protein itself, incubations were performed with lipid-free apolipoproteins. Wnt3a was incubated with murine L cells in the absence or presence of lipid free apolipoprotein and the effect on cellular β-catenin levels measured by immunoblot (**Figure 3-4**). In this case, whereas incubations with apoE3-NT led to dramatic decline in Wnt3a-induced β-catenin stabilization, apoA-I had little effect.

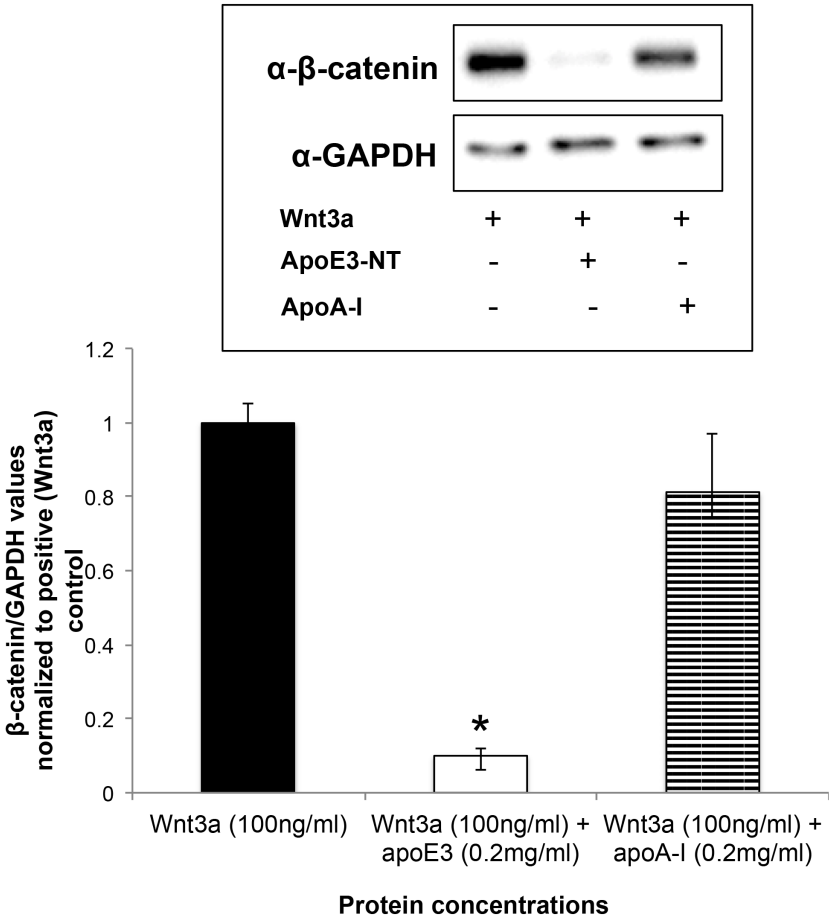

Figure 3-4. Effect of lipid free apolipoprotein on Wnt3a-stimulated β-catenin stabilization. L cells were incubated with 100 ng/ml Wnt3a in the absence or presence of 0.2 mg/ml apolipoprotein (apoE3-NT or apoA-I) for 3h. Following incubation, the cells were lysed and 10 µg lysate protein was applied to a 10% SDS-PAGE gel. Separated proteins were transferred to a PVDF membrane and, after blocking, probed with antibodies directed against β-catenin and GAPDH. Bar graph represents densitometric analysis of β-catenin/GAPDH normalized to incubations with Wnt3a alone. The results are representative of 3 independent experiments.

Effect of EDTA on apoE3-NT mediated modulation of Wnt3a signaling activity

To determine if the apoE3-NT dependent attenuation of Wnt3a-induced β-catenin stabilization requires apoE3-NT binding to LDL-A repeats present on LRP5/6, EDTA was included in assays to chelate calcium ions bound to LRP5/6 LDL-A repeats (predicted apoE3-NT binding site on LRP5/6; Yamamoto and Ryan 2007). On the other hand, Wnt3a binds to the β-propeller regions of LRP5/6, structural elements that are devoid of calcium binding sites and, presumably, unaffected by EDTA-mediated calcium chelation. The degree of Wnt3a-induced stabilization of β-catenin was unaffected by inclusion of EDTA in the assay mixture (**Figure 3-5**). Furthermore, EDTA had no effect on apoE3-NT mediated attenuation of Wnt3a stimulated β-catenin stabilization.

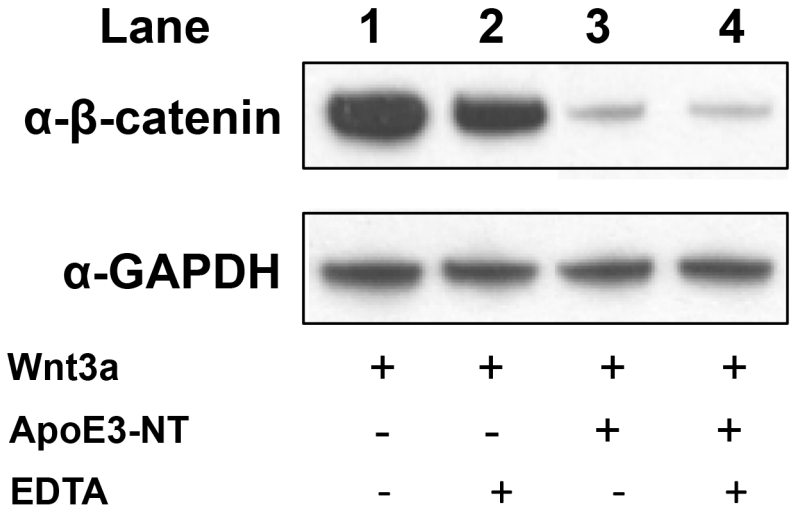

Figure 3-5. Effect of EDTA on apoE3-NT dependent modulation of Wnt3a-stimulated β-catenin stabilization. L cells were incubated with 100ng/ml Wnt3a in the absence or presence of (0.2mg/ml) apoE3-NT and (2mM) EDTA for 3h. Following incubation, the cells were lysed and 10 µg lysate protein applied to a 10% SDS-PAGE gel. Separated proteins were transferred to PVDF membrane and, after blocking, probed with antibodies directed against β-catenin and GAPDH.

Effect of ligand presentation order on Wnt3a-stimulated β-catenin stabilization

Conceivably, upon binding apoE3-NT, LRP5/6 undergoes endocytosis and, thereby, is rendered unavailable to bind Wnt3a. Similarly, if LRP5/6 is engaged with Wnt3a prior to exposure to apoE3-NT, the ability of this protein to attenuate signaling activity may be affected. To test this, L cells were incubated for 1 h with Wnt3a, followed by the addition of apoE3-NT for 3 h and vice versa (**Figure 3-6**). As control, a similar protocol was employed with Wnt3a and apoA-I. Compared to Wnt3a alone, the addition of apoE3-NT induced a decline in Wnt3a-stimulated β-catenin levels. This decline in levels of β-catenin remained unchanged irrespective of the order of presentation of apoE3-NT and Wnt3a. In control incubations with apoA-I, no changes in Wnt3a-stimulated β-catenin stabilization were observed.

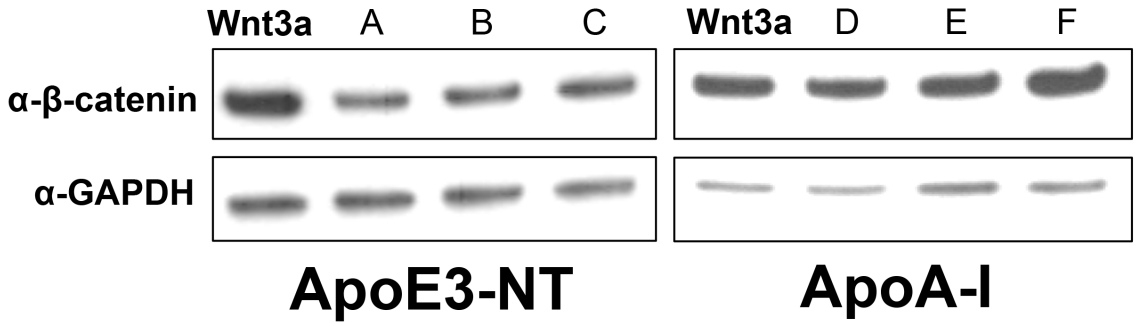

Figure 3-6. Effect of incubation conditions on apoE3-NT modulation of Wnt3a-stimulated β-catenin stabilization. L cells were incubated with 100 ng/ml Wnt3a in the absence or presence of 0.2 mg/ml apolipoprotein (apoE3-NT or apoA-I) for 4h. Following incubation, the cells were lysed and 10 µg lysate protein applied to a 10% SDS-PAGE gel. Separated proteins were transferred to PVDF membrane and, after blocking, probed with antibodies directed against β-catenin and GAPDH. Lane 1) Wnt3a alone; Lane 2) pre-incubation with Wnt3a followed by apoE3-NT; Lane 3) apoE3-NT preincubation followed by Wnt3a. Panel B) the same lane assignments and incubation conditions except that apoA-I was used instead of apoE3-NT.

3.5. Discussion

The central roles played by LRP5/6 in canonical Wnt signaling and apoE mediated lipoprotein metabolism, respectively, are well established. Considering the significant differences between these ligands, we sought to investigate if interplay exists between Wnt3a and apoE3-NT. Given the rapid and profound effect of Wnt3a on L cell β-catenin levels, assays were designed to assess effectors of this activity. Initially, it was determined that FBS is not a required component of the cell culture medium for Wnt3a signaling activity detection. Since FBS contains apolipoproteins, assays were conducted in serum free medium.

Wnt proteins aggregate in solution in the absence of serum or detergent (26, 27). However, the process of aggregation and the gradual loss of Wnt signaling activity occurs over a period of 8h (27). Cell based assays conducted in the serum-free media reported here employed an incubation time of 3 h, and, in this time frame, no significant loss of Wnt3a stimulated β-catenin stabilization occurred, as compared to incubations in media containing FBS. The relatively short assay time in the present study may explain the difference in results of Fuerer and coworkers (28) who observed a loss of Wnt signaling activity at longer incubation times in the absence of serum.

The presence of a covalently bound fatty acyl chain on Wnts has led to speculation on how this protein transits between neighboring cells. Several groups have demonstrated that liposomes, agrosomes and/or lipoprotein particles transport Wnt proteins (29–32). Mammalian Wnt3a was shown to be specifically released onto HDL particles endogenously produced by enterocytes (33). Lalefar et al. (2016) successfully demonstrated that pre-incubation of phospholipids with Wnt3a followed by addition of recombinant apoA-I yielded biologically active Wnt3a “nanodisks” with hematopoietic stem cell regeneration capacity. It is important to note that formation of liposomes and rHDL particles in the presence of Wnt provides an opportunity for its fatty acyl group to interact with phospholipids, thus facilitating Wnt stabilization in solution. In the current study, when cells were presented with Wnt3a and rHDL particles composed of phospholipid and apoE3-NT or apoA-I, Wnt3a stimulated β-catenin stabilization was diminished (**Figure 3-3**). Considering that the rHDL particles were prepared in the absence of Wnt3a, when presented together in media devoid of FBS or detergent, rHDL particles likely serve as a “sink” for Wnt3a to associate and bury its fatty acyl group within the hydrophobic milieu of the particle. As a result Wnt3a may form a stable association such that it does not engage its cognate receptors at the cell surface.

Caruso et al. demonstrated that Wnt7a canonical signaling activity was reduced by full-length apoE in undifferentiated rat adrenal medulla cells transfected with plasmids to constitutively express LRP5/6. These authors concluded that apoE mediated modulation of Wnt7a-stimulated signaling was influenced by expression of LRP5/6 (20). These results lend further support to the findings in the present study where addition of lipid-free recombinant apoE3-NT but not apoA-I, resulted in down regulation of Wnt3a-stimulated canonical signaling in L cells, thereby confirming the specificity of apoE3-NT as a mediator of Wnt3a canonical signaling activity.

ApoE3 is known to bind to LDL-A modules in LDLR family members (25). LRP5/6 has three LDL-A modules with five conserved acidic residues, DXXXDXXDXXDE, the side chains of which are involved in calcium coordination. Mutations in any of these

residues results in impaired folding of LDL-A modules and defects in ligand binding (34). We speculated that, if modulation of Wnt3a stimulated β-catenin stabilization was dependent upon apoE3-NT binding to LDL-A modules in LRP5/6, then EDTA-mediated sequestration of calcium would impair its ability to bind and, thereby, affect its Wnt modulatory activity. Surprisingly, however, EDTA treatment did not alter the modulation of Wnt3a signaling in the presence of apoE3-NT. Given this result, it could be that apoE3-NT binds to a region distinct from the LDL-A repeat portion of LRP5/6, initiating a process of receptor-mediated endocytosis wherein the cell surface concentration of LRP5/6 is decreased, limiting the availability for Wnt signaling activation. There is also the possibility that the amphipathic helices that form the apoE3-NT helix bundle are able to complex with Wnt3a, rendering it biologically inactive. Taken together, further studies are required to fully demonstrate the specifics of the receptor binding interaction of lipid-free apoE3-NT and LRP5/6 or Wnt3a.

3.6. References

1. Brown, S. D., Twells, R. C. J., Hey, P. J., Cox, R. D., Levy, E. R., Soderman, A. R., Metzker, M. L., Caskey, C. T., Todd, J. A., and Hess, J. F. (1998) Isolation and Characterization ofLRP6,a Novel Member of the Low Density Lipoprotein Receptor Gene Family. *Biochem. Biophys. Res. Commun.* **248**, 879–888
2. Bennet, A. M., Di Angelantonio, E., Ye, Z., Wensley, F., Dahlin, A., Ahlbom, A., Keavney, B., Collins, R., Wiman, B., de Faire, U., and Danesh, J. (2007) Association of apolipoprotein E genotypes with lipid levels and coronary risk. *JAMA*. **298**, 1300–11
3. He, X., Semenov, M., Tamai, K., and Zeng, X. (2004) LDL receptor-related proteins 5 and 6 in Wnt/beta-catenin signaling: arrows point the way. *Development*. **131**, 1663–77
4. Humphrey, W., Dalke, A., and Schulten, K. (1996) VMD: visual molecular dynamics. *J. Mol. Graph.* **14**, 33–8, 27–8
5. Bourhis, E., Wang, W., Tam, C., Hwang, J., Zhang, Y., Spittler, D., Huang, O. W., Gong, Y., Estevez, A., Zilberleyb, I., Rouge, L., Chiu, C., Wu, Y., Costa, M., Hannoush, R. N., Franke, Y., and Cochran, A. G. (2011) Wnt Antagonists Bind through a Short Peptide to the First β-Propeller Domain of LRP5/6. *Structure*. **19**, 1433–1442
6. Gong, Y., Bourhis, E., Chiu, C., Stawicki, S., DeAlmeida, V. I., Liu, B. Y., Phamluong, K., Cao, T. C., Carano, R. A. D., Ernst, J. A., Solloway, M., Rubinfeld, B., Hannoush, R. N., Wu, Y., Polakis, P., and Costa, M. (2010) Wnt isoform-specific interactions with coreceptor specify inhibition or potentiation of signaling by LRP6 antibodies. *PLoS One*. **5**, e12682
7. Nusse, R., and Varmus, H. (2012) Three decades of Wnts: a personal perspective on how a scientific field developed. *EMBO J.* **31**, 2670–84
8. Wang, X., Xiao, Y., Mou, Y., Zhao, Y., Blankesteijn, W. M., and Hall, J. L. (2002) A Role for the β-Catenin/T-Cell Factor Signaling Cascade in Vascular Remodeling. *Circ. Res.*
9. Quasnichka, H., Slater, S. C., Beeching, C. A., Boehm, M., Sala-Newby, G. B., and George, S. J. (2006) Regulation of Smooth Muscle Cell Proliferation by β-Catenin/T-Cell Factor Signaling Involves Modulation of Cyclin D1 and p21 Expression. *Circ. Res.*
10. Dravid, G., Ye, Z., Hammond, H., Chen, G., Pyle, A., Donovan, P., Yu, X., and Cheng, L. (2005) Defining the Role of Wnt/β-Catenin Signaling in the Survival, Proliferation, and Self-Renewal of Human Embryonic Stem Cells. *Stem Cells*. **23**, 1489–1501
11. Naito, A. T., Shiojima, I., Akazawa, H., Hidaka, K., Morisaki, T., Kikuchi, A., and Komuro, I. (2006) Developmental stage-specific biphasic roles of Wnt/beta-catenin signaling in cardiomyogenesis and hematopoiesis. *Proc. Natl. Acad. Sci.* **103**, 19812–19817
12. Månsson-Broberg, A., Rodin, S., Bulatovic, I., Ibarra, C., Löfling, M., Genead, R., Wärdell, E., Felldin, U., Granath, C., Alici, E., Le Blanc, K., Smith, C. I. E., Salašová, A., Westgren, M., Sundström, E., Uhlén, P., Arenas, E., Sylvén, C., Tryggvason, K., Corbascio, M., Simonson, O. E., Österholm, C., and Grinnemo,

K.-H. (2016) Wnt/β-Catenin Stimulation and Laminins Support Cardiovascular Cell Progenitor Expansion from Human Fetal Cardiac Mesenchymal Stromal Cells. *Stem Cell Reports*. **6**, 607–617

13. Fujino, T., Asaba, H., Kang, M.-J., Ikeda, Y., Sone, H., Takada, S., Kim, D.-H., Ioka, R. X., Ono, M., Tomoyori, H., Okubo, M., Murase, T., Kamataki, A., Yamamoto, J., Magoori, K., Takahashi, S., Miyamoto, Y., Oishi, H., Nose, M., Okazaki, M., Usui, S., Imaizumi, K., Yanagisawa, M., Sakai, J., and Yamamoto, T. T. (2003) Low-density lipoprotein receptor-related protein 5 (LRP5) is essential for normal cholesterol metabolism and glucose-induced insulin secretion. *Proc. Natl. Acad. Sci.* **100**, 229–234
14. Magoori, K., Kang, M.-J., Ito, M. R., Kakuuchi, H., Ioka, R. X., Kamataki, A., Kim, D.-H., Asaba, H., Iwasaki, S., Takei, Y. A., Sasaki, M., Usui, S., Okazaki, M., Takahashi, S., Ono, M., Nose, M., Sakai, J., Fujino, T., and Yamamoto, T. T. (2003) Severe Hypercholesterolemia, Impaired Fat Tolerance, and Advanced Atherosclerosis in Mice Lacking Both Low Density Lipoprotein Receptor-related Protein 5 and Apolipoprotein E. *J. Biol. Chem.* **278**, 11331–11336
15. Kim, D. H., Inagaki, Y., Suzuki, T., Ioka, R. X., Yoshioka, S. Z., Magoori, K., Kang, M. J., Cho, Y., Nakano, A. Z., Liu, Q., Fujino, T., Suzuki, H., Sasano, H., and Yamamoto, T. T. (1998) A new low density lipoprotein receptor related protein, LRP5, is expressed in hepatocytes and adrenal cortex, and recognizes apolipoprotein E. *J. Biochem.* **124**, 1072–6
16. Wilson, C., Wardell, M. R., Weisgraber, K. H., Mahley, R. W., and Agard, D. A. (1991) Three-dimensional structure of the LDL receptor-binding domain of human apolipoprotein E. *Science*. **252**, 1817–22
17. Weisgraber, K. H., Innerarity, T. L., Harder, K. J., Mahley, R. W., Milne, R. W., Marcel, Y. L., and Sparrow, J. T. (1983) The receptor-binding domain of human apolipoprotein E. Monoclonal antibody inhibition of binding. *J. Biol. Chem.* **258**, 12348–54
18. Ye, Z., Go, G.-W., Singh, R., Liu, W., Keramati, A. R., and Mani, A. (2012) LRP6 Protein Regulates Low Density Lipoprotein (LDL) Receptor-mediated LDL Uptake. *J. Biol. Chem.* **287**, 1335–1344
19. Mani, A., Radhakrishnan, J., Wang, H., Mani, A., Mani, M.-A., Nelson-Williams, C., Carew, K. S., Mane, S., Najmabadi, H., Wu, D., and Lifton, R. P. (2007) LRP6 mutation in a family with early coronary disease and metabolic risk factors. *Science*. **315**, 1278–82
20. Caruso, A., Motolese, M., Iacovelli, L., Caraci, F., Copani, A., Nicoletti, F., Terstappen, G. C., Gaviraghi, G., and Caricasole, A. (2006) Inhibition of the canonical Wnt signaling pathway by apolipoprotein E4 in PC12 cells. *J. Neurochem.* **98**, 364–371
21. Witkowski, A., Krishnamoorthy, A., Su, B., Beckstead, J. A., and Ryan, R. O. (2015) Isolation and characterization of recombinant murine Wnt3a. *Protein Expr. Purif.* **106**, 41–48
22. Fisher, C. A., Wang, J., Francis, G. A., Sykes, B. D., Kay, C. M., and Ryan, R. O. (1997) Bacterial overexpression, isotope enrichment, and NMR analysis of the N-terminal domain of human apolipoprotein E. *Biochem. Cell Biol.* **75**, 45–53
23. Ryan, R. O., Forte, T. M., and Oda, M. N. (2003) Optimized bacterial expression

of human apolipoprotein A-I. *Protein Expr. Purif.* **27**, 98–103
24. Brunner, D., Frank, J., Appl, H., Schöffl, H., Pfaller, W., and Gstraunthaler, G. (2010) Serum-free cell culture: the serum-free media interactive online database. *ALTEX*. **27**, 53–62
25. Yamamoto, T., and Ryan, R. O. (2007) Anionic phospholipids inhibit apolipoprotein E—Low-density lipoprotein receptor interactions. *Biochem. Biophys. Res. Commun.* **354**, 820–824
26. Fuerer, C., Habib, S. J., and Nusse, R. (2010) A study on the interactions between heparan sulfate proteoglycans and Wnt proteins. *Dev. Dyn.* **239**, 184–90
27. Tüysüz, N., van Bloois, L., van den Brink, S., Begthel, H., Verstegen, M. M. A., Cruz, L. J., Hui, L., van der Laan, L. J. W., de Jonge, J., Vries, R., Braakman, E., Mastrobattista, E., Cornelissen, J. J., Clevers, H., and ten Berge, D. (2017) Lipid-mediated Wnt protein stabilization enables serum-free culture of human organ stem cells. *Nat. Commun.* **8**, 14578
28. Fuerer, C., Habib, S. J., and Nusse, R. (2010) A study on the interactions between heparan sulfate proteoglycans and Wnt proteins. *Dev. Dyn.* **239**, 184–90
29. Neumann, S., Coudreuse, D. Y. M., van der Westhuyzen, D. R., Eckhardt, E. R. M., Korswagen, H. C., Schmitz, G., and Sprong, H. (2009) Mammalian Wnt3a is released on lipoprotein particles. *Traffic*. **10**, 334–43
30. Panáková, D., Sprong, H., Marois, E., Thiele, C., and Eaton, S. (2005) Lipoprotein particles are required for Hedgehog and Wingless signalling. *Nature*. **435**, 58–65
31. Morrell, N. T., Leucht, P., Zhao, L., Kim, J.-B., ten Berge, D., Ponnusamy, K., Carre, A. L., Dudek, H., Zachlederova, M., McElhaney, M., Brunton, S., Gunzner, J., Callow, M., Polakis, P., Costa, M., Zhang, X. M., Helms, J. A., and Nusse, R. (2008) Liposomal Packaging Generates Wnt Protein with In Vivo Biological Activity. *PLoS One*. **3**, e2930
32. Greco, V., Hannus, M., and Eaton, S. (2001) Argosomes: a potential vehicle for the spread of morphogens through epithelia. *Cell*. **106**, 633–45
33. Neumann, S., Coudreuse, D. Y. M., van der Westhuyzen, D. R., Eckhardt, E. R. M., Korswagen, H. C., Schmitz, G., and Sprong, H. (2009) Mammalian Wnt3a is released on lipoprotein particles. *Traffic*. **10**, 334–43
34. Guo, Y., Yu, X., Rihani, K., Wang, Q.-Y., and Rong, L. (2004) The role of a conserved acidic residue in calcium-dependent protein folding for a low density dipoprotein (LDL)-A module: Implications in structure and function for the LDL receptor superfamily. *J. Biol. Chem.* **279**, 16629–16637

CHAPTER 4

The saposin-like sub-domain of human Wnt3a

4.1. Abstract

Wnt signaling is essential for embryonic development and adult homeostasis in multicellular organisms. A conserved feature among Wnt family proteins is the presence of two structural domains. Within the N-terminal (NT) domain there exists a motif that is superimposable upon saposin-like protein (SAPLIP) family members. SAPLIPs are found in plants, microbes and animals and possess lipid surface seeking activity. To investigate the function of the Wnt3a saposin-like sub-domain (SLD), recombinant SLD was studied in isolation. Bacterial expression of this Wnt fragment was achieved only when the core SLD included 82 NT residues of Wnt3a (NT-SLD). Unlike SAPLIPs, NT-SLD required the presence of detergent to achieve solubility at neutral pH. Deletion of two hairpin loop extensions present in NT-SLD, but not other SAPLIPs, had no effect on the solubility properties of NT-SLD. Far UV circular dichroism spectroscopy of NT-SLD yielded 50 to 60% α-helix secondary structure. Limited proteolysis of isolated NT-SLD in buffer and detergent micelles showed no differences in cleavage kinetics. Unlike prototypical saposins, NT-SLD exhibited weak membrane-binding affinity and lacked cell lytic activity. In cell-based canonical Wnt signaling assays, NT-SLD was unable to induce stabilization of β-catenin or modulate the extent of β-catenin stabilization induced by full-length Wnt3a. Taken together, the results indicate neighboring structural elements within full-length Wnt3a affect SLD conformational stability. Moreover, SLD function(s) in Wnt proteins appear to have evolved away from those commonly attributed to SAPLIP family members.

Keywords: Canonical Wnt signal transduction, circular dichroism spectroscopy, detergent, fluorescence spectroscopy, limited proteolysis, liposomes, saposin, Wnt3a.

4.2. Introduction

Evolutionally conserved Wnt proteins initiate a signaling cascade that is key to normal embryonic development and homeostasis throughout the adult life of metazoans (1). In mammals, Wnts comprise a family of secreted ~350 amino acid, lipid-modified / glycosylated, cysteine-rich proteins (2) that signal via canonical (β-catenin dependent) and non canonical (β-catenin independent) pathways (3). In the well-characterized canonical pathway, Wnt engages the co-receptors “frizzled” (Fzd) and low density lipoprotein receptor related proteins 5 or 6 (LRP5/6), leading to stabilization of cytoplasmic β-catenin which migrates to the nucleus and functions as a transcriptional activator. Nuclear β-catenin co-activates the lymphoid enhancer binding factor/T cell specific transcription factor to regulate transcription of Wnt target genes. In the absence of Wnt, cytoplasmic β-catenin is phosphorylated, ubiquitinylated and degraded by proteasomes (4). Spatiotemporal expression of 19 different Wnt genes, 10 Fzd and 2 LRP give rise to diversity and complexity in mammalian Wnt signaling (5). Thus, it is not surprising that dysregulation in Wnt signaling underlies diseases including cancer, metabolic syndrome and neurodegenerative disorders (6–9).

The X-ray crystal structure of *Xenopus* Wnt8 engaged with the cysteine-rich domain (CRD) of Fzd8 revealed two independently folded structural domains joined by a linker segment (10). The N-terminal (NT) domain is comprised of six α-helices organized in a bundle. Extending from this core helix bundle are two narrow, elongated β-hairpins. The extreme tip of the first hairpin bears a conserved serine that serves as the site of posttranslational attachment of a palmitoleic acid moiety, which is required for intracellular trafficking and secretion of Wnt (11). This monounsaturated fatty acid also contributes to Wnt8 interaction with Fzd8 CRD (10). The smaller Wnt C-terminal (CT) domain adopts a long twisted β-hairpin reminiscent of a cysteine knot growth factor fold. As with hairpins in the NT domain, those in the CT domain are stabilized by a series of disulfide bonds (10, 12).

Based on structural analysis, a discrete region within the NT domain of Wnt8 was identified as resembling a saposin-like protein (SAPLIP) fold (13, 14). Prototypical SAPLIPs exist either as independently folded proteins or sub-domains within larger protein structures. SAPLIPs consist of a bundle of 4-5 amphipathic α-helices with 3 intra-domain disulfide bonds (15). It has been postulated that, when presented with an appropriate lipid surface, the SAPLIP helix bundle unfurls, exposing a hydrophobic interior that interacts with lipid surfaces (16, 17). This conformational flexibility facilitates the biological functions of SAPLIPs including membrane interaction, pore formation and/or cell lysis (18–20). In fact, SAPLIPs encompass a large protein family that manifest diverse functions including pulmonary surface tension regulation, antimicrobial activity, eukaryotic cell lysis and/or cofactor for sphingolipid degradative enzymes (15, 21–25).

The identification of a protein fold resembling SAPLIPs as a structural element within the NT domain of Wnt family members raises the possibility that Wnts adopt alternate conformational states via their saposin-like sub-domain (SLD). The hypothesis that Wnt3a-SLD possesses functions ascribed to SAPLIP family members was examined in the present study. Constructs encoding SLD alone, SLD plus 82 NT residues (NT-SLD) and an NT-SLD lacking two Wnt-specific β-hairpins (NT-SLD(nh))

were produced in *E. coli*. Results obtained indicate SLD expression is dramatically improved when 82 NT residues of Wnt3a are attached to the core SLD sequence. Furthermore, although β-hairpin deleted SLD more closely resembles prototypical SAPLIPs, no differences in protein expression level or solubility properties were observed. Overall, the data suggest Wnt3a SLD has evolved to rely on other elements of the Wnt structure to maintain a stable fold and does not manifest classical functions associated with SAPLIPs in isolation.

4.3. Materials and Methods

Chemicals and reagents

Bacterial growth medium, dodecyltrimethylammonium chloride (DTAC), sodium dodecyl sulfate (SDS), reduced and oxidized glutathione were from Sigma-Aldrich. Dithiothreitol (DTT) was from Thermo Fisher Scientific. Thrombin was from Cayman Chemical. 3-[(3-cholamidopropyl)dimethylammonio]-1-propanesulfonate (CHAPS) was purchased from A.G. Scientific Inc. Oligonucleotide primers were from Elim Oligo. Murine Wnt3a was expressed in stably transfected *Drosophila* S2 cells and isolated from conditioned media according to (26). Dulbecco's Modified Eagle's Medium (DMEM), fetal bovine serum (FBS), penicillin and streptomycin and Halt Protease Inhibitor cocktail were obtained from Thermo Fisher Scientific. Precast 4-20% and 10% acrylamide slab gels were from Bio-Rad Laboratories. Mouse embryonic fibroblast L cells were provided by Dr. Roel Nusse (27). 1,2-dimyristoyl-sn-glycero-3-phosphocholine (DMPC) was purchased from Avanti Polar Lipids Inc. Gel Code Blue and Imperial Protein stain was from Thermo Scientific. CellTiter 96 Non-Radioactive Cell Proliferation (MTT; 3-[4,5-dimethylthiazol-2-yl]-2,5-diphenyltetrazolium bromide) assay kit was from Promega. Prestained Precision Plus protein standards were purchased from BioRad. Anti mouse β-catenin was purchased from BD Transduction Laboratories and anti-glyceraldehyde-3-phosphate dehydrogenase (GAPDH) was from Millipore. Horseradish Peroxidase (HRP)-conjugated anti mouse secondary antibody was from Vector Labs and WesternBright ECL HRP substrate was from Advansta.

Expression vector construction

A cDNA encoding human *WNT3A* (Transomic Technologies) served as template for amplification of a 420 bp sequence corresponding to the SLD using the following primers: FwdSLDNde1 (5' - gggccccatatggtgctggac - 3') and RevSLDXho1 (5' - ctccaccacctcgagcatctccga - 3'). The same human *WNT3A* template was used to amplify a 666 bp sequence (NT-SLD) using FwdNTSLDNde1 (5'-atcatatgagctacccgatctggtggtcg - 3') and RevSLDXho1. Finally, a 531 bp cDNA SLD construct missing the 2 β-hairpin extensions NT-SLD no hairpins(nh) was custom ordered from GenScript. All 3 constructs were ligated into a pET22b plasmid vector (Novagen) at Nde1 and Xho1 (New England Biolabs). Each construct was sequence verified and transformed into SHuffle T7 Express *E. coli* cells (New England Biolabs) to facilitate disulfide bond formation (28).

Recombinant protein production and purification

Bacteria were cultured in NZCYM media plus ampicillin (50 μg/ml) at 30 °C. When the OD_{600} reached 0.6, SLD synthesis was induced by the addition of isopropyl β-D-1-thiogalactopyranoside (1 mM final concentration). Following overnight culture, bacteria were pelleted by centrifugation, re-suspended in 50 mM Tris-HCl, pH 7.2, 0.1 M NaCl, 0.1 mM EDTA, 1 mM DTT and disrupted by probe sonication. Preliminary expression studies revealed that NT-SLD and NT-SLD(nh) localized to inclusion bodies.

Subsequently, *E. coli* cells were processed according to Burgess (2009). Briefly, Triton X-100 (1% final concentration) was added to a sonicated cell lysate, incubated on ice for 10 min and centrifuged at 20,000g for 15 min. This process was repeated at least 6 times or until a white pellet appeared. The precipitate was re-suspended in buffer without Triton X-100 and centrifuged at 20,000g for 15 min to pellet inclusion bodies. The washed pellet was re-suspended in 50 mM Tris-HCl, pH 7.2 containing 6 M guanidine (Gdn HCl, 0.1 M NaCl, 0.1 mM DTT) and incubated at 42-50 °C to dissolve the pellet. Following this, the sample was centrifuged at 20,000g for 15 min. The supernatant was filtered (0.22 µm) to remove particulate matter and applied to a Hi-Trap affinity column (GE Healthcare) as per the manufacturer's instructions. Bound protein was eluted in 20 mM Tris-HCl, pH 7.2, 0.5 M NaCl, 0.5 M imidazole, 6 M Gdn HCl, dialyzed against H_2O, lyophilized and stored at -20 °C.

Recombinant protein solubilization

Lyophilized protein was re-suspended (4 mg/ml) in 2% DTAC (w/v) in the presence of 2 µM oxidized glutathione and 10 µM reduced glutathione (30). The sample was "dilution-folded" in 10 mM sodium phosphate, pH 7, 0.6 M arginine HCl to a final protein concentration of ~0.02 mg/ml, thereby lowering the DTAC concentration below its critical micelle concentration (~30 mM) (31). Subsequently, the sample was concentrated with an Amicon stirred cell fitted with a 10K molecular weight cutoff membrane and dialyzed against 10 mM Na phosphate, pH 7, 0.6 M arginine HCl to remove residual DTAC. Protein concentrations were determined by the Bicinchoninic acid assay (Thermo Fisher Scientific) and purity assessed by SDS-polyacrylamide gel electrophoresis (PAGE). In some cases, sample protein content was determined spectrophotometrically (280 nm) using an extinction coefficient of 45210 M^{-1} cm^{-1} for NT-SLD and 22710 M^{-1} cm^{-1} for NT-SLD(nh).

Far UV circular dichroism spectroscopy

Far UV circular dichroism (CD) spectroscopy measurements were performed on a Jasco 810 spectrapolarimeter. Scans were collected thrice to obtain an average value, using a 0.1 cm path length and 0.2 mg/ml protein concentration. For low pH measurements, NT-SLD was dissolved in 50 mM Na citrate, 20 mM NaCl, pH 3 and measured in the presence of 1% SDS and 50% trifluoroethanol. In another set of experiments, NT-SLD or NT-SLD(nh) were dissolved in 2% DTAC and spectra collected in the presence of 20 mM Na phosphate, pH 7.2, 1mM DTT. Ellipticity values were converted into molar ellipticity (degrees cm^2 $dmol^{-1}$) using mean residue weight values of 25,035 Da for NT-SLD (228 residues) and 20,127 Da for NT-SLD(nh) (185 residues). Protein secondary structure content was calculated using CDSSTR, a variable selection method and SMP180 reference set through DichroWeb (32–34).

Limited proteolysis

NT-SLD and NT-SLD(nh) were incubated in the presence and absence of thrombin (Sigma-Aldrich) at a 1:3 thrombin : SLD protein ratio for 1, 2 and 4 h at 37 °C in 10 mM

Na phosphate, pH 7, 0.6 M arginine HCl in the presence or absence of 1% CHAPS (w/v). Following incubation, proteins were separated by SDS-PAGE and visualized with Imperial protein stain.

Liposome preparation

Ten mg DMPC in chloroform was dried under N_2 gas in a 10 ml round bottom flask and dried further under vacuum overnight. The dried lipid film was dispersed in 500 µl 10 mM Na phosphate, pH 7, 0.6 M arginine HCl and vortexed. The lipid suspension was extruded with 21 passes through a 100 nm polycarbonate membrane in a Thermobarrel extruder maintained at 30–37 °C. The resulting liposome preparation was incubated with NT-SLD or NT-SLD(nh) at 37 °C for 1 h (20:1 liposome to protein ratio; 2 mg liposomes and 100 µg protein in a final volume = 200 µl). Following incubation, liposome-associated SLDs were separated from free SLDs by sucrose gradient centrifugation. Samples were mixed with an equal volume of 80% sucrose and transferred to a centrifuge tube. The 40% sucrose solution was topped with a 20% sucrose solution followed by an 8% sucrose solution. The tube contents were then centrifuged at 200,000g for 3 h at 4 °C. Following centrifugation, fractions (200 µl) were collected from the top and analyzed for liposome content turbidimetrically (310 nm) and protein content by SDS-PAGE.

Tryptophan fluorescence spectroscopy

Specified SLDs were excited at 280 nm and emission recorded between 300 and 450 nm (2 nm slit width) on a Horiba Jobin Yvon FluoroMax-4 luminescence spectrometer. Spectra were obtained in 10 mM Na phosphate, pH 7, 0.6 M arginine HCl in the presence and absence of 2% DTAC.

Biological membrane lytic activity

L cells (6000 cells/well, 96-well plate) were cultured in high glucose DMEM containing 10% FBS, 100 U/ml penicillin and 100 µg/ml streptomycin overnight at 37 °C. After 24 h, the cells were replenished with fresh medium supplemented with specified concentrations of NT-SLD or NT-SLD(nh). After 24 h incubation with SLDs, cell viability was measured with MTT assay.

Canonical Wnt3a signaling activity

L cells (0.5×10^6 cells/well, 12-well plate) were incubated with specified amounts of NT-SLD or NT-SLD(nh) for 3 h at 37 °C and harvested using RIPA cell lysis buffer (50 mM Tris, 150 mM NaCl, 0.1% SDS, 0.5% sodium deoxycholate, 1% Triton X-100) containing 1X Halt protease inhibitor cocktail mix. The protein concentration of cell lysates was measured and 10 µg aliquots heated to 95 °C for 10 min in the presence of SDS reducing buffer, applied to precast 10% polyacrylamide gels and electrophoresed at 120 V. Separated proteins were transferred to a polyvinylidene difluoride membrane, blocked in 5% BSA and probed with anti mouse β-catenin (1:2,000 dilution) and anti

mouse GAPDH (1:2,500 dilution). Positive bands were detected with HRP-conjugated anti mouse secondary antibody (1:5,000 dilution). Assays were performed in triplicate.

Protein Bioinformatics

The three dimensional structure of *Xenopus* Wnt8 in complex with Fz8 CRD (10) was analyzed *in silico* using Research Collaboratory for Structural Bioinformatics Protein Data Bank entry 4FOA.

4.4. Results

Bacterial expression of recombinant Wnt3a SLD

To study the Wnt SLD motif in isolation, a plasmid vector encoding amino acids 83-VLDK…ASEM-222 of mature human *WNT3A* was transformed into *E. coli*. Despite several attempts, no SLD expression was detected in the culture supernatant or pellet fractions of bacteria cultured for 4 to 24 h at 30 °C or 16 °C. Computer assisted analysis of predicted α-helix segments in the SLD motif revealed helix 'a' is mostly hydrophobic while helices 'b', 'c' and 'd' are amphipathic, similar to the helix pattern found in SAPLIPs (35). 3D view analysis of the *Xenopus* Wnt8 crystal structure provided evidence that residues in the extreme N-terminus of the protein (**Figure 4-1A**) orient perpendicular to the core SLD 4-helix bundle in a "protective" belt-like manner that shields helix 'a'. Based on this, the original SLD construct was modified to include 82 NT residues from Wnt3a (**Figure 4-1B**). Unlike the original SLD construct, robust expression of NT-SLD (residues 1-SYPI…ASEM-222) was observed, with large amounts of recombinant protein accumulating in inclusion bodies. To better mimic the structure of SAPLIPs, a third construct was generated wherein two hairpin extensions present in Wnt SLDs but not other saposin family proteins, were deleted (residues 112 to 141 comprising hairpin 1 were replaced by the amino acid sequence Gly-Ala-Gly while residues 178 to 205 comprising hairpin 2 were replaced by Gly-Ala-Gly-Ala-Gly). The resulting construct, NT-SLD(nh), expressed well in *E. coli*, with the protein product accumulating in inclusion bodies.

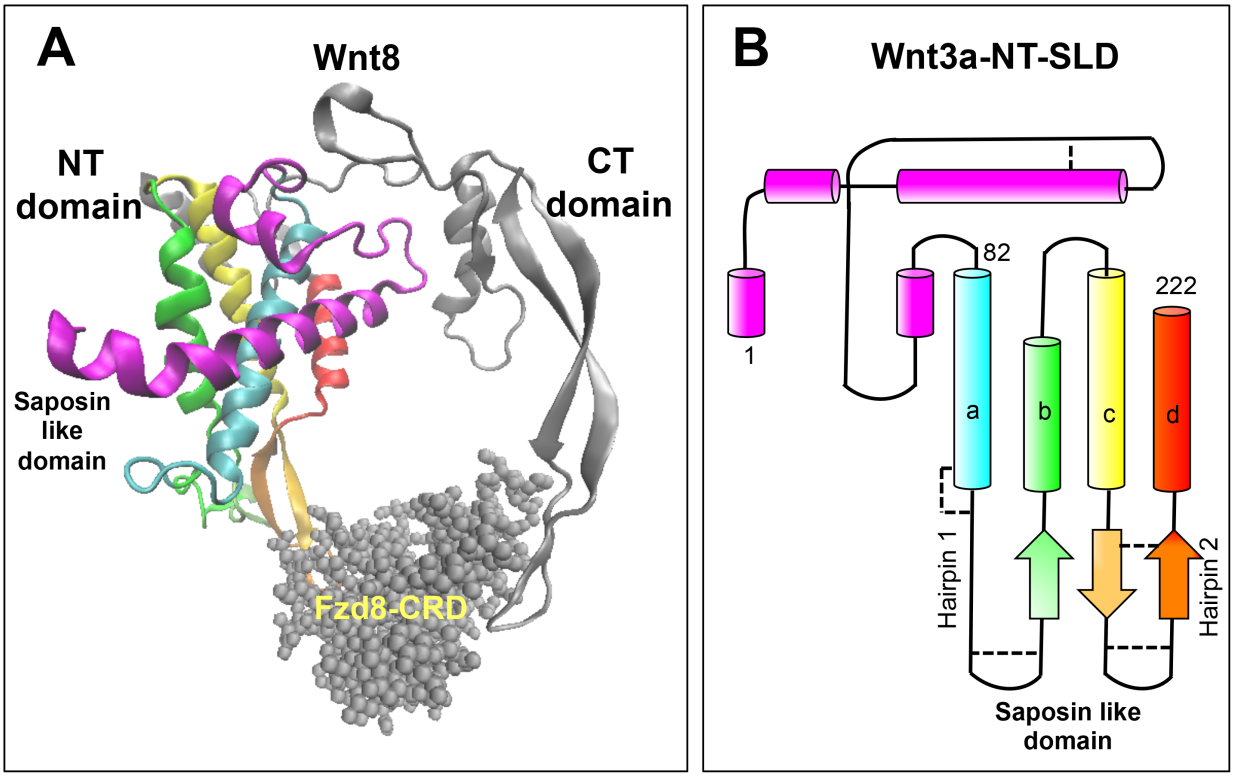

Figure 4-1. Structural models of *Xenopus* Wnt8 and NT-SLD. Panel A) Structure of *Xenopus* Wnt8 complexed with Fzd8-CRD (Protein Data Bank entry 4FOA) was generated using Visual Molecular Dynamics (36). The first NT 82 amino acids are in magenta, the SLD is multicolour and the CT domain is in grey. Fzd8-CRD is shown as grey space-fill. Panel B) Schematic representation of secondary structure elements of human Wnt3a NT-SLD, adapted from (37). Cylinders depict α-helices; block arrows indicate β-sheet and dotted lines connect cysteine disulfide bonds. Individual α-helices are color-coded: magenta (N terminal 82 amino acids), cyan (SLD helix a), green (helix b), yellow (helix c) and red (helix d).

Solution properties of recombinant Wnt3a-NT-SLDs

The relative purity of isolated NT-SLD and NT-SLD(nh) were assessed by SDS-PAGE (**Figure 4-2**). Although isolated NT-SLD was fully soluble in 50 mM sodium citrate, pH 3, 150 mM NaCl, it was insoluble in neutral pH buffers. However, solubility was conferred to NT-SLD at neutral pH when DTAC (2% w/v) was introduced. Subsequent removal of DTAC by dilution and dialysis against 10 mM sodium phosphate pH 7, 0.6 M arginine HCl retained NT-SLD solubility at neutral pH in the absence of detergent. To determine the effect of hairpin deletion on NT-SLD solubility, NT-SLD(nh) was purified and isolated from inclusion bodies using the same process. This ~20 kDa protein was soluble at pH 3 and also required the presence of 0.6 M arginine HCl to retain solubility in neutral pH buffer upon removal of detergent.

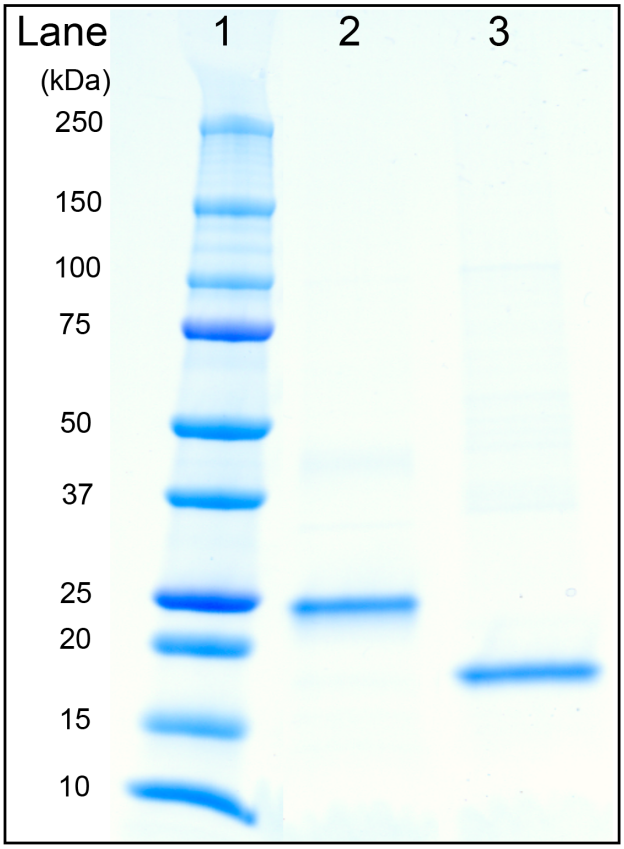

Figure 4-2. SDS-PAGE of isolated SLD proteins. Lane assignments: lane 1) prestained Precision Plus protein standard, lane 2) NT-SLD (expected molecular weight = 25 kDa) and lane 3) NT-SLD(nh) (expected molecular weight = 20 kDa). Five µg protein was applied to each well and, following electrophoresis, the gel was stained with Gel Code Blue.

Far UV CD spectroscopy of SLDs

To evaluate the secondary structure content of NT-SLD and NT-SLD(nh), far UV CD spectra were collected. NT-SLD in 50 mM Na citrate, pH 3, 20 mM NaCl yielded a spectrum with little negative ellipticity. Upon addition of 1% SDS or 50% trifluoroethanol, however, distinct minima appeared at 208 nm and 222 nm, consistent with induction of α-helix secondary structure (**Figure 4-3**). At neutral pH (10 mM sodium phosphate, pH 7, 0.6 M arginine HCl) the absorption properties of L-arginine interfered with the SLD signal. Subsequently, spectra of NT-SLD and NT-SLD(nh) were collected in 20 mM sodium phosphate, pH 7.2, 2% DTAC. The spectra displayed strong minima at 208 and 222 nm and secondary structure calculations indicated 49% α-helix for NT-SLD and 63% for NT-SLD(nh). Inclusion of oxidized / reduced glutathione and DTT had no effect on the secondary structure content of NT-SLD or NT-SLD(nh).

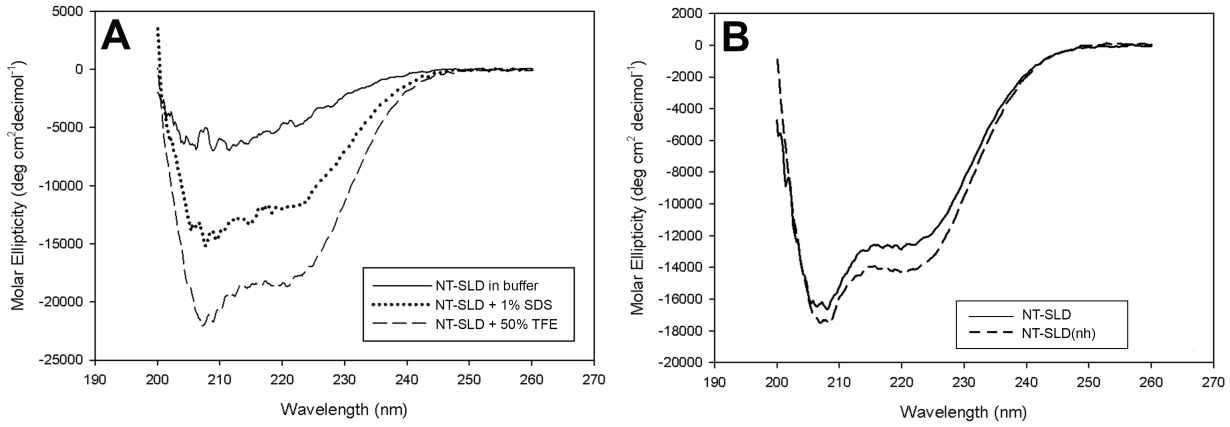

Figure 4-3. Far UV CD spectroscopy of SLDs. Panel A) Spectra of NT-SLD (0.2 mg/ml) in 50 mM Na citrate pH 3, 20 mM NaCl (solid line), 50 mM Na citrate, pH 3, 20 mM NaCl plus 1% SDS (dotted line) or 50 mM sodium citrate, pH 3, 20 mM NaCl plus 50% trifluoroethanol (TFE) (dashed line). Panel B) NT-SLD (solid line) and NT-SLD(nh) (dashed line) in 20 mM $NaPO_4$, pH 7.2, 2% DTAC.

SLD interaction with liposomes

To assess their membrane interaction properties, NT-SLD and NT-SLD(nh) were incubated with liposomes. Following incubation, lipid-bound and free SLDs were separated by sucrose gradient centrifugation, fractionated and analyzed (**Figure 4-4**). Turbidimetric measurement of light scattering intensity detected liposomes in gradient fractions 2 and 3 while fractions 4 and 5 were essentially free of liposomes. In the absence of liposomes, NT-SLD and NT-SLD(nh) were recovered in fractions 4 and 5 while in the presence of liposomes, a portion of NT-SLD and NT-SLD(nh) shifted to lower density, liposome-containing fractions.

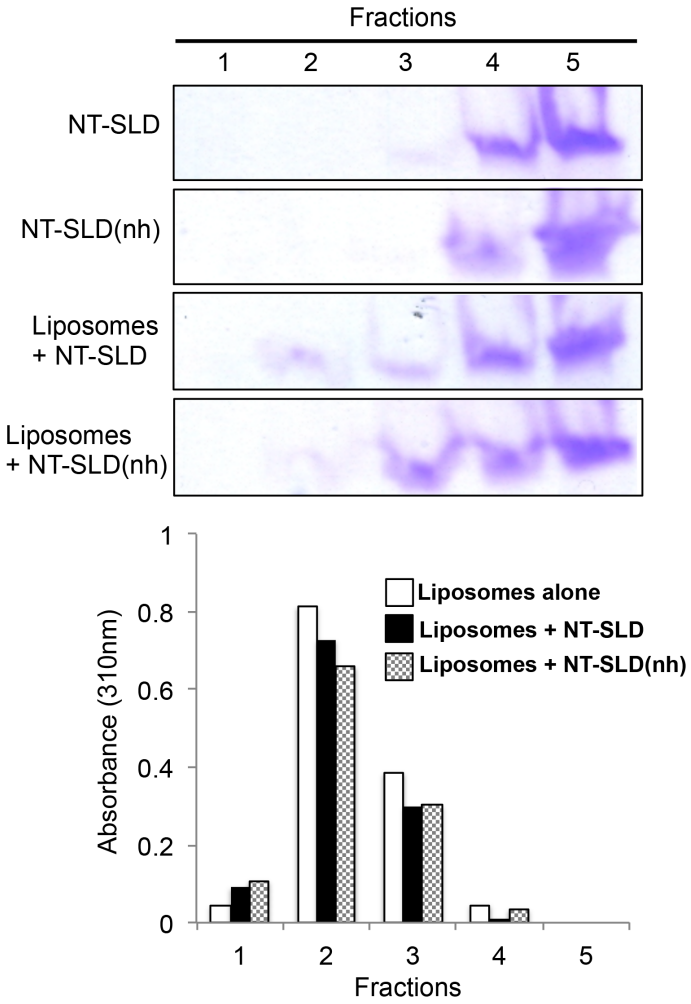

Figure 4-4. SLD-liposome binding interactions. Liposomes were incubated with NT-SLD or NT-SLD(nh) at a liposome:protein ratio = 20:1. After 1 h incubation, the sample was subjected to sucrose gradient centrifugation. Following centrifugation, five fractions (200 µl each) were collected from the top. An aliquot of each fraction was analyzed by SDS-PAGE and proteins visualized by Imperial protein stain. The liposome content of each fraction was measured by light scattering measurements at 310 nm and presented graphically. Results presented are representative of two independent experiments.

Fluorescence analysis of SLD-detergent micelle interaction

Given that NT-SLD exhibited limited binding to liposomes yet was stabilized in the presence of detergent micelles, the effect of DTAC on the intrinsic fluorescence of SLDs was examined (**Figure 4-5**). Fluorescence emission spectra were collected for each SLD in the absence and presence of 2% DTAC. NT-SLD has seven Trp residues (positions 5, 6, 68, 132, 134, 199 and 200) while NT-SLD(nh) has three (positions 5, 6, 68). In the absence of DTAC, fluorescence emission spectra (excitation 280 nm) of NT-SLD and NT-SLD(nh) gave rise to wavelengths of maximum fluorescence emission of 346 nm and 341 nm, respectively. In the presence of DTAC, a ~2 fold increase in quantum yield was recorded for NT-SLD and NT-SLD(nh), with no shift in the wavelength of maximum fluorescence emission.

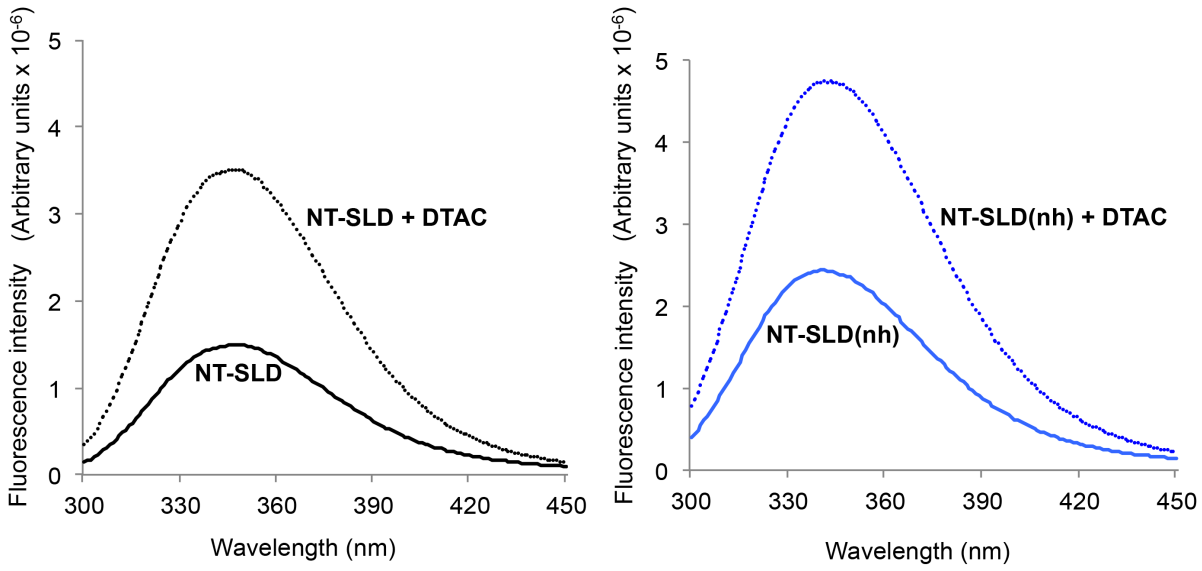

Figure 4-5. Fluorescence emission spectra of SLDs. Left) Tryptophan fluorescence emission spectra (excitation 280nm) of (a) NT-SLD (1 mg/ml) in 10 mM Na phosphate, pH 7, 0.6 M arginine HCl, recorded from 300 to 450 nm in the absence (solid black line) and presence (dotted black line) of 2% DTAC. Right) NT-SLD(nh) (1 mg/ml) in 10 mM Na phosphate, pH 7, 0.6 M arginine HCl, recorded from 300 to 450 nm in the absence (solid blue line) and presence of 2% DTAC (dotted blue line).

Limited proteolysis of SLDs

To probe whether binding to detergent micelles induces a conformational change in NT-SLD or NT-SLD(nh) similar to that reported for SAPLIPs (38), limited proteolysis experiments were performed. Based on the previously reported thrombin sensitivity of Wnt3a (26) and its binding to CHAPS micelles (39), thrombolytic cleavage of SLDs was evaluated in the absence and presence of CHAPS. Whereas thrombin prefers to cleave Arg-Gly sequences (40), the SLDs under investigation lack this sequence element. However, NT-SLD and NT-SLD(nh) contain an Arg-Ser sequence that is sensitive to thrombin digestion (41). Under the conditions employed, a time-dependent increase in NT-SLD and NT-SLD(nh) proteolysis was observed, as judged by substrate reduction / product accumulation over the course of 4 h (**Figure 4-6**). The proteolytic fragments generated from NT-SLD were 17 kDa and 7 kDa in size while those from NT-SLD(nh) were 14 kDa and 5 kDa. Cleavage of NT-SLD(nh) was monitored by the appearance of the 14 kDa fragment since the 5 kDa fragment was not detected under these electrophoresis conditions. No significant differences in thrombin sensitivity were observed between NT-SLD and NT-SLD(nh) in the presence or absence of CHAPS micelles.

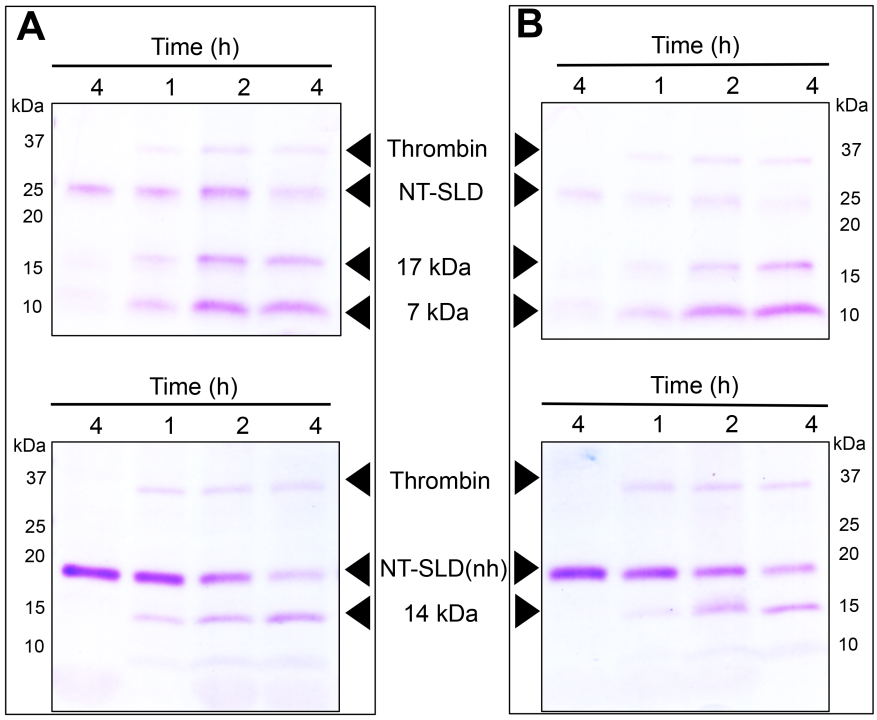

Figure 4-6: Thrombin-mediated proteolysis of NT-SLDs. NT-SLD and NT-SLD(nh) were incubated in the absence and presence of thrombin in 10 mM Na phosphate, pH 7, 0.6 M arginine HCl, labeled as buffer (panel A) and buffer plus 1% CHAPS (panel B) in final volume of 10 µl for 1, 2 and 4 h at 37°C. Control SLD incubations in the absence of thrombin were incubated for 4 h at 37°C. Following incubation, samples were subjected to SDS-PAGE and stained with Imperial protein stain. The results are representative of two experiments.

Effect of NT-SLDs on cell membrane lysis

A known property of certain SAPLIPs is cell membrane lysis (25, 42). To determine if NT-SLD or NT-SLD(nh) possess cell lytic activity, the proteins were incubated with cultured fibroblasts. Following incubation with varying concentrations of NT-SLD or NT-SLD(nh), cell viability was assayed (**Figure 4-7**). Compared to buffer treated control cells, no differences in cell viability were detected in cells incubated with either protein.

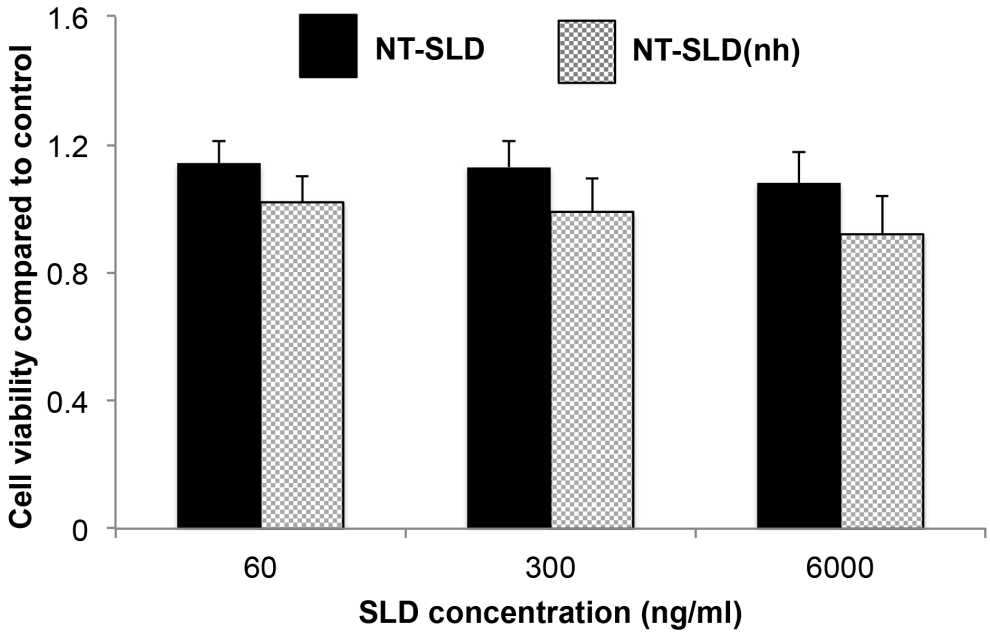

Figure 4-7. Effect of SLDs on L cell viability. Cultured murine L cells were incubated in the absence and presence of increasing concentrations of NT-SLD or NT-SLD(nh) for 24 h. Following incubation, cell viability was measured by the MTT assay. SLDs were presented to the cells in 10 mM Na phosphate, pH 7, 0.6 M arginine HCl. Values reported are the mean ± standard error (n=3).

Wnt3a canonical signaling in the presence of NT-SLDs

To assess their affect on canonical Wnt3a signaling activity, cultured fibroblasts were treated with increasing concentrations of NT-SLD or NT-SLD(nh) followed by determination of cellular β-catenin levels (a measure of canonical Wnt signaling; (26). Similar to untreated control cells, β-catenin levels were below the limits of detection following incubation with either NT-SLD or NT-SLD(nh) (**Figure 4-8**). By contrast, levels of β-catenin increased dramatically in response to treatment with 60 ng/ml full-length Wnt3a. This level of activation was unaffected by inclusion of increasing concentrations of NT-SLD or NT-SLD(nh).

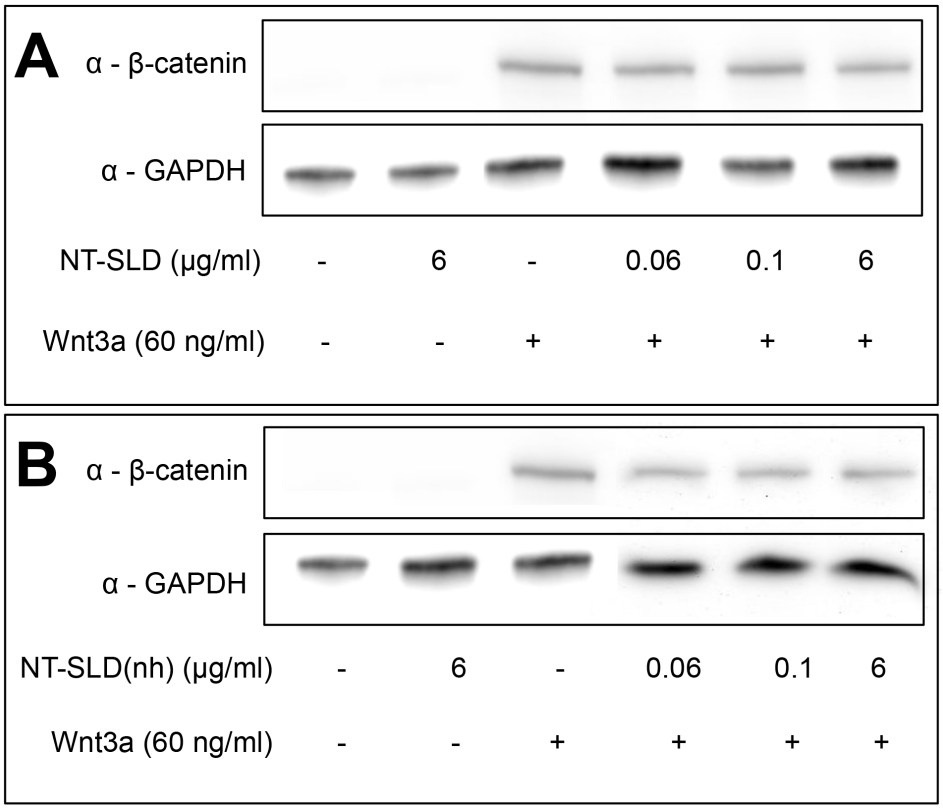

Figure 4-8. Effect of SLD on canonical Wnt signaling activity. L cells were incubated with indicated concentrations of Wnt3a and (A) NT-SLD or (B) NT-SLD(nh) for 3 h. Following incubation, the cells were lysed and 10 μg lysate protein applied to a 10% SDS-PAGE gel. Separated proteins were transferred to a PVDF membrane and probed with antibodies directed against β-catenin and GAPDH. The results are representative of three independent experiments.

4.5. Discussion

The Wnt protein structure provides valuable information pertinent to its post-secretory migration via diffusion, and /or interaction with carriers, that ultimately leads to engagement of cell surface receptors and manifestation of biological activity (43, 44). At the target cell surface, bipartite binding of Wnt's globular NT domain and CT cytokine-like domain to Fzd CRD has led to the hypothesis that, during evolution of Wnts, a gene fusion event occurred to create its two domain structure (37). Such an event may have included a SAPLIP gene, which became integrated into the molecular architecture of Wnt. Analysis of *Xenopus* Wnt8 X-ray structure reveals the presence of a saposin-like sub-domain as a structural feature of Wnt (13). If so, has this domain retained or lost functional properties associated with SAPLIP family members? To address this, a reductionist approach was employed to evaluate the functional properties of this sub-domain in isolation. Initial experiments were performed to determine the feasibility of bacterial expression of human Wnt3a SLD. When the expression construct included only those residues identified as being part of the saposin structure, little or no SLD protein was produced. On the other hand, when the construct was expanded to include 82 NT amino acids of human Wnt3a, protein production greatly increased. The reason for this is unclear but may be related to a potential structural role imparted by these 82 residues. In the X-ray structure of *Xenopus* Wnt8 these residues adopt an α-helix that contacts helix 'a' of SLD. Thus, it is conceivable that Wnt SLD is unstable in the absence of this region of the Wnt protein. Another feature unique to Wnt SLD is the presence of two elongated hairpins that extend from the SLD. Given that these structural features are not present in SAPLIPs, a construct was generated in which these elements were deleted. Among 3 different plasmid constructs generated, SLD, NT-SLD and NT-SLD(nh), the latter two led to recombinant protein production upon transformation into *E. coli*. The expressed proteins were isolated in mg quantities, permitting their structural and functional properties to be investigated.

To our knowledge, the present study is the first investigation into the molecular properties of an isolated Wnt sub-domain in which structural and biochemical analyses were used to evaluate its potential functionality in the context of full-length Wnt. Based on secondary structure analysis, it was observed that, similar to other SAPLIP family members (45, 46), isolated NT-SLD and NT-SLD(nh) adopt α-helix secondary structure in aqueous media, albeit only under special circumstances. Although both of the SLDs studied were soluble in low pH buffer, they lack secondary structure under this condition. This property is unlike many SAPLIPs, which are known to retain secondary structure and function at low pH (25). These results suggest additional structural elements within full-length Wnt3a affect the structural integrity of the SLD sub-domain.

A general feature of SAPLIPs is the presence of a loosely packed helix bundle core that is predicted to facilitate conformational opening and closing in response to pH change or exposure to lipid (15, 38). The presence of three intramolecular disulfide bonds in SAPLIPs may define the limits of conformational flexibility and dictate the route of helix bundle opening and closing. As a result, members of the SAPLIP protein family interact reversibly with membranes, either at cell surface or an organelle to facilitate cell lysis, lipid modifying enzyme activity or transport processes (25, 47). While the SLD of Wnt also possesses a loosely packed core, corresponding disulfide bonds are lacking,

such that fewer restrictions exist to limit conformational flexibility (10, 14). Although SLDs interact with detergent micelles, classic helix bundle opening to engage the membrane surface of liposomes did not occur to a significant extent.

Further information about SLD conformational flexibility and changes in protein microenvironment was obtained in studies with detergent micelles using fluorescence spectroscopy. Although the wavelength of maximum Trp fluorescence emission did not shift upon SLD binding to micelles, a large enhancement in quantum yield was noted. The increase in quantum yield is indicative of SLD binding to the micelle surface while the location of SLD Trp residues outside the core helix bundle structure may underlie the absence of a blue shift in Trp fluorescence emission maximum upon micelle binding.

In an effort to monitor changes in conformation upon SLD interaction with micelles, thrombin cleavage sensitivity studies were performed. Previous studies revealed thrombin recognizes an Arg-Ser sequence element in Wnt3a as a cleavage site (26). Thus, we hypothesized that, if this region of the protein changes its orientation and exposure to solvent, differences in thrombin cleavage sensitivity may be observed in the presence / absence of detergent micelles. The results obtained indicate that micelle interaction did not confer protection from thrombolytic cleavage as compared to the same SLDs in aqueous media. This may be explained by the location of the Arg-Ser sequence near one end of the SLD, a region that is not predicted to make intimate contact with the micelle surface. More information may be gained by examining the cleavage sensitivity of SLD variants in which the cleavage site is relocated within the protein sequence.

Among Wnt family protein members, *Drosophila* WntD is unique in that it is neither glycosylated nor fatty acylated yet it signals through the Fzd4 receptor to affect patterning, adult immune responses and primordial germ cells migration to gonads (14). Similarly, recombinant NT-SLD and NT-SLD(nh) studied herein lack fatty acylation. Given the binding interaction identified between the fatty acyl chain on *Xenopus* Wnt8 and Fzd8 CRD by X-ray crystallography (10), it is possible, if not likely, that the lack of a fatty acyl group in SLDs generated in this study interferes with their ability to modulate canonical Wnt signaling activity. The finding that SLDs did not interfere or enhance the ability of full length Wnt3a to induce β-catenin stabilization suggests these proteins do not interact with one another. Future studies will be required to determine the effect of post-translational SLD fatty acylation on canonical Wnt signaling activity. It would also be interesting to examine liposome binding of lipid-modified SLD. Such studies would reveal if fatty acylated SLD alone could accentuate or interfere with Wnt signaling. Based on the findings of the present study, the evidence suggests that Wnt3a SLD has deviated from ancestral SAPLIPs such that, while maintaining the overall protein fold, it serves a predominantly structural role in the broader context of Wnt proteins.

4.6. References

1. Nusse, R. (2008) Wnt signaling and stem cell control. *Cell Res.* **18**, 523–527
2. Holstein, T. W. (2012) The evolution of the Wnt pathway. *Cold Spring Harb. Perspect. Biol.* **4**, a007922
3. Staal, F. J. T., Luis, T. C., and Tiemessen, M. M. (2008) WNT signalling in the immune system: WNT is spreading its wings. *Nat. Rev. Immunol.* **8**, 581–593
4. Schulte, G. (2015) Frizzleds and WNT/β-catenin signaling – The black box of ligand–receptor selectivity, complex stoichiometry and activation kinetics. *Eur. J. Pharmacol.* **763**, 191–195
5. Angers, S., and Moon, R. T. (2009) Proximal events in Wnt signal transduction. *Nat. Rev. Mol. Cell Biol.* **10**, 468
6. Moon, R. T., Kohn, A. D., Ferrari, G. V. De, and Kaykas, A. (2004) WNT and β-catenin signalling: diseases and therapies. *Nat. Rev. Genet.* **5**, 691–701
7. Schinner, S. (2009) Wnt-signalling and the metabolic syndrome. *Horm. Metab. Res.* **41**, 159–63
8. Berwick, D. C., and Harvey, K. (2012) The importance of Wnt signalling for neurodegeneration in Parkinson's disease. *Biochem. Soc. Trans.* **40**, 1123–8
9. Libro, R., Bramanti, P., and Mazzon, E. (2016) The role of the Wnt canonical signaling in neurodegenerative diseases. *Life Sci.* **158**, 78–88
10. Janda, C. Y., Waghray, D., Levin, A. M., Thomas, C., and Garcia, K. C. (2012) Structural basis of Wnt recognition by Frizzled. *Science*. **337**, 59–64
11. Takada, R., Satomi, Y., Kurata, T., Ueno, N., Norioka, S., Kondoh, H., Takao, T., and Takada, S. (2006) Monounsaturated fatty acid modification of Wnt protein: its role in Wnt secretion. *Dev. Cell*. **11**, 791–801
12. Kumar, S., Žigman, M., Patel, T. R., Trageser, B., Gross, J. C., Rahm, K., Boutros, M., Gradl, D., Steinbeisser, H., Holstein, T., Stetefeld, J., and Özbek, S. (2014) Molecular dissection of Wnt3a-Frizzled8 interaction reveals essential and modulatory determinants of Wnt signaling activity. *BMC Biol.* **12**, 44
13. Bazan, J. F., Janda, C. Y., and Garcia, K. C. (2012) Structural architecture and functional evolution of Wnts. *Dev. Cell*. **23**, 227–32
14. Chu, M. L.-H., Ahn, V. E., Choi, H.-J., Daniels, D. L., Nusse, R., and Weis, W. I. (2013) Structural Studies of Wnts and identification of an LRP6 binding site. *Structure*. **21**, 1235–42
15. Anderson, D. H., Sawaya, M. R., Cascio, D., Ernst, W., Modlin, R., Krensky, A., and Eisenberg, D. (2003) Granulysin crystal structure and a structure-derived lytic mechanism. *J. Mol. Biol.* **325**, 355–65
16. Munford, R. S., Sheppard, P. O., and O'Hara, P. J. (1995) Saposin-like proteins (SAPLIP) carry out diverse functions on a common backbone structure. *J. Lipid Res.* **36**, 1653–63
17. Bruhn, H. (2005) A short guided tour through functional and structural features of saposin-like proteins. *Biochem. J.* **389**, 249–57
18. Michalek, M., and Leippe, M. (2015) Mechanistic Insights into the Lipid Interaction of an Ancient Saposin-like Protein. *Biochemistry*. **54**, 1778–1786
19. Rossmann, M., Schultz-Heienbrok, R., Behlke, J., Remmel, N., Alings, C., Sandhoff, K., Saenger, W., and Maier, T. (2008) Crystal structures of human

saposins C andD: implications for lipid recognition and membrane interactions. *Structure*. **16**, 809–17
20. Winkelmann, J., Leippe, M., and Bruhn, H. (2006) A novel saposin-like protein of Entamoeba histolytica with membrane-fusogenic activity. *Mol. Biochem. Parasitol.* **147**, 85–94
21. Liepinsh, E., Andersson, M., Ruysschaert, J. M., and Otting, G. (1997) Saposin fold revealed by the NMR structure of NK-lysin. *Nat. Struct. Biol.* **4**, 793–5
22. Piatigorsky, J., Norman, B., Dishaw, L. J., Kos, L., Horwitz, J., Steinbach, P. J., and Kozmik, Z. (2001) J3-crystallin of the jellyfish lens: similarity to saposins. *Proc. Natl. Acad. Sci. U. S. A.* **98**, 12362–7
23. Bornhauser, B. C., Olsson, P.-A., and Lindholm, D. (2003) MSAP Is a Novel MIR-interacting Protein That Enhances Neurite Outgrowth and Increases Myosin Regulatory Light Chain. *J. Biol. Chem.* **278**, 35412–35420
24. Hecht, O., Van Nuland, N. A., Schleinkofer, K., Dingley, A. J., Bruhn, H., Leippe, M., and Grötzinger, J. (2004) Solution structure of the pore-forming protein of Entamoeba histolytica. *J. Biol. Chem.* **279**, 17834–41
25. Yang, L., Johansson, J., Ridsdale, R., Willander, H., Fitzen, M., Akinbi, H. T., and Weaver, T. E. (2010) Surfactant Protein B Propeptide Contains a Saposin-Like Protein Domain with Antimicrobial Activity at Low pH. *J. Immunol.* **184**, 975–983
26. Witkowski, A., Krishnamoorthy, A., Su, B., Beckstead, J. A., and Ryan, R. O. (2015) Isolation and characterization of recombinant murine Wnt3a. *Protein Expr. Purif.* **106**, 41–48
27. Willert, K., Brown, J. D., Danenberg, E., Duncan, A. W., Weissman, I. L., Reya, T., Yates, J. R., and Nusse, R. (2003) Wnt proteins are lipid-modified and can act as stem cell growth factors. *Nature*. **423**, 448–52
28. Kong, B., and Guo, G. L. (2014) Soluble expression of disulfide bond containing proteins FGF15 and FGF19 in the cytoplasm of Escherichia coli. *PLoS One*. **9**, e85890
29. Burgess, R. R. (2009) Chapter 17 Refolding Solubilized Inclusion Body Proteins. in *Methods in enzymology*, pp. 259–282, **463**, 259–282
30. Kudou, M., Yumioka, R., Ejima, D., Arakawa, T., and Tsumoto, K. (2011) A novel protein refolding system using lauroyl-l-glutamate as a solubilizing detergent and arginine as a folding assisting agent. *Protein Expr. Purif.* **75**, 46–54
31. Oviedo-Roa, R., Martínez-Magadán, J. M., Muñoz-Colunga, A., Gómez-Balderas, R., Pons-Jiménez, M., and Zamudio-Rivera, L. S. (2013) Critical micelle concentration of an ammonium salt through DPD simulations using COSMO-RS-based interaction parameters. *AIChE J.* **59**, 4413–4423
32. Abdul-Gader, A., Miles, A. J., and Wallace, B. A. (2011) A reference dataset for the analyses of membrane protein secondary structures and transmembrane residues using circular dichroism spectroscopy. *Bioinformatics*. **27**, 1630–6
33. Whitmore, L., and Wallace, B. A. (2008) Protein secondary structure analyses from circular dichroism spectroscopy: Methods and reference databases. *Biopolymers*. **89**, 392–400
34. Sreerama, N., and Woody, R. W. (2000) Estimation of protein secondary structure from circular dichroism spectra: comparison of CONTIN, SELCON, and CDSSTR methods with an expanded reference set. *Anal. Biochem.* **287**, 252–60

35. Qi, X., and Grabowski, G. A. (2001) Differential membrane interactions of saposins A and C: Implications for the functional specificity. *J. Biol. Chem.* **276**, 27010–27017
36. Humphrey, W., Dalke, A., and Schulten, K. (1996) VMD: visual molecular dynamics. *J. Mol. Graph.* **14**, 33–8, 27–8
37. MacDonald, B. T., Hien, A., Zhang, X., Iranloye, O., Virshup, D. M., Waterman, M. L., and He, X. (2014) Disulfide bond requirements for active Wnt ligands. *J. Biol. Chem.* **289**, 18122–36
38. Popovic, K., Holyoake, J., Pomès, R., and Privé, G. G. (2012) Structure of saposin A lipoprotein discs. *Proc. Natl. Acad. Sci. U. S. A.* **109**, 2908–12
39. Lalefar, N. R., Witkowski, A., Simonsen, J. B., and Ryan, R. O. (2016) Wnt3a nanodisks promote ex vivo expansion of hematopoietic stem and progenitor cells. *J. Nanobiotechnology*. **14**, 66
40. Waugh, D. S. (2011) An overview of enzymatic reagents for the removal of affinity tags. *Protein Expr. Purif.* **80**, 283–93
41. Le Bonniec, B. F., Myles, T., Johnson, T., Knight, C. G., Tapparelli, C., and Stone, S. R. (1996) Characterization of the P2' and P3' specificities of thrombin using fluorescence-quenched substrates and mapping of the subsites by mutagenesis. *Biochemistry*. **35**, 7114–22
42. Bryksa, B. C., Bhaumik, P., Magracheva, E., De Moura, D. C., Kurylowicz, M., Zdanov, A., Dutcher, J. R., Wlodawer, A., and Yada, R. Y. (2011) Structure and mechanism of the saposin-like domain of a plant aspartic protease. *J. Biol. Chem.* **286**, 28265–75
43. Miyabayashi, T., Teo, J.-L., Yamamoto, M., McMillan, M., Nguyen, C., and Kahn, M. (2007) Wnt/beta-catenin/CBP signaling maintains long-term murine embryonic stem cell pluripotency. *Proc. Natl. Acad. Sci. U. S. A.* **104**, 5668–73
44. Nusse, R., and Varmus, H. (2012) Three decades of Wnts: a personal perspective on how a scientific field developed. *EMBO J.* **31**, 2670–84
45. Egas, C., Lavoura, N., Resende, R., Brito, R. M., Pires, E., de Lima, M. C., and Faro, C. (2000) The saposin-like domain of the plant aspartic proteinase precursor is a potent inducer of vesicle leakage. *J. Biol. Chem.* **275**, 38190–6
46. Waring, A. J., Chen, Y., Faull, K. F., Stevens, R., Sherman, M. A., and Fluharty, A. L. (1998) Porcine Cerebroside Sulfate Activator (Saposin B) Secondary Structure: CD, FTIR, and NMR Studies. *Mol. Genet. Metab.* **63**, 14–25
47. Alattia, J.-R., Shaw, J. E., Yip, C. M., and Privé, G. G. (2006) Direct Visualization of Saposin Remodelling of Lipid Bilayers. *J. Mol. Biol.* **362**, 943–953

CONCLUDING REMARKS

The primary focus of this dissertation has been around the biochemistry and behavior of molecules that exhibit hydrophobic properties. In the study about nutlins, the small molecule hydrophobic inhibitor of MDM2, I demonstrated that reconstituted HDL is a viable platform for solubilization and delivery of biologically active nutlin-3a in the form of nanodisks (ND) thus improving nutlin-3a solubility in aqueous media. Nutlin-3a ND administration to different glioblastoma cell lines induces apoptosis and cell cycle arrest by activating upstream regulators of p53 specifically in cell lines possessing a wild type p53 tumor suppressor protein pathway. With improved solubility, further studies can be carried out to test the bioavailability of nutlin-3a ND in vivo and its potential use in other tumor models.

In the study about Wnts, an improvised system was established using *Drosophila* S2 cells that were stably transfected with murine Wnt3a to enhance the yield of recombinant Wnt3a and optimized using 3 chromatographic steps. Biological activity of Wnt3a isolated in the presence of CHAPS detergent was confirmed by measuring levels of stabilized β-catenin protein in mouse embryonic fibroblast L cells as a result of activation of canonical signaling pathway. Upon generating sufficient quantities of Wnt3a, I undertook a series of Wnt3a characterization studies. One of which was to evaluate modulation of Wnt3a mediated canonical signaling pathway in the presence of apoE3. I found that in a lipid free environment, the N terminus of apoE3 is able to down regulate Wnt3a mediated stabilization of β-catenin protein. In fact reconstituted high density lipoprotein made of apoE3 or apoA-I were also able to down regulate Wnt3a mediated canonical signaling most likely by complexing with Wnt3a. However, the specificity demonstrated by lipid free apoE3 requires further investigation into the potential interactions between apoE3 and Wnt3a and or LRP5/6 receptor.

As a part of the characterization studies using full length Wnt3a, I found that Wnt3a is susceptible to thrombin digestion within its lipidated N terminal region that contains the saposin like sub-domain (SLD). Using a reductionist approach I expressed and purified the SLD that required the presence of the first 82 N terminal residues of Wnt3a, due to its interaction with the helical core (NT-SLD). Saposin like proteins (SAPLIPs) have lipid / membrane binding properties. However, the functional properties of Wnt3a-NT-SLD do not appear to be associated with SAPLIP family members. Based on the findings of the study, it is apparent that the Wnt3a SLD has deviated away from ancestral SAPLIPs such that, while maintaining the overall protein fold, it serves a predominantly structural role in the broader context of Wnt proteins.